



# JOURNAL OF APPLIED RESEARCH ON SCIENCE AND TECHNOLOGY



Approved during 2022-2024

INSTITUTE OF RESEARCH AND DEVELOPMENT  
RAJAMANGALA UNIVERSITY OF TECHNOLOGY THANYABURI

ISSN Online  
2773-9473

Volume 23 Issue 3  
September – December 2024

# JARST

# RMUTT

## **Journal of Applied Research on Science and Technology (JARST)**

E-ISSN : 2773-9473

Vol. 23 No. 3 September - December

The Journal of Applied Research on Science and Technology (JARST) aims to disseminate and share knowledge and ideas in the form of high-quality articles to academia, professionals, industrialists, and an important forum for exchanging knowledge between researchers, academics, faculty members and students both national and international, which will bring benefits in building academic cooperation and network that will lead to sustainable use of research. The articles that will be published in this journal must not be ever presented and published or in the evaluation processes in any other journals. Any piracy occurred will be only under the responsibility of the authors. The journal will not be responsible for such consequences.

### **Aims and Scope**

The scope of the journal includes the following areas of research: General Engineering, General Materials Science, General Agricultural and Biological Sciences, General Computer Science, and General Mathematics with particular emphasis on issues that deepen in the basic and applied research. The JARST includes full length original, novel research articles and review articles. Accepted articles are immediately available online and are freely accessible without any restrictions or any other obligations to researchers and scholarly people globally.

### **Review Process**

#### **1. Evaluation by the Editor-in-Chief**

The Editor-in-Chief will see whether the topic and theme of the article are appropriate and congruent with the stipulated objectives and format of the Journal. Plagiarism and benefits relating to theory and business contribution will also be investigated. The submitted paper may be returned to the author for preliminary revising or, if the aforesaid criteria are not met, rejected.

#### **2. Evaluation by Review**

All submitted manuscripts must be reviewed by at least two expert reviewers in the related fields. Reviewers will evaluate the quality of submitted article for publication via the double-blinded review system.

#### **3. Evaluates the Reviews**

The Editor-in-Chief make decision for article publication based on the external readers' evaluation. The said decision is either accepting the article for publication, rejecting it, or resending it back to the author for further elaborating revision.

### **Period of Issued Journal**

The Journal of Applied Research on Science and Technology (JARST) will be 3 issues/year, as follows:

1<sup>st</sup> issue: January - April

2<sup>nd</sup> issue: May - August

3<sup>rd</sup> issue: September - December

### **Advisory Board**

Sommai Pivsa-Art  
Krischonme Bhumkittipich  
Kiattisak Sangpradit  
Sorapong Pavasupree  
Boonyang Plangklang  
Syuji Fujii

Rajamangala University of Technology Thanyaburi, Thailand  
Rajamangala University of Technology Thanyaburi, Thailand  
Rajamangala University of Technology Thanyaburi, Thailand  
Rajamangala University of Technology Thanyaburi, Thailand  
Rajamangala University of Technology Thanyaburi, Thailand  
Osaka Institute of Technology, Japan

## Editor-in-Chief

Amorn Chaiyasat Rajamangala University of Technology Thanyaburi, Thailand

## Assistant Editors

Warinthon Poonsri Rajamangala University of Technology Thanyaburi, Thailand  
 Jakkree Srinonchat Rajamangala University of Technology Thanyaburi, Thailand

## Editorial Board

Arumugam Priyadharsan	Saveetha Institute of Medical and Technical Sciences, India
Arunachala Mada Kannan	Arizona State University, USA
Chaudhery Mustansar Hussain	New Jersey Institute of Technology, USA
Enggee Lim	Xi'an Jiaotong-Liverpool University, China
Hemanatha P.W. Jayasuriya	Sultan Qaboos University, Oman
Hideto Minami	Kobe University, Japan
Katsuyuki Takahashi	Iwate University, Japan
Kelvin Huang-Chou Chen	National Pingtung University, Taiwan
Pankaj B. Pathare	Sultan Qaboos University, Oman
Peeyush Soni	Indian Institute of Technology Kharagpur, India
Ryo Honda	Kanazawa University, Japan
Tran Hung Tra	Nha Trang University, Viet Nam
Venkataswamy Gurusamy Venkatesh	EM Normandie, France
Vilas Mahadeo Salokhe	Kaziranga University, India
Yukiya Kitayama	Osaka Metropolitan University, Japan
Chatchai Ponchio	Rajamangala University of Technology Thanyaburi, Thailand
Chatthai Kaewtong	Maharakham University, Thailand
Daniel Crespy	Vidyasirimedhi Institute of Science and Technology, Thailand
Pakorn Opaprakasit	Sirindhorn International Institute of Technology, Thailand
Warayuth Sajomsang	Thailand National Nanotechnology Center, Thailand
Jaturong Langkapin	Rajamangala University of Technology Thanyaburi, Thailand
Thammasak Rojviroon	Rajamangala University of Technology Thanyaburi, Thailand

## Managing Department

Jittima Singto	Rajamangala University of Technology Thanyaburi, Thailand
Monticha Ruttanapan	Rajamangala University of Technology Thanyaburi, Thailand
Mullika Kongpetsak	Rajamangala University of Technology Thanyaburi, Thailand
Nuthawan Thamawatchakorn	Rajamangala University of Technology Thanyaburi, Thailand
Phakhawan Lunkham	Rajamangala University of Technology Thanyaburi, Thailand
Saranya Suwinai	Rajamangala University of Technology Thanyaburi, Thailand
Thitirat Vijanpon	Rajamangala University of Technology Thanyaburi, Thailand
Wasin Buayang	Rajamangala University of Technology Thanyaburi, Thailand

## Contact

Institute of Research and Development, Rajamangala University of Technology Thanyaburi (RMUTT)  
 39 Moo 1, Klong 6, Khlong Luang Pathum Thani 12110 Thailand  
 Website: <https://ph01.tci-thaijo.org/index.php/rmutt-journal/index>  
 Phone: +66 2 5494492, +66 2 5494681  
 Fax: +66 2 5494680  
 Email: jarst@rmutt.ac.th

### Editorial Note

The Journal of Applied Research on Science and Technology (JARST) is an academic journal prepared by Institute of Research and Development, Rajamangala University of Technology Thanyaburi (RMUTT). The JARST aims to disseminate and share knowledge and ideas in the form of high-quality articles related General Engineering, General Materials Science, General Agricultural and Biological Sciences, General Computer Science, and General Mathematics to researchers, academics, faculty members and students both national and international.

This journal published eight research articles. Each of the research articles presented interesting concepts such as Water pollution influencing contamination of *Vibrio* bacteria in the coastal aquaculture area of Chanthaburi and Trat Provinces, Enhancing torrefaction process efficiency for biochar production from filter cake residue in the sugar industry, The development of real-time energy monitoring system using IoT base, A study on the behavior of pulling power and flammability of mold walls mixed with high-density polyethylene plastic waste, The fabrication of wood alternative material from cassava rhizome and cassava peel pulp, Phytochemical screening and toxicity assessment of compounds isolated from the leaves of *Mangifera indica* L. for the control of *Spodoptera litura* (Lepidoptera; Noctuidae), Synthesis of biocompatible hydroxyapatite from quail eggshell, oyster shell, and periwinkle snail shell and Characterization and bioactive protein hydrolysates from two-spotted cricket (*Gryllus bimaculatus* De Geer) and short-tail cricket (*Brachytrupes portentosus* Lichtenstein). Therefore, this journal is a channel disseminating the knowledge areas of physical sciences and life sciences which related persons could apply it for further benefits.

Lastly, the editorial team would like to considerably thank you for supporting and pushing forward this journal to occur and well accomplish. We are hopeful of your good cooperation and continuing support in the future.

Editorial Team

## Contents

Research Articles	Page
<b>Water pollution influencing contamination of <i>Vibrio</i> bacteria in the coastal aquaculture area of Chanthaburi and Trat Provinces</b> <i>Jakkapan Potipat, Chawanrat Somnuek and Sutthinee Mekprayoon</i>	255295
<b>Enhancing torrefaction process efficiency for biochar production from filter cake residue in the sugar industry</b> <i>Nopporn Rattanachoung</i>	256081
<b>The development of real-time energy monitoring system using IoT base</b> <i>Kamolwan Wongwut and Daungkamol Angamnuaysiri</i>	255911
<b>A study on the behavior of pulling power and flammability of mold walls mixed with high-density polyethylene plastic waste</b> <i>Thaweesak Rungsaktaweekul, Piyapong Kesawadkorn, Teerin Kongpun and Apised Suwansaard</i>	257122
<b>The fabrication of wood alternative material from cassava rhizome and cassava peel pulp</b> <i>Nichapha Minaboon, Prachoom Khamput, Kongpop Watcharasawe and Attapole Malai</i>	255879
<b>Phytochemical screening and toxicity assessment of compounds isolated from the leaves of <i>Mangifera indica</i> L. for the control of <i>Spodoptera litura</i> (Lepidoptera; Noctuidae)</b> <i>Poonnanan Phankaen, Vasakorn Bullangpoti, Wanchai Pluempanupat, Chatwadee Saiyaitong, Parinthorn Temyarasilp and Nutchaya Kumrungsee</i>	255634
<b>Synthesis of biocompatible hydroxyapatite from quail eggshell, oyster shell, and periwinkle snail shell</b> <i>Phurinart Suandork and Marchin Hongsuwong</i>	257693
<b>Characterization and bioactive protein hydrolysates from two-spotted cricket (<i>Gryllus bimaculatus</i> De Geer) and short-tail cricket (<i>Brachytrupes portentosus</i> Lichtenstein)</b> <i>Achara Chaiongkarn, Pattarawadee Kendkwasingh, Premsuda Saman and Supatjaree Ruengsomwong</i>	257207





## Water pollution influencing contamination of *Vibrio* bacteria in the coastal aquaculture area of Chanthaburi and Trat Provinces

Jakkapan Potipat<sup>1\*</sup>, Chawanrat Somnuek<sup>1</sup> and Sutthinee Mekprayoon<sup>2</sup>

<sup>1</sup>Department of Environmental Science, Faculty of Science and Technology, Rambhai Barni Rajabhat University, Chanthaburi 22000, THAILAND

<sup>2</sup>Department of Chemistry, Faculty of Science and Technology, Rambhai Barni Rajabhat University, Chanthaburi 22000, THAILAND

\*Corresponding author: jakkapan.p@rbru.ac.th

### ABSTRACT

Since 1982, the Eastern coastal area of Thailand has been developed from the Eastern Seaboard Project (ESP) to the Eastern Economic Corridor (EEC). The marine ecosystem of Chanthaburi and Trat Provinces was polluted by anthropogenic activities such as agriculture, transportation, tourism, fisheries, and urban communities. This study aims to investigate the marine environmental quality and the contamination of the *Vibrio* bacteria (*V. cholerae*, *V. parahaemolyticus* and *V. vulnificus*) in the coastal aquaculture area of Chanthaburi and Trat Provinces. Environmental sampling areas were designated at seven stations eastward from Tamai to Klongyai districts (about 150 km long stretch). The physicochemical parameters, including temperature, salinity, conductivity, pH, dissolved oxygen (DO),  $\text{NH}_3$ , and major anions e.g.  $\text{NO}_2^-$ ,  $\text{PO}_4^{3-}$  of seawater samples were measured at designated stations. Marine samples, including cockles (*Anadara granosa*), mussels (*Perna viridis*), oysters (*Saccostrea cucullata*) and white shrimp (*Litopenaeus vannamei*) were collected from aquaculture areas located in the estuarine ecosystem with simple random sampling. Our studies revealed that major inorganic substance concentrations followed this consequence order  $\text{PO}_4^{3-} > \text{NH}_3 > \text{NO}_2^-$ . The physicochemical properties indicated that seawater quality has been varied within the marine quality standard class III for aquaculture. The prevalence of *V. parahaemolyticus* and *V. vulnificus* showed in all bivalve samples were detected at 0.36 to 4.30 MPN/g and below the detection limit (0.3 MPN/g), respectively, whereas *V. cholerae* was not detected. This study also concluded that the periods of environmental sampling did not significantly influence the seawater quality and the level of *Vibrio* contamination. However, the difference of infection rates for *V. parahaemolyticus* and *V. vulnificus* depended on the marine species.

**Keywords:** Water pollution, *Vibrio* bacteria, Coastal aquaculture area

### INTRODUCTION

*Vibrio* is a Gram-negative bacteria, typically with lipopolysaccharide in the outer membrane, that belongs to the Proteobacteria phylum, Gammaproteobacteria class, the most diverse class of Gram-negative bacteria. The Vibrionaceae family comprises aquatic bacteria that mostly thrive in warm waters and tolerate various salinity levels, including freshwater, brackish, and marine waters [1].

Nowadays, the global aquaculture sector has grown continuously, and it is currently an important contributor to aquatic animal protein for human consumption [2]. The Thai government has to decide how they will control their national aquaculture production. Multiple bivalve species are economically important both natural and farmed populations, while white shrimp are produced mainly for export [3, 4]. Foodborne infections with the genus *Vibrio* are a serious

problem in Thailand and a major cause of gastroenteritis, particularly from traditional consumption of raw or undercooked seafood. Most of these patients are affected by *V. parahaemolyticus* and *V. cholerae* and to a lesser extent by *V. vulnificus* [5]. *Vibrios* belong to the microbiota of infectious bivalves, which can concentrate bacteria in their edible tissues and body fluids, including the hemolymph [6]. The aquacultural harvests from the Gulf of Thailand were more contaminated than *Vibrio*, while bivalves and white shrimps showed a high frequency of contamination [7-9].

The marine mollusks showed a great correlation to environmental variability investigation in the coastal areas and river mouth ecosystems [10]. Bivalve molluscs as bioindicator organisms have been used to assess pollution levels in the aquatic environment [11]. The bivalve species, including oysters (*Saccostrea*

*cucullata*), mussels (*Perna viridis*), and cockles (*Anadara granosa*) are abundance species and commercial seafood in the Eastern part of Thailand [7, 12]. Whereas the white shrimp (*Litopenaeus vannamei*) is used to focus on the potential *Vibrio* disease, due to *Vibrio* is recognized as a major cause of seafood-borne illness [13, 14].

Coastal water pollution is an increasingly significant environmental effect and public health illness [15]. Untreated wastewater and urban runoff are the principal sources of marine pollution [16]. These pollutants can inhibit the growth, reproduction, and survival of flora and fauna, leading to a decline in biodiversity. Physicochemical parameters are a limiting factor in the marine ecosystem and the most important environmental variable [17]. The various physicochemical measurements carried out in the coastal seawaters reveal the relationships between environmental quality and intensive anthropogenic activities [18, 19]. Hence, the physicochemical properties of seawater, including temperature, salinity, conductivity, pH, dissolved oxygen (DO), ammonia (NH<sub>3</sub>), and major anions (NO<sub>2</sub><sup>-</sup>, PO<sub>4</sub><sup>3-</sup>) are fundamental indicators for the assessment of changing the marine environment and reflecting land use development. Numerous indices regarding seawater quality and pollution status were conducted in Thailand, while the operation of these parameters was followed by a manual seawater sampling and analysis of PCD Thailand and international standards [20, 21].

The inner eastern coastal area of Thailand is the most important coastal aquaculture area and is a central source of recreation, as well as travel destinations, conservation areas, and comfort zones. In recent years, Thailand's Special Economic Zone (SEZ) was approved by the Thai government in 2015, covering the Chanthaburi and Trat coastal areas [22]. These marine zones have

seen significant spatial development in the past decade. As a result, they have transformed into important shrimp farming areas, tourism hotspots, and urban communities. Several reports indicated that anthropogenic activities as a source of water pollution are fed back into the marine ecosystem [23-26].

Here, we designed an analysis of water pollution influencing contamination and abundance of *Vibrio* bacteria by collecting marine samples along the Chanthaburi and Trat coastal areas from 2014 to 2022. Precisely, we determined the correlation between water quality parameters and the infection of *Vibrio* in commercial marine seafood with the statistical data.

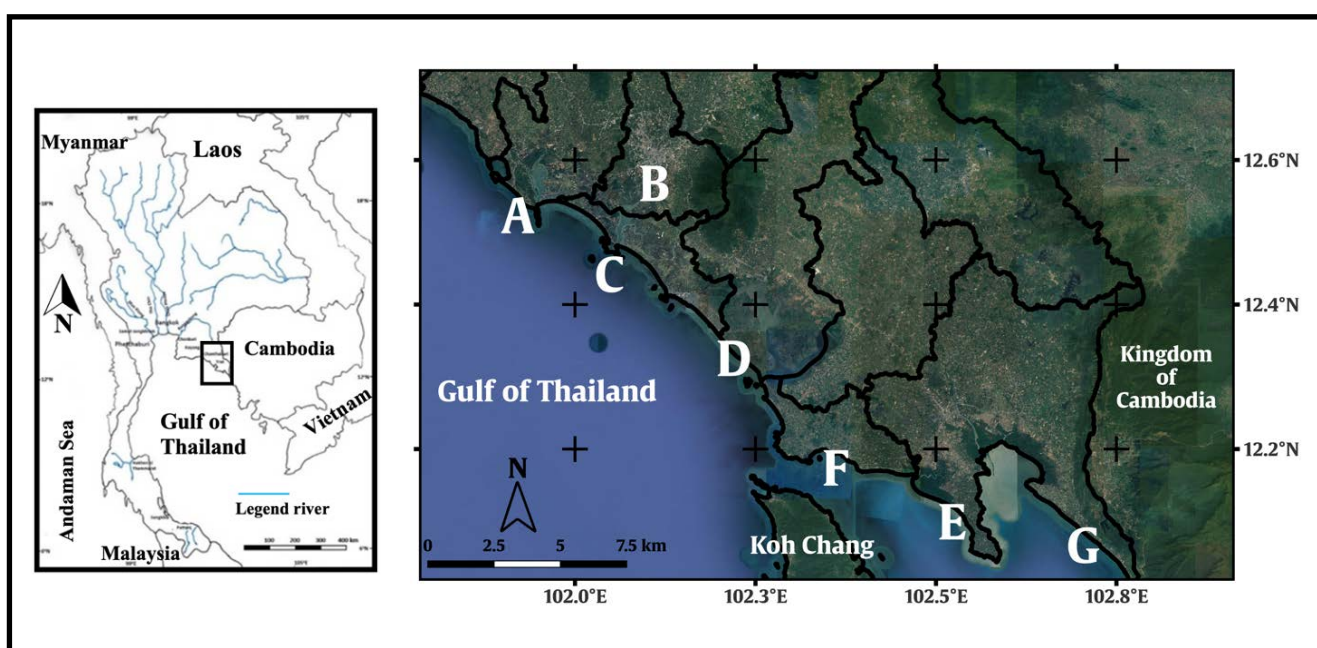
## MATERIALS AND METHODS

### Environmental sampling station

The eastern coastal areas cover two provinces, namely Chanthaburi and Trat Provinces, which were considered the locations for the marine sampling (Figure 1). The seawater samples were selected to represent environmental quality at designated stations. All study sites were recorded by Global Positioning System (GPS) (SD ± 5 m) as shown in Table 1.

Three bivalve species, including cockles (*Anadara granosa*), mussels (*Perna viridis*), and oysters (*Saccostrea cucullata*), as well as white shrimps (*Litopenaeus vannamei*) were collected from coastal aquaculture areas using simple random sampling. The surface seawater samples were collected at a depth of 100 cm using a vertical sampling procedure for physicochemical analysis.

All species samples were dredged and cleaned with seawater and stored in 4.0 °C iceboxes to the medical laboratory within 24 hours after collection.



**Figure 1** The map of sampling stations along the coastal area of Chanthaburi and Trat Provinces.

**Table 1** Use details of the sampling stations.

Stations	Latitude	Longitude	Description
Chanthaburi coastal areas			
Tha Mai (A)	12.621421°	102.004851°	Tourism landmarks and fisheries
Mueang Chanthaburi (B)	12.606965°	102.104579°	Several anthropogenic activities (Urban community, transportation and oxidation pond treatment)
Laem Sing (C)	12.481633°	102.073803°	Aquaculture in river mouth areas
Khlong (D)	12.454718°	102.221408°	Agriculture, homestay and fisheries
Trat coastal areas			
Mueang Trat (E)	12.243642°	102.515117°	Urban community, disposal site and fisheries
Laem Ngop (F)	12.225371°	102.369298°	Eco-tourism and fisheries
Khlong Yai (G)	12.200052°	102.296142°	Border trade and fisheries

**Table 2** The vulnerability assessment of the coastal marine ecosystem of Chanthaburi and Trat Provinces.

Variables	Chanthaburi	Trat
Habitat		
In-shore shallow Seawater	Low	Low to Middle
Sandy beaches	Low	Middle
Rocky beaches	Low	Middle
Inter-tidal mudflats	Middle	Middle to High
Estuaries	Very high	Very high
Seagrass beds	Loss	Loss
Mangroves	Very high	Very high
Selected species		
Cetaceans (3 species)	Very high	Very high
Dugong	Loss	Loss
Migratory shorebirds	Low	Low
Red-backed sea eagle	Low to Middle	Low to Middle

Source: Modification from [34].

### Physicochemical measurement

The physicochemical properties were recorded in situ in each station using the electrochemical analyzer (Consort C 932) and salinometer which were calibrated before use. Dissolved Oxygen (DO) is measured by azide modification of the Winkler's titration [20]. Direct nesslerization was performed for  $\text{NH}_3$  detection, whereas the colorimetric technique was used to determine nitrite ( $\text{NO}_2^-$ ) and phosphate ( $\text{PO}_4^{3-}$ ) [27, 28].

### Bacteriological analysis

Marine samples were prepared by rinsing and scrubbing them under running deionized water to remove debris from the shell, and they were opened using a sterile knife. The edible tissues in an equal amount of phosphate-buffered saline (PBS; pH 7.4) were homogenized in a sterile blender for 90 s [29].

The observation of *Vibrio* contamination was prepared following methods outlined in the Bacteriological Analytical Manual (BAM) for food sampling/preparation [30]. *V. cholerae*, *V. parahaemolyticus*, and *V. vulnificus*

were isolated from marine species by cultured in alkaline peptone water (APW) and thiosulfate citrate bile sucrose (TCBS), which was modified from BAM [31]. Each APW culture sample was sub-cultured on TCBS agar and incubated at 35°C for 18 - 24 hours to observe fermentative colonies. *Vibrio* densities in contaminated samples were calculated using the scored MPN table, and each dilution was measured in triplicate [32].

### Data analysis and quality control

A prevalence of *Vibrio* for each of the four species was tested for significant differences by analysis of Chi-square;  $p < 0.05$  was accepted for significant value. The influence of time on study periods and the physicochemical parameters of seawaters were analyzed using one-way analysis of variance (ANOVA) with  $p < 0.05$  was classified as statistically significant. Post hoc comparisons, LSD (Least Significant Difference) were applied to report differences among the sampling periods;  $p < 0.05$  was accepted as a significant value. The statistical inferences for hypothesis



tests were confirmed with a 5% significance level. All statistical analyses were performed using SPSS 18.0 software (Serial No.5083337). The quality control procedures were implemented through rigorous standardization by the PCD (Pollution Control Department), in accordance with seawater analysis guidelines.

## RESULTS AND DISCUSSION

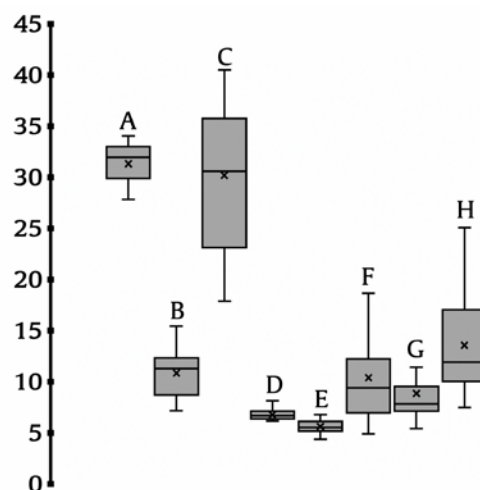
### *Land use of coastal area of Chanthaburi and Trat Provinces*

The eastern coastal region of Thailand has been an important part of the country's economic development. The real gross regional product (GRP) of the eastern region increased significantly from around 500,000 THB in 1994 to 1.7 million THB in 2018 [33]. The terrestrial area of Chanthaburi and Trat Provinces is the most agricultural landscape. It covers more than 60 percent of the total land use. The agricultural areas are a mixture of many kinds of tropical fruits known for their tasteful flavor. The coastal areas of Chanthaburi and Trat Provinces are affected by four major river basins, including the Wang-Ta-Nord, Chanthaburi, Welu, and Trat river basins, as shown in Table 2. Land use activities from the river basins during heavy rainfall may also significantly affect the marine coastal area and the dynamic of *Vibrio* spp. abundance [35].

### *Physicochemical parameters*

The physicochemical parameters are used to determine environmental quality along the coastal

areas of Chanthaburi and Trat Provinces. Table 3 reported the annual average of physicochemical properties from 2014, 2018 and 2022. The variation in seawater quality was elucidated with a Box plot diagram based on the minimum, maximum, first, median, and third quartile (Figure 2). The seawater quality monitoring in study sites could be categorized as a marine water quality standard class III. Additionally, the investigation of seawater samples revealed that the environmental quality of study areas was unpolluted.



**Figure 2** Box plot of physicochemical parameters of seawater samples (A: Temperature; B: Salinity; C: Conductivity; D: pH; E: Dissolved Oxygen (DO); F: Ammonia-Nitrogen; G: Nitrite-Nitrogen and H: Phosphate-Phosphorus).

**Table 3** Seawater quality along the coastal areas of Chanthaburi and Trat Provinces, Thailand of 2014, 2018 and 2022.

Physicochemical parameters	Year 2014	Year 2018	Year 2022	Criterion*
Temperature (°C)	29 - 33	30 - 34	28 - 34	a
Salinity (g/L)	31.14 ± 1.57	32.14 ± 1.35	30.86 ± 2.19	b
Conductivity (µS/cm)	8 - 13	9 - 14	9 - 16	-
pH	10.29 ± 1.70	11.71 ± 1.98	12.71 ± 2.50	-
Dissolved Oxygen (mg/L)	18.39 - 32.45	23.54 - 40.26	19.55 - 40.11	7.0 - 8.5
Ammonia-Nitrogen (µg/L)	24.83 ± 5.14	33.90 ± 5.44	32.10 ± 6.96	≥ 4
Nitrite-Nitrogen (µg/L)	7.04 - 8.11	7.09 - 8.95	7.36 - 8.09	≤ 70
Phosphate-Phosphorus (µg/L)	7.43 ± 0.37	7.66 ± 0.65	7.75 ± 0.34	55 <sup>c</sup>
	5.32 - 7.09	6.08 - 7.65	6.05 - 7.11	≤ 45
	6.24 ± 0.65	6.72 ± 0.55	6.55 ± 0.44	
	5.83 - 10.18	6.78 - 20.12	9.17 - 13.47	
	8.05 ± 1.68	11.34 ± 4.28	11.29 ± 1.48	
	7.15 - 18.21	6.32 - 12.13	8.09 - 11.37	
	10.67 ± 4.44	8.87 ± 1.89	9.39 ± 1.23	
	10.46 - 25.32	9.64 - 20.23	8.31 - 19.56	
	15.61 ± 5.17	13.09 ± 3.90	13.91 ± 4.39	

\*The announcement of the National Environment Board No.27 (B.E. 2549) regarding the specification of the standard of seawater

a - Naturally but changing by no more than 1 °C

b - Changing no more than 10 percent of the lowest value

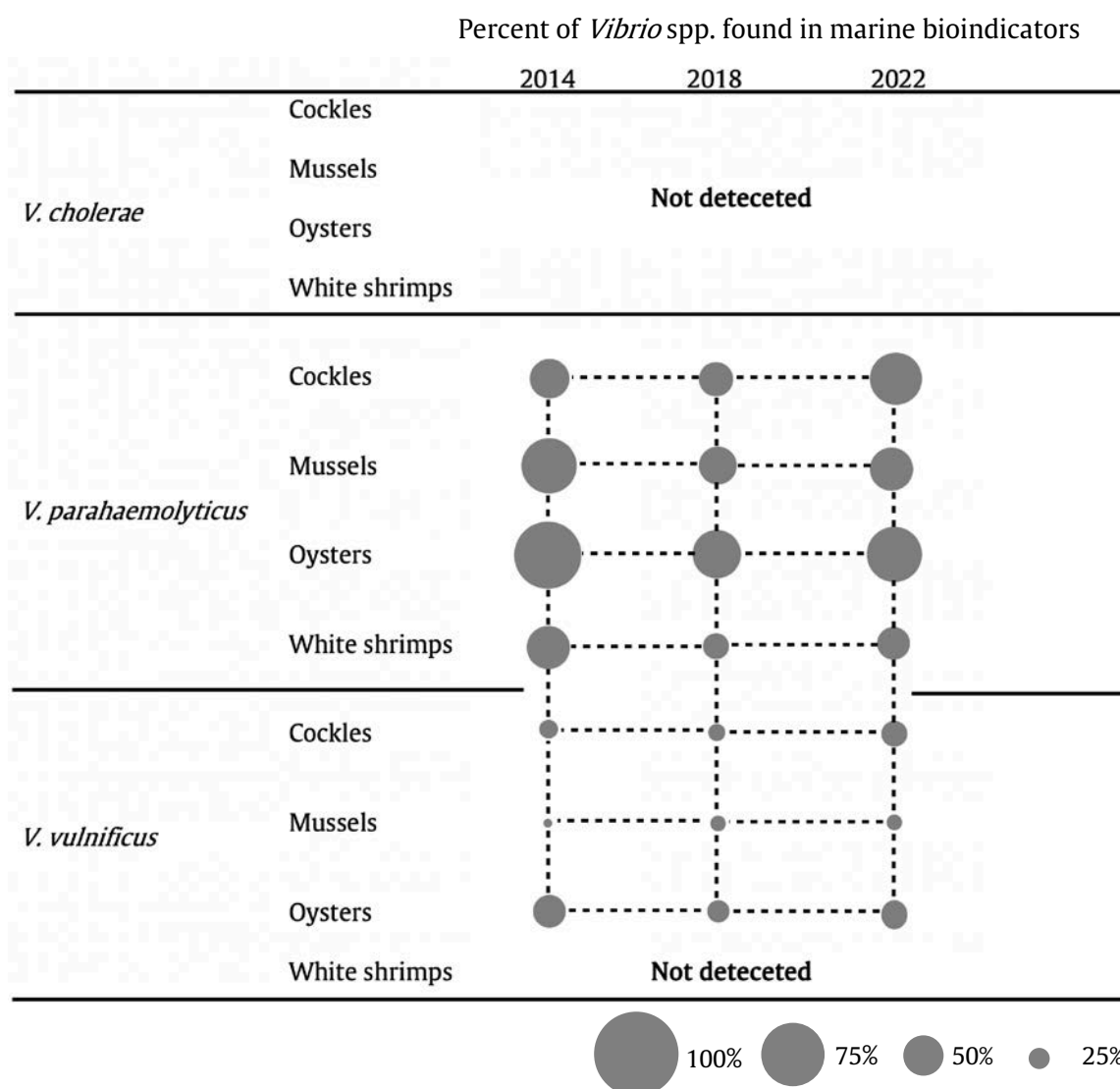
c - AMEQC (ASEAN Marine Environmental Quality Criteria)

The statistical comparison did not reveal a significant difference between the seawater quality and the sampling periods ( $p > 0.05$ ), except for conductivity. Multiple comparisons (LSD) revealed a significant difference in conductivity values across the study periods period ( $p < 0.05$ ). The conductivity variation in seawater is affected by the presence of inorganic dissolved solids such as chloride, nitrate, phosphate, and other anions. Mostly, essential nutrients enter the marine environment through urban rinsing, irrigation drainage, and agricultural runoff, while the high nutrient levels in seawater may lead to phytoplankton abundance and eutrophication [36]. In this study, the sampling sites revealed the degree of variation in terrestrial water pollution, which is frequently observed in estuarine coastal areas due to locally accumulated contaminants from domestic wastewater, fertilizer usage in orchards, and natural watershed erosion. A septic tank with an anaerobic filter was recommended for practice in solving water pollution problems in urban areas [37]. Conversely,

nanomaterials, biosolids, and electrobiological techniques have efficiently removed nutrients from agricultural wastewater [38, 39].

#### Contamination of *Vibrio* bacteria

The contamination of *Vibrio* spp. was investigated in the marine samples collected along the coastal aquaculture area of Chanthaburi and Trat Provinces, which produced seafood products for Thailand's domestic consumption and also exported. The results showed the infection of *V. parahaemolyticus* in all marine species, but *V. cholerae* was not detected, except in three bivalve species that were contaminated with *V. vulnificus* (Table 4; Figure 3). However, abundance of *Vibrio* species was below the seafood safety standard for fishery products, indicating no potential risks for human consumption. The main contaminated source of *Vibrio* bacteria is the discharge from untreated wastewater, urban sewage and infectious leachate, especially during extremely heavy rainfall, which are very threatening to the downstream ecosystem [19].



**Figure 3** Distribution of *Vibrio* contamination in marine samples along the coastal areas of Chanthaburi and Trat Provinces from 2014 to 2022.

**Table 4** Contamination of *Vibrio* spp. (MPN/g) in 25 g samples of marine species along the coastal aquaculture areas of Chanthaburi and Trat Provinces (7 stations) from 2014 to 2022 ( $n = 63$ ).

Species	<i>V. cholerae</i>		<i>V. parahaemolyticus</i>		<i>V. vulnificus</i>	
	Prevalence (percent)	MPN/g	Prevalence (percent)	MPN/g	Prevalence (percent)	MPN/g
Cockles	-	n.d.	55.56	0.36 - 1.25	25.40	< 0.3
Mussels	-	n.d.	63.49	0.74 - 2.80	15.87	< 0.3
Oysters	-	n.d.	73.02	0.36 - 4.30	36.51	< 0.3
White shrimps	-	n.d.	47.62	< 0.3 - 3.0	-	n.d.
Safety levels*		n.d.		< 30/g (MPN)		< 30/g (MPN)

n.d. - not detected

\*FDA and EPA safety levels of fishery products in regulation and guidance.

**Table 5** Growth characteristics of *V. parahaemolyticus* in the marine environment

Variables	Optimum	Range
Temperature (°C)	37	5 - 43
pH	7.8 - 8.6	4.8 - 11
NaCl (%)	1.5 - 3.0	0.5 - 10
Water Activity (WA)	0.981	0.940 - 0.996
Atmosphere (O <sub>2</sub> consumption)	Aerobic	Aerobic-Anaerobic

Source: Modification from International Commission for Microbiological Specifications for Foods

The study found a high abundance of *V. parahaemolyticus* in all marine samples. The chi-square test showed a significant difference in the prevalence of *V. parahaemolyticus* in the marine species ( $p < 0.05$ ), and the sampling periods were not a significant difference ( $p > 0.05$ ). *V. parahaemolyticus* is commonly found in coastal areas and estuarine ecosystems, and it has been isolated in various marine animals [40]. *V. parahaemolyticus* is a mildly halophilic, mesophilic microorganism, and its general growth characteristics are shown in Table 5. Hence, the physicochemical variation can play an important role in the significant contamination of *V. parahaemolyticus* in marine habitats [41-44].

The contamination of *V. vulnificus* was detected in all samples of bivalves at below detection limit (0.3 MPN/g) but was not found in the white shrimp samples during the study periods (Table 4). The statistical analysis revealed a notable disparity in the infection levels of *V. vulnificus* in bivalve samples, with a significance level of  $p < 0.05$ . A microbiological survey concerned the levels of pathogenic *V. vulnificus* in marine bivalves across various global locations. The reporting indicated infection rates of 17.2% in oysters and 8.0% in mussels [45, 46]. The prevalence rate of *V. vulnificus* contamination is commonly observed in shellfish maturity within coastal areas, but in this study, *V. vulnificus* was not detected in the white shrimp samples. The confirmation of *V. vulnificus* appeared to have the same disease symptoms as naturally infected shrimp. However, the circulating hemocytes of *Litopenaeus vannamei* play a crucial role in self-purification and activate several *Vibrio* pathogens [47]. Furthermore, physicochemical parameters, such as salinity and

temperature, influence the occurrence of *V. vulnificus*, while the natural depuration pond was prepared to decrease *Vibrio* contamination [48, 49].

## CONCLUSIONS

The present study concludes that physicochemical parameters were within the seawater permissible standard at all sampling stations in the coastal aquaculture area of Chanthaburi and Trat Provinces. The major land use concerns that have polluted the marine coastal area from anthropogenic activities such as recreational renovation, aquaculture, and infrastructure improvement. *V. parahaemolyticus* is an abundant species in the aquaculture area and is commonly isolated from edible bivalves and white shrimp tissues. However, *V. parahaemolyticus* densities also included the permissible limit. The depuration processes were recommended to decontaminate the cultivated fishery products.

## ACKNOWLEDGEMENT

This research was financially supported by the national budget of the National Research Council of Thailand (NRCT) from 2012 to 2018. The authors also would like to greatly thank the Faculty of Science and Technology, Rambhai Barni Rajabhat University for the experimental facilities provided during the study period.

### Ethics approvals

Ethical approval was exempted from this study as it operated within the local fishing communities' methods.

## REFERENCES

- Wright AC, Hill RT, Johnson JA, Roghman MC, Colwell RR, Morris JG. Distribution of *Vibrio vulnificus* in the Chesapeake Bay. Appl Environ Microbiol. 1996;62:717-24.
- FAO (Food and Agriculture Organization of the United Nations). The state of world fisheries and aquaculture 2016. Rome: Food and Agriculture Organization of the United Nations; 2016.
- Ferreira JG, Falconer L, Kittiwonich J, Ross L, Saurel C, Wellman K, et al. Analysis of production and environmental effects of Nile tilapia and white shrimp culture in Thailand. Aquaculture. 2015; 447:23-36.
- Oliveira GFM, Couto MCM, Lima MF, Bomfim TCB. Mussels (*Perna perna*) as bioindicator of environmental contamination by Cryptosporidium species with zoonotic potential. Int J Parasitol Parasites Wildl. 2016;5:28-33.
- FEHD (Food and Environmental Hygiene Department). *Vibrio* species in seafood. Hong Kong: The Government of the Hong Kong Special Administrative Region; 2005.
- Destoumieux-Garzón D, Canesi L, Oyanedel D, Travers MA, Charrière GM, Pruzzo C, et al. *Vibrio*-bivalve interactions in health and disease. Appl Microbiol Int. 2020;22(10):4323-41.
- Nakaguchi Y. Contamination by *Vibrio parahaemolyticus* and its virulent strains in seafood marketed in Thailand, Vietnam, Malaysia, and Indonesia. Trop Med Health. 2013;41(3):95-102.
- Yokyingyong P. Risk assessment of *Vibrio parahaemolyticus* in white shrimp (*Litopenaeus vannamei*) from retail market [thesis]. Faculty of Veterinary Science: Chulalongkorn University; 2019.
- Jeamsripong S, Chuanchuen R, Atwill ER. Assessment of bacterial accumulation and environmental factors in sentinel oysters and estuarine water quality from the Phang Nga estuary area in Thailand. Int J Env Res Pub He. 2018;15:1-17.
- Nuangjui M, Pimpang B, Chulalaksananukul W, Glinwong C. Biomonitoring by using rapid-read pathogenic bacteria indicator in sediments and bivalve mollusks: southern Gulf of Thailand, a mangrove area case study. Trends Sci. 2023;20(4):1-14.
- Boening DW. An evaluation of bivalves as biomonitors of heavy metals pollution in marine waters. Environ Monit Assess. 1999;55(3):459-70.
- Cheevaporn V, Menasveta P. Water pollution and habitat degradation in the Gulf of Thailand. Mar Pollut Bull. 2003;47:43-51.
- Gopal S, Otta SK, Kumar S, Karunasagar I, Nishibuchi M, Karunasagar I. The occurrence of *Vibrio* species in tropical shrimp culture environments; implications for food safety. Int J Food Microbiol. 2005;102(2): 151-59.
- Somboon M, Purivirojkul W, Limsuwan C, Chuchird N. Effect of *Vibrio* spp. In white feces infected shrimp in Chanthaburi, Thailand. Fish Res Bull Kasetsart Univ. 2012;36(1):7-15.
- Pendergraft MA, Belda-Ferre P, Petras D, Morris CK, Mitts Ba, Aron AT, et al. Bacterial and chemical evidence of coastal water pollution from the Tijuana River in sea spray aerosol. Environ Sci Technol. 2023;57:4071-81.
- Fedderson F, Boehm AB, Giddings SN, Wu X, Liden D. Modeling untreated wastewater evolution and swimmer illness for four wastewater infrastructure scenarios in the San Diego-Tijuana (US/MX) border region. GeoHealth. 2021;5:1-20.
- Elahi N, Ahmed Q, Bat L, Yousuf F. Physicochemical parameters and seasonal variation of coastal water from Balochistan coast, Pakistan. J Coast Life Med. 2015;3(3):199-203.
- Narendra Babu K, Omana PK, Mohan M. Water and sediment quality of Ashtamudi estuary, a Ramsar site, southwest coast of India-a statistical appraisal. Environ Monit Assess. 2010;165:307-19.
- Bonisławska M, Nędzarek A, Rybczyk A, Tański A. Influence of anthropogenic pollution on the physicochemical conditions of the waters of the lower section of the Sępólna River. Water. 2024; 16(1):w16010035.
- APHA (American Public Health Association). Standard methods for the examination of water and wastewater. 20th ed. Washington DC: APHA, AWAA & WEF; 1998.
- PCD (Pollution Control Department). Manual seawater sampling and analysis. Bangkok: Teachers' Council Printing House; 2001.
- Kanjananil B. The role of the state in the development of Special Economic Zone: the case study of Trat. Rajapark J. 2018;12(26):78-89.
- Sarakhan N. The environment education model for sustainable mangrove forest management in the Eastern part of Thailand. App Environ Res. 2014; 41(4):29-40.
- PCD (Pollution Control Department). Thailand state of pollution report 2015. Bangkok: Ministry of Natural Resources and Environment; 2015.
- PCD (Pollution Control Department). Thailand state of pollution report 2016. Bangkok: Ministry of Natural Resources and Environment; 2016.



26. Kunsook C, Dumrongrojwatthana P. Species diversity and abundance of marine crabs (Portunidae: Decapoda) from a collapsible crab trap fishery at Kung Krabaen Bay, Chanthaburi Province, Thailand. *Trop Life Sci Res.* 2017;28(1):45-67.
27. Traichaiyaporn S. Water quality analysis. Chiang Mai: Faculty of Science, Chiang Mai University; 2000.
28. Daungsavat M, Somsiri J. Water properties and analysis for fisheries research. Bangkok: Department of Fisheries, Ministry of Agriculture and Cooperatives; n.d.
29. Brumfield KD, Chen AJ, Gangwar M, Usmani M, Hasan NA, Jutla AS, et al. Environmental factors influencing occurrence of *Vibrio parahaemolyticus* and *Vibrio vulnificus*. *Appl Environ Microbiol.* 2023;89(6):1-19.
30. Andrews WH, Hammack TS. Chapter 1: Food sampling and preparation of sample homogenate. In: Jinneman K, Chair Member. *Bacteriological Analytical Manual (BAM)*. FDA; 2019. p. 1-10.
31. Kaysner CA, DePaola A, Jones J. Chapter 9: *Vibrio*. In: Jinneman K, Chair Member, editor. *Bacteriological Analytical Manual (BAM)*. FDA; 2004. p. 1-41.
32. Miwa N, Nishio T, Arita Y, Kawamori F, Masuda T, Akiyama M. Evaluation of MPN method combined with PCR procedure for detection and enumeration of *Vibrio parahaemolyticus* in seafood. *Food Hyg Safe Sci.* 2003;44(6):289-93.
33. Tontisirin N, Anantsuksomsri S. Economic development policies and land use changes in Thailand: from the Eastern Seaboard to the Eastern Economic Corridor. *Sustainability.* 2021;13:6153.
34. Bezuijen MR, Morgan C, Mather, RJ. A rapid vulnerability assessment of coastal habitats and selected species to climate risks in Chanthaburi and Trat (Thailand), Koh Kong and Kampot (Cambodia) and Kien Giang, Ben Tre, Soc Trang and Can Gio (Vietnam). Gland, Switzerland: IUCN (International Union for Conservation of Nature); 2011.
35. Cantet F, Hervio-Heath D, Caro A, Le Mennec C, Monteil C, Quéméré C, et al. Quantification of *Vibrio parahaemolyticus*, *Vibrio vulnificus* and *Vibrio cholerae* in French Mediterranean coastal lagoons. *Res Microbiol.* 2013;164(8):867-74.
36. Akinde SB, Obire O. *In-situ* physico-chemical properties of the Deep Atlantic Ocean water column and their implications on heterotrophic bacterial distribution in the Gulf of Guinea. *Adv Appl Sci Res.* 2011;2(6):470-82.
37. Thongkao K. The assessment of domestic wastewater quality for the guideline of water treatment and remediation in urban area. *SNRU J Sci Technol.* 2016;8(1):155-62.
38. Janczukowicz W, Rodziejewicz J. Water and wastewater management in agriculture. *Appl Sci.* 2024;14:2488.
39. Rusanescu CO, Rusanescu M, Constantin GA. Wastewater management in agriculture. *Water.* 2022;14:3351.
40. Yokyingyong P. Risk assessment of *Vibrio parahaemolyticus* in white shrimp (*Litopenaeus vannamei*) from retail market [thesis]. Bangkok: Chulalongkorn University; 2019.
41. Blackwell KD, Oliver JD. Ecology of *Vibrio vulnificus*, *Vibrio cholerae* and *Vibrio parahaemolyticus* in North Carolina estuaries. *J Microbiol.* 2008;46(2):146-53.
42. Hsieh JL, Fries JS, Noble RT. Dynamics and predictive modeling of *Vibrio* spp. in the Neuse river estuary, North Carolina, USA. *Environ Microbiol.* 2008;10(1):57-64.
43. Chonsin K, Hemmanee B, Hongkul R, Changkaew K, Noisumdaeng P, Suthienkul O. Detection of bacteriophages specific to *Vibrio parahaemolyticus* in marine water samples, Surat Thani, Thailand. *Thai J Public Health.* 2021;5(1):7-15.
44. Padovan A, Siboni N, Kaestli M, King WL, Seymour JR, Gibb K. Occurrence and dynamics of potentially pathogenic vibrios in the wet-dry tropics of northern Australia. *Mar Environ Res.* 2021;169:105405.
45. Beneduce L, Vernile A, Spano G, Massa S, Lamacchia F, Oliver JD. Occurrence of *Vibrio vulnificus* in mussel farms from the Varano lagoon environment. *Lett Appl Microbiol.* 2010;51(4):443-9.
46. Kirs M, DePaola A, Fyfe R, Jones JL, Krantz J, Van Laanen A, et al. A survey of oysters (*Crassostrea gigas*) in New Zealand for *Vibrio parahaemolyticus* and *Vibrio vulnificus*. *Int J Food Microbiol.* 2011;147(2):149-53.
47. Liu CH, Yeh ST, Cheng SY, Chen JC. The immune response of the white shrimp *Litopenaeus vannamei* and its susceptibility to *Vibrio* infection in relation with the moult cycle. *Fish Shellfish Immun.* 2004;16(2):151-61.
48. Kelly MT. Effect of temperature and salinity on *Vibrio (Beneckea) vulnificus* occurrence in a Gulf Coast Environment. *Appl Environ Microbiol.* 1982;44(4):820-4.
49. Chen YP. Reduction and management of *Vibrio vulnificus* in gulf coast oyster (*Crassostrea Virginica*) [dissertation]. LA: Louisiana State University; 1996.



## Enhancing torrefaction process efficiency for biochar production from filter cake residue in the sugar industry

Nopporn Rattanachoung\*

Department of Physical and Material Sciences, Faculty of Liberal Arts and Science, Kasetsart University, Nakhon Pathom 73140, THAILAND

\*Corresponding author: faasnor@ku.ac.th

### ABSTRACT

The torrefaction process is a promising technique for enhancing the quality of solid biomass fuels. This study investigates the effects of torrefaction on biochar produced from filter cake residue, a byproduct of the sugar industry. The primary objectives were to evaluate the impact of process parameters on biochar properties and identify optimal conditions for maximizing the higher heating value (HHV). Filter cake residue was subjected to torrefaction at temperatures ranging from 220–340°C under an inert atmosphere. The influence of particle size (20, 60, and 100 mesh), nitrogen flow rate (20–30 ml/min), temperature (220–340°C), and residence time (30–90 min) on biochar properties was examined using response surface methodology. Proximate analysis revealed that torrefaction significantly reduced moisture, volatile matter, and ash content while increasing fixed carbon content. The maximum HHV of 21.9571 MJ/kg was achieved at a particle size of 20 mesh, nitrogen flow rate of 25 ml/min, temperature of 340°C, and residence time of 60 min. The experimental results agreed with predicted values from the developed models, with an average error of 3.64%. Optimal torrefaction conditions were determined to be a particle size of 21.77 mesh, nitrogen flow rate of 22.50 ml/min, temperature of 311.13°C, and residence time of 42.58 min, yielding a maximum HHV of 18.4853 MJ/kg. These findings demonstrate the potential of torrefaction for upgrading filter cake residue into a high-quality solid biofuel, providing a sustainable solution for waste utilization in the sugar industry.

**Keywords:** Biomass, Torrefaction process, Filter cake residue

### INTRODUCTION

Biomass is considered a highly significant energy source because it is a natural energy reservoir that can be utilized for energy production without contributing to the greenhouse effect. This is attributed to the fact that carbon dioxide generated during combustion is utilized for photosynthesis in plant growth, leading to cyclic carbon circulation without substantial atmospheric release. Moreover, biomass fuel is cost-effective as it can be produced domestically sustainably, reducing the need to import and generate local income [1]. Recognizing these advantages, the government acknowledges the importance and benefits of biomass energy. Thailand has formulated policies to promote energy security to boost research and development in alternative energy derived from biomass, aligning with Thailand's Thirteenth economic and societal development plan (2023–2027) [2].

Biochar, a carbon-rich material produced from biomass or organic substances from natural decay or agricultural waste, is generated through a controlled pyrolysis process at low oxygen levels. This process is called pyrolysis under anaerobic or limited oxygen

conditions. In this way, biochar with various properties suitable for use as fuel is obtained. An ideal biochar possesses a high heating value (HHV) and meets other standard criteria. However, the production of biochar from biomass is not yet fully efficient. Factors such as temperature and time during torrefaction result in heat loss and insufficient product yield. Consequently, extensive expenses are incurred [3]. Hence, this research addresses this issue by determining the most suitable conditions for producing biochar from filter cake residue, a type of biomass.

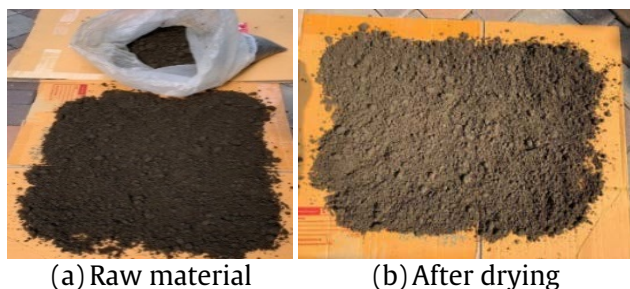
This study investigates the effects of the torrefaction process on biofuel produced from filter cake residue and identifies the most suitable conditions. The study examines the influence of variables affecting the torrefaction process, including biomass particle size, nitrogen gas flow rate, temperature, and torrefaction time [4–7].

### MATERIALS AND METHODS

#### Material preparation

The biomass material used in this research is filter cake residue obtained from a sugar factory.

Figure 1(a) shows the raw material of filter cake residue used in the research. The material was dried under sunlight for 2 days, as shown in Figure 1(b). It was ground to fine particles and sieved through three sizes of (a) 20, (b) 60, and (c) 100 mesh, as shown in Figure 2. All three-size powders were put into ziplock bags for further analysis under the torrefaction process. However, the proximate composition of the sample, that is, volatile matter, moisture, fixed carbon, and ash, was determined. The samples used were raw filter cake residue and filter cake residue after the torrefaction process.



**Figure 1** Filter cake residue: (a) raw material and (b) after drying.



**Figure 2** Filter cake residue with different particle sizes of (a) 20, (b) 60, and (c) 100 mesh.

#### *Experimental design using design expert program*

In the torrefaction process, the independent variables for the experiments include biomass particle size (mesh), nitrogen gas flow rate (ml/min), temperature (°C), and time (min). The dependent variable is biomass's higher heating value (HHV) in MJ/kg.

In this work, the Box-Behnken design (BBD) method using the Design Expert V.13.0 program was employed for statistical analysis and prediction of the experimental outcomes. The study focused on the influence of 3 levels (minimum, mean, maximum) of 4 variables ( $X_1$ ,  $X_2$ ,  $X_3$ ,  $X_4$ ) as presented in Table 1, under the conditions specified in Table 2.

**Table 1** Experimental design by BBD method.

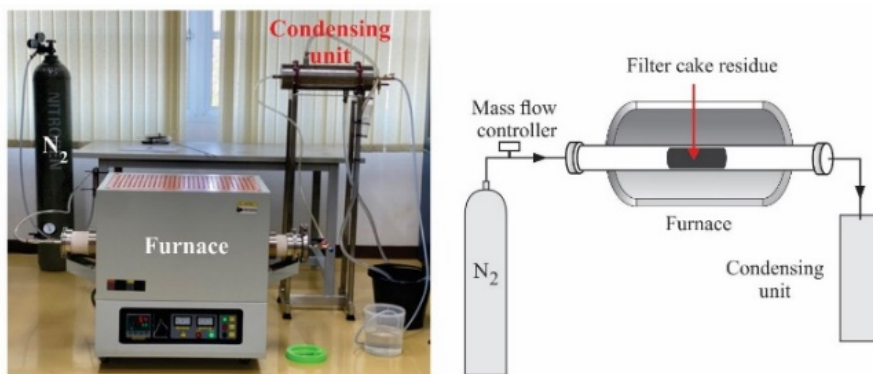
Parameter	Symbol	Unit	Min.	Mean	Max.
Particle size	$X_1$	mesh	20	60	100
N <sub>2</sub> flow rate	$X_2$	ml/min	20	25	30
Temperature	$X_3$	°C	220	280	340
Time	$X_4$	min	30	60	90
High heating value	$Y_1$	MJ/kg	-	-	-

**Table 2** Conditions of torrefaction process.

Run No.	Particle size (mesh)	Flow N <sub>2</sub> (ml/min)	Temperature (°C)	Time (min)	HHV (MJ/kg)
1	60	20	340	60	18.3352
2	60	20	280	30	16.6152
3	20	25	280	30	19.6237
4	60	20	280	90	16.4797
5	100	25	280	90	16.7569
6	60	30	340	60	20.2209
7	100	25	280	30	16.8694
8	20	25	220	60	18.7078
9	60	30	280	90	18.1508
10	100	25	220	60	16.5795
11	100	25	340	60	18.5945
12	60	25	220	30	16.7533
13	20	30	280	60	20.5835
14	60	25	340	90	19.4425
15	60	25	220	90	16.6551
16	60	25	280	60	16.5356
17	60	25	280	60	17.5356
18	60	30	280	30	18.2773
19	100	30	280	60	17.2832
20	100	20	280	60	16.1719
21	20	25	280	90	19.4872
22	60	25	280	60	17.8356



Run No.	Particle size (mesh)	Flow N <sub>2</sub> (ml/min)	Temperature (°C)	Time (min)	HHV (MJ/kg)
23	60	25	280	60	17.3412
24	60	25	280	60	17.2914
25	60	20	220	60	15.9001
26	20	20	280	60	17.8521
27	20	25	340	60	21.9571
28	60	30	220	60	17.3487
29	60	25	340	30	19.3419



**Figure 3** Shows (a) a photograph and (b) a schematic diagram of the experimental setup of the torrefaction process.

In this work, the Box-Behnken design (BBD) method using the Design Expert V.13.0 program was employed for statistical analysis and prediction of the experimental outcomes. The study focused on the influence of 3 levels (minimum, mean, maximum) of 4 variables ( $X_1$ ,  $X_2$ ,  $X_3$ ,  $X_4$ ) as presented in Table 1, under the conditions specified in Table 2.

It is seen from Table 2 that the maximum HHV of 21.9571 MJ/kg was obtained from run no. 27, where particle size, N<sub>2</sub> flow rate, temperature, and time were 20 mesh, 25 ml/min, 280°C and 30 min, respectively. The HHVs obtained from the design model were then compared with those of the experimental torrefaction process, as described in the next Section.

#### *Torrefaction process*

Figure 3 shows the schematic diagram of the torrefaction experiment. The reactor for loading filter cake residue was made of cylindrical stainless steel with a length of 160 mm and a diameter of 54.6 mm. It was placed inside a horizontal tube furnace with a length of 120 cm (Vacuum 1,400 degree Tube Furnace, Model PN:SK2-7-14PD3). The sample temperature was measured using 4 thermocouples introduced through the top flange of the reactor. A temperature controller of the furnace controlled the temperature.

About 20 g of filter cake residue sample was uniformly distributed inside the sample basket and placed in the uniform heated zone of the reactor prior to the experiment. The reactor lid was closed, and a mass flow controller controlled nitrogen gas flow into the reactor. The nitrogen flow rate was maintained for 30 min to remove the air from the reactor chamber and ensure inert condition. The sample was heated

from the room to the desired temperature with a rate of 10°C min<sup>-1</sup> under a nitrogen atmosphere. The gas leaving the torrefaction reactor was cooled by a condensing unit using two lines of the condenser ice bath, where most of the tar and water were collected. To compare the HHVs obtained from the design model, as shown in Table 2, with those obtained from the experimental torrefaction process, we conducted the experiments at 4 conditions, including run no. 27 (maximum HHV of 21.9571 MJ/kg), run no. 25 (minimum HHV of 15.9001 MJ/kg), run no. 13 and run no. 19.

#### *Measurement of Higher Heating Value (HHV)*

The heating value indicates the amount of energy released during fuel combustion (biomass) per unit weight in the form of heat. The heating value of each fuel type varies depending on the characteristics and components of the biomass. Higher heating value (HHV) refers to the heat energy released from the complete combustion of fuel (Gross calorific value), including the latent heat of vaporization of water.

Generally, the higher heating value from biomass is analyzed using a Bomb calorimeter, which measures the heat energy from burning samples in the calorimeter. It operates on the principle that the energy accumulated in the chemical bonds of the substance is released when the substance is burned, known as the heat of combustion. In the Bomb calorimeter, biomass combustion causes a temperature change. Then, the higher heating value is determined as the heat released during combustion from initial to final temperatures as described by the equation:

$$HHV = \frac{W\Delta T}{m}$$



where  $\Delta T$  is the increased temperature ( $^{\circ}\text{C}$ ),  $W$  is the energy equivalent (EE) of Bomb calorimeter ( $\text{cal}/^{\circ}\text{C}$ ) and  $m$  is the weight of the sample (g). In this work, the Bomb calorimeter manufactured by IKA was designed for scientists. The Model Calorimeter C1 was used to measure the high heating value of the combustion of biomass filter cake. It consisted of the calorimeter, combustion chamber, and chiller.

## RESULTS AND DISCUSSION

Table 3 shows the proximate analysis of raw filter cake residue and torrefied filter cake residue after the torrefaction process of run no. 27 (particle size,  $\text{N}_2$  flow rate, temperature, and time were 20 mesh, 25 ml/min,  $280^{\circ}\text{C}$  and 30 min, respectively). Raw filter cake residue has a very high amount of volatile matter and high moisture content, resulting in its low heating value. In addition, the raw filter cake has low carbon that carbon, which also results in its low heating value. For

torrefied filter cake residue, the volatile matter decreased from 72.76 to 51.70%, and the ash decreased from 2.15 to 1.81%, while the fixed carbon increased from 15.40 to 38.74%, increasing the heating value.

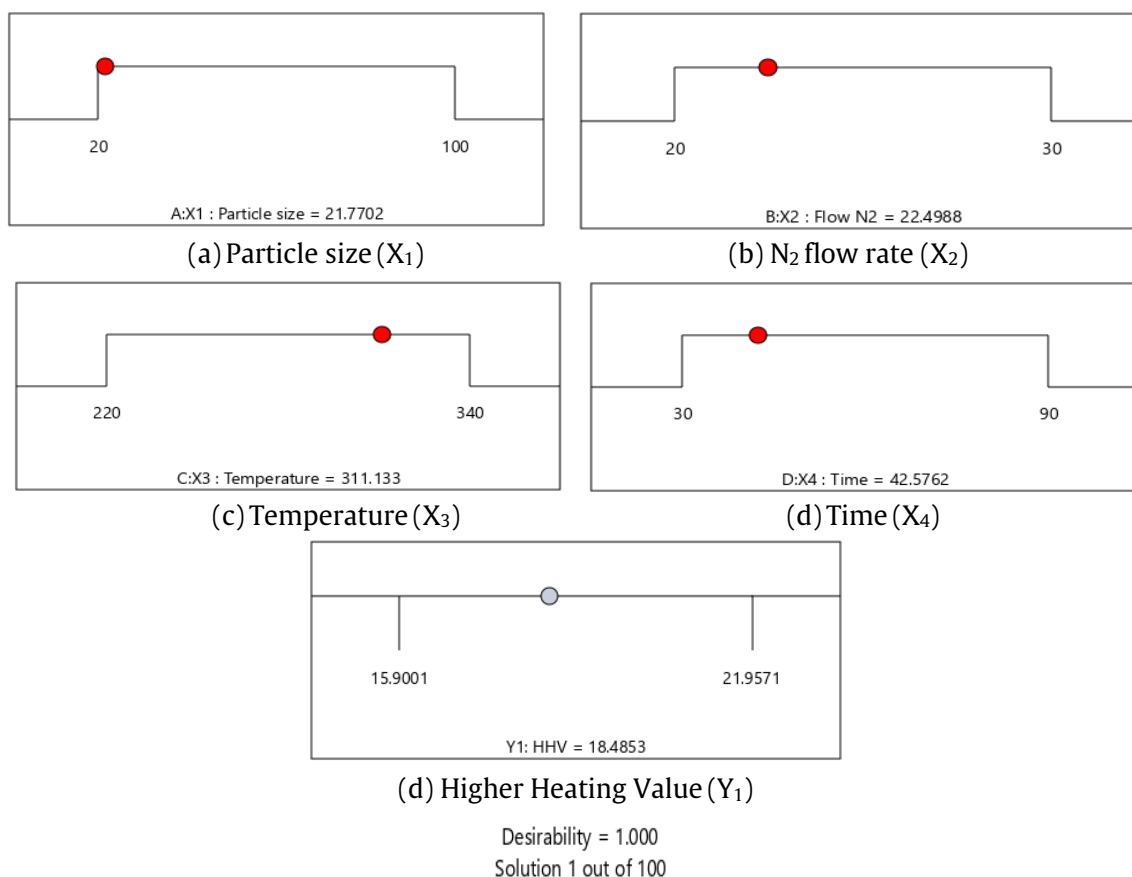
**Table 3** Proximate analysis (wt%, d.b.).

Proximate composition	Before torrefaction	After torrefaction
Volatile matter	72.76	51.70
Moisture	9.69	7.75
Fixed carbon	15.40	38.74
Ash	2.15	1.81

The experimental torrefaction process was conducted for 4 biomass samples of run nos. 27, 13, 19, and 25 as described in Section Measurement of Higher Heating Value (HHV). The results of those samples on HHVs are given in Table 4. The average difference value of HHV between the simulation model and experiment was 3.64%.

**Table 4** Torrefaction process experiment at 4 conditions.

Run No.	Particle size (mesh)	$\text{N}_2$ flow rate (ml/min)	Temperature ( $^{\circ}\text{C}$ )	Time (min)	HHV (MJ/kg) Simulation	HHV (MJ/kg) Experiment	Error
27	20	25	340	60	21.9571	20.7453	5.52
13	20	30	280	60	20.5835	19.9954	2.86
19	100	30	280	60	17.2832	16.9853	1.72
25	60	20	220	60	15.9001	15.1872	4.48



**Figure 4** Optimal conditions for the torrefaction process of filter cake residue.

To find the optimum point for the torrefaction process of filter cake residue in this work, by using the Design Expert v13.0 program, the most suitable conditions for the process were obtained, as shown in Figure 4. That is: a) particle size ( $X_1$ ) was 21.7702 mesh, b)  $N_2$  flow rate ( $X_2$ ) was 22.4988 mL/min, c) temperature ( $X_3$ ) was 311.1330°C, and d) time ( $X_4$ ) was 42.5762 min and gave the maximum HHV of 18.4853 MJ/kg.

## CONCLUSIONS

This study investigated the torrefaction process to enhance the fuel properties of filter cake residue, a waste biomass material from the sugar industry. The raw filter cake was sun-dried, ground, and sieved to obtain three particle sizes: 20, 60, and 100 mesh. Design Expert v.13.0 software was employed to design the experiments and analyze the results. The influence of four independent variables, namely particle size ( $X_1$ ),  $N_2$  flow rate ( $X_2$ ), temperature ( $X_3$ ), and residence time ( $X_4$ ), on the higher heating value (HHV) of the torrefied biomass was examined. Proximate analysis revealed that torrefaction significantly altered the composition of the filter cake residue. Volatile matter, moisture, and ash contents decreased while fixed carbon content increased, resulting in an overall improvement in the heating value of the biomass. The experimental HHV values agreed with the predicted values, with an average deviation of 3.64%.

Response surface methodology was employed to identify the optimal torrefaction conditions for maximizing the HHV of the torrefied filter cake. The optimal parameters were determined to be a particle size of 21.77 mesh,  $N_2$  flow rate of 22.50 mL/min, temperature of 311.13°C, and residence time of 42.58 min. Under these conditions, a maximum HHV of 18.4853 MJ/kg was predicted. The findings of this study demonstrate the potential of torrefaction as an effective technique for upgrading the fuel properties of filter cake residue. A high-quality solid biofuel can be produced from this abundant waste biomass by optimizing the process parameters. Using filter cake residue for biofuel production provides a sustainable solution for waste management in the sugar industry and contributes to developing renewable energy sources.

Further research is recommended to investigate the feasibility of scaling up the torrefaction process and to assess the techno-economic and environmental aspects of utilizing torrefied filter cake as a biofuel. Additionally, the properties and performance of the torrefied biomass in various combustion systems should be evaluated to ensure its suitability as a fuel substitute.

## REFERENCES

1. Indam P, Mueanmat C, Rattanawilai S. Selection of factors affecting the torification process of palm bunches using an experimental design. *KKU Research Journal (Graduate Studies)*. 2019;19(4):86-99.
2. Business/industry trends 2020-2022: Electricity generation business [Internet]. 2021 [cited 2021 June 21]. Available from: <https://www.krungsri.com/th/research/industry/industryoutlook/Energy-Utilities/Power-Generation/IO/io-power-generation-20>.
3. Biochar production and guidelines for its use [Internet]. Chiang Mai: Maejo University; [cited 2021 Oct 11] Available from: <https://erp.mju.ac.th/articleDetail.aspx?qid=1072>.
4. Acharya B, Sule I, Dutta A. A review on advances of torrefaction technologies for biomass processing. *Biomass Conversion and Biorefinery*. 2012;2(4):349-69.
5. Asadullah M, Adi AM, Suhada N, Malek NH, Saringat MI, Azdarpour A. Optimization of palm kernel shell torrefaction to produce energy densified bio-coal. *Energ Convers Manage*. 2014;88:1086-93.
6. Li MF, Li X, Bian J, Chen CZ, Yu YT, Sun RC. Effect of temperature and holding time on bamboo torrefaction. *Biomass and Bioenergy*. 2015;83:366-72.
7. Granados DA, Ruiz RA, Vega LY, Chejne F. Study of reactivity reduction in sugarcane bagasse as consequence of a torrefaction process. *Energy*. 2017;139:818-27.



## The development of real-time energy monitoring system using IoT base

Kamolwan Wongwut<sup>1</sup> and Daungkamol Angamnuaysiri<sup>2\*</sup>

<sup>1</sup>Department of Electrical Engineering, Faculty of Engineering and Industrial Technology, Phetchaburi Rajabhat University, Phetchaburi 76000, THAILAND

<sup>2</sup>Department of Information Communication Engineering, Faculty of Engineering and Industrial Technology, Phetchaburi Rajabhat University, Phetchaburi 76000, THAILAND

\*Corresponding author: daungkamol.fame@gmail.com

### ABSTRACT

This paper aims to develop a real-time energy monitoring system based on smart metering to enhance energy efficiency in the single-phase residential sector. Based on the concept of low-cost IoT devices, this intelligent meter system is designed to monitor household energy consumption. It provides real-time information on a graphical Node-RED Dashboard, making it easy for households to track and manage their energy usage. The hardware of the power metering system included the Node MCU ESP8266, the PZEM-004T, and a cloud server built on the Raspberry Pi for storing electricity consumption data by using Node-RED to connect devices via an application programming interface system. This system can help analyze the electricity consumption behavior in the residential sector. It is a guideline for selecting the electricity rate between the TOD and TOU rates. The results found that in the electrical energy measurements of households 1 and 2, the mean deviations were 0.8758% and 0.5523%, respectively. The electricity cost-saving results when changing the electricity tariff from the TOD rate of households 1 and 2 to the TOU rate. It was found that electricity costs can be saved by 0.2807% and 1.0936%, respectively. The most critical variable is electricity consumption during peak periods. In the case study of household 1, if the electricity consumption during the peak period is less than 13%, it will be appropriate to select the Time of Use rate. In household 2, if there is electricity consumption during the peak period, less than 38% would be appropriate to choose the type of electricity user with a TOU rate.

**Keywords:** Energy monitoring system, Node-RED, IoT base, Residential sector, Smart metering

### INTRODUCTION

Electricity is a critical factor in life and tends to use more energy. Due to the country's economic growth, it is growing steadily. Whether in the household, commercial, industry, transport, or agriculture sectors. Electric power is essential to various activities, including driving the country's economy, and all of these rely on electricity as the main factor. It is expected that the energy demand will continue to increase in the future. Efficient and sustainable energy use is an essential goal for both the public and private sectors. Many agencies have been continuously campaigning, especially the energy-saving efforts of the household sector. However, arousing public consciousness can save energy to a certain extent. Suppose technology is developed as a tool to help measure electrical energy. In that case, it can show the behavior of consumers using electricity daily to bring information to analyze the energy-saving results of each household. Each household will have different periods of electricity consumption. Some households may use less electricity during the day but more at night. It may give power users a way to adjust

their electricity usage behavior in line with the time of use tariff, a government policy that encourages reducing peak demand and saving energy.

The Time of Use (TOU) tariff is a pricing structure for electricity consumption where electricity costs vary depending on the time of day. Instead of a flat rate for electricity throughout the day, TOU tariffs divide the day into different time blocks, typically categorized as on-peak and off-peak. Besides, the Time of Day (TOD) tariff is another term used to describe a pricing structure for electricity consumption, like the TOU tariff. Under a TOD rate, the cost of electricity varies depending on the time of day when it is consumed. Like TOU rates, TOD rates typically divide the day into different periods, such as on-peak and off-peak, each with its corresponding electricity rate. **Peak Period:** This is when electricity demand is highest, usually during daytime hours when businesses are operational and household energy usage is at its peak. Electricity rates during peak periods are typically higher, reflecting the higher cost of supplying electricity during high demand. **Off-peak Period:** This is when electricity demand is lowest, often during late-night or early morning hours when businesses are

closed, and overall energy consumption is reduced. Electricity rates during off-peak periods are usually lower to incentivize consumers to shift their energy usage away from peak times. The goal of TOD tariffs, like TOU tariffs, is to encourage consumers to adjust their electricity usage patterns to periods of lower demand, thereby helping to balance electricity supply and demand, reduce strain on the grid during peak periods, and potentially lower overall energy costs for consumers and utilities. The TOU tariff varies according to the time of use. The study was based on the electricity tariff rate (2023) of the Provincial Electricity Authority (PEA) [1]. Electricity rates during the day and night will be different. The TOU tariff varies according to the time of use. The study was based on the electricity tariff rate (2023) of the Provincial Electricity Authority (PEA) [1]. Electricity rates during the day and night will be different. The cost of electricity will be expensive during the period when the system has a high demand for electricity (on-peak) between 09.00 a.m. and 10.00 p.m. on working days (Monday-Friday), with an electricity rate of 5.1135 baht per unit (in the case of a voltage of 22-33 kV). The electricity rate equals 5.7982 baht per unit (in the case of a voltage lower than 22 kV) because electricity has to operate power plants that use all fuel types. Both cheap and expensive to produce enough electricity to meet demand, But when the system has low electricity demand (off-peak) between 10:00 p.m. and 9:00 a.m. on weekdays (Monday-Friday) and during the time between 00.00-24.00 on Saturday-Sunday, National Labor Day standard public holidays (excluding plowing day and substitution holidays) with an electricity rate of 2.6037 baht per unit (in the case of voltage 22-33 kV) and an electricity rate of 2.6369 baht per unit (in the case of voltage below 22 kV). Electricity costs will be cheaper because the utilities can operate power plants that use cheap fuel. The standard electricity tariff is calculated as a progressive rate; the more electricity used, the more expensive it will be. If comparing the standard electricity rate with the TOU electricity rate during the off-peak period, there will be a difference of about 40%, which means that the TOU electricity rate during the off-peak period is about 40% cheaper than the standard electricity rate. The possibility of an energy-saving effect and efficient energy use will result in the most value for the user. The electricity cost-saving chart changes from time of day (TOD) to time of use (TOU). It was based on the electricity tariff rate (2015) of the Provincial Electricity Authority (PEA). The customer can use this chart as a guideline to change the TOU rate by analyzing their electrical usage behavior parameter. The chart is plotted to evaluate the percentage of energy savings [2]. Nowadays, communication technology is more advanced and has been applied to various applications based on the IoT concept. It creates a network of connections between various devices via the wireless internet. The adoption of the IoT system is an additional function

of energy management. It is one way to increase energy efficiency. We present a cutting-edge, real-time, low-cost, internet-of-things energy monitoring system developed in this work. The design and development of electrical energy monitoring systems are of various types, such as the IoT-based Smart Energy Meter for Home Appliances designed using an Arduino microcontroller. This innovative smart meter automatically measures energy consumption and calculates the bill with the help of IoT and GSM techniques. The energy consumption units are measured from the user's location to calculate the bill. The generated bill is sent to the user's smartphone through SMS [3]. They proposed electrical energy measurement and monitoring for an IoT home electrical load. The electrical energy measurement and monitoring application used an IoT system based on an ESP8266 microcontroller and a low-cost PZEM-004T current sensor. It measured such parameters by connecting it with a Node MCU ESP8266 unit, a board with built-in Wi-Fi capability. Electrical energy was displayed on a smartphone with the Blynk application, and the data was saved to a cloud system. Abnormal high-energy alerts were sent on a LINE application [4]. The IoT is based on intelligent energy meters for smart grids. The power meter is connected to the ESP8266 12E via an optocoupler. The system also has an OLED display. ULN2003 is used in the driver cycle to relay and shift loads. The current sensor is also installed to detect power theft [5]. An intelligent energy meter monitoring system. It consists of an Arduino, an energy meter, a WIFI module, a relay, and a transformer. An energy meter measures the live current, voltage, and power. The microcontroller reads these parameters and sends them to the cloud. Node MCU is a Wi-Fi device that has a microcontroller in it. This paper measures electricity consumption in home appliances and automatically generates its bill using IoT [6]. A prototype of an advanced meter based on the ESP8266 module with two-way communication over the MQTT protocol [7]. The intelligent energy monitoring systems for energy savings consist of the ZigBee module (IEEE 802.15.4), ESP-12 module, Blynk app, and cloud computing for interfacing the information between the meters and the consumer [8]. Schneider Industry installed an IoT-based energy monitoring system. It can read different electrical parameters. The computing system uses Raspbian, an open-source Linux-based operating system [9]. The hardware included PZEM-004T modules with non-invasive current transformer sensors, Arduino WeMos, and an ESP8266 microcontroller. The software unit, an algorithm using Matlab software, is developed to send measurement data to the ThingSpeak cloud. The proposed system can monitor and analyze the PQ parameters in real time, including frequency, root mean square (RMS) voltage, RMS current, active power, and the power factor of a low-voltage load [10]. The hardware included a Raspberry Pi 3, an Arduino Uno board, and



an ESP8266 Wemos D1 mini to communicate with the PZEM-004T via RS-232. The software included Android Studio and the Raspbian operating system [11]. The hardware included the NodeMCU and sensor PZEM-004T microcontroller. The software included the ThingSpeak cloud server [12] and the Blynk application [13]. The controller, NB-IoT connection module, and cloud are the three main components of an IOT-based innovative energy meter system [14]. An energy consumption monitoring system based on IoT for residential rooftops uses the ESP8266 controller chipset to build the sensing peripheral node, which controls a relay and a PZEM-004T current sensor [15]. Besides, the energy is measured, and a product arrangement is given to create a bill for energy consumption and implement it in LabVIEW software. An IOT-based platform is created to monitor the metering infrastructure in real-time [16] remotely. Overall, Energy monitoring systems promote energy-conscious behavior by raising awareness of energy usage habits. Homeowners can visualize their energy consumption data, set energy-saving goals, reduce energy waste, and contribute to a more sustainable future.

The primary objective of our research is to enhance energy efficiency in the residential sector by developing a household energy monitoring system. This system, which displays real-time information on a graphical Node-RED Dashboard, is connected to a cloud server on the Raspberry Pi for storing electricity consumption data. The system uses Node-RED to connect devices via APIs (Application Programming Interface) system, and the electrical data obtained from the electrical energy measurement system is used to analyze the variables on the behavior of electricity consumption of each household. This analysis is a guideline for selecting the electricity rate between the TOD and TOU rates. Using the relationship equation of the base electricity rate and the variables on electricity consumption behavior, we can calculate the result of saving electricity bills when changing the electricity tariff from the TOD to the TOU rate. The research materials and methods, results and discussions, and conclusions are presented in the following sections.

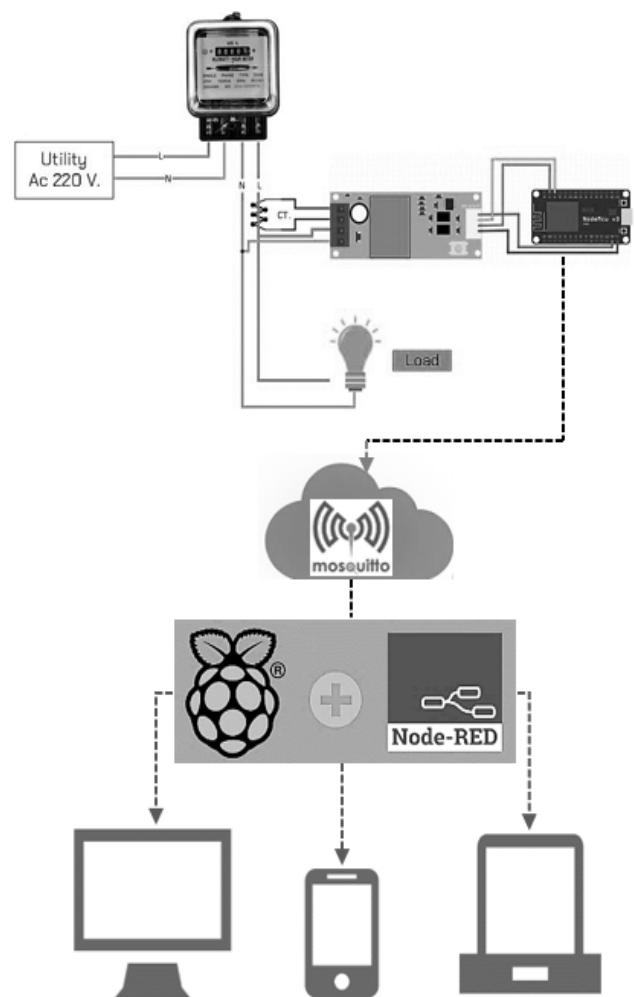
## MATERIALS AND METHODS

This paper aims to 1) develop an energy monitoring system for the residential sector. The data were real-time on a graphic with a Node-RED Dashboard, 2) Building a cloud server on the Raspberry Pi for storing electricity consumption data by using Node-RED to connect devices through Application Programming Interface (APIs, and 3) analyzing variables on electricity consumption behavior in the household. It will guide the selection of electricity tariffs between the TOD and TOU rates.

The functional structure design of the real-time electrical energy monitoring system consists of three parts.

### A. The design of a real-time electrical energy monitoring system

The real-time data display system is designed with a Node-RED Dashboard on the graphic. The purpose of MQTT is to make our systems send and receive data more efficiently, including wasting the device's energy. In the IOT system, we want to send real-time data and want our devices to use only a little energy unnecessarily. The hardware includes a microcontroller and electrical data measurement sensors such as voltage, current, power, energy, frequency, and power factor. The microcontroller will receive various values from the sensor, which processes and transmits data to Node-Red over a wireless Internet network. Display graphical data on the Node-RED Dashboard and use the data to analyze the variables affecting the electricity consumption behavior of each household. To be a guideline for selecting the electricity tariff between the standard rate and the time of use (TOU) rate. The working process of the system as shown in Figure 1.



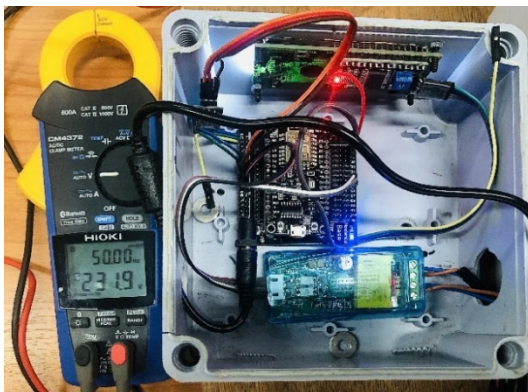
**Figure 1** The proposed real-time electrical energy monitoring system design with Node-RED Dashboard.

### B. The creating a cloud server on Raspberry Pi

The creation of a cloud server on Raspberry Pi for storing electricity consumption data using Node-RED connects devices via APIs, as shown in Figure 2.



**Figure 2** Node-RED uses the cloud server on Raspberry Pi.



**Figure 3** Installation of the proposed system for the experiment.

Data protection protocols and measures can be implemented to ensure user information confidentiality in energy monitoring systems. Encryption: All data transmitted between the energy monitoring system and any external devices or servers should be encrypted using robust encryption algorithms. This prevents unauthorized access to the data during transmission. Access Control: Implement access control mechanisms to restrict access to sensitive user information. Only authorized users should have access to the data, and different access privileges can be assigned based on roles and responsibilities.

### C. The installing an electrical energy metering system for the experiment

The hardware includes NodeMCU ESP8266-V3 and AC Digital Power Energy Meter Module PZEM-004T. The software consists of storing and displaying

data with the cloud server on Raspberry Pi using Node-RED. The real-time data of power measurement can be transmitted via a wireless system of devices based on the smart meter concept, as shown in Figure 3.

### D. The analysis of electricity cost savings

The relationship equation of the base electricity cost with the behavioral variables of electricity usage type 1 residential house considered the TOD of the group of electrical energy consumers not exceeding 150 units per month as in equation (1).

$$\begin{aligned} \text{Base}_{\text{TOD}} = & 2.3488 + 0.6394 - \left( \frac{9.5910}{\text{kWh}_{\text{Total}}} \right) \\ & + 0.2523 - \left( \frac{6.3075}{\text{kWh}_{\text{Total}}} \right) \\ & + 0.3832 - \left( \frac{13.4120}{\text{kWh}_{\text{Total}}} \right) \\ & + 0.0934 - \left( \frac{9.3400}{\text{kWh}_{\text{Total}}} \right) \\ & + 0.5047 - \left( \frac{75.7050}{\text{kWh}_{\text{Total}}} \right) \\ & + 0.1999 - \left( \frac{79.9600}{\text{kWh}_{\text{Total}}} \right) \end{aligned} \quad (1)$$

The group of electrical energy consumers exceeds 150 units per month, as shown in equation (2).

$$\begin{aligned} \text{Base}_{\text{TOD}} = & 3.2484 + 0.9734 - \left( \frac{146.01}{\text{kWh}_{\text{Total}}} \right) \\ & + 0.1999 - \left( \frac{79.96}{\text{kWh}_{\text{Total}}} \right) \end{aligned} \quad (2)$$

The time of use rate (TOU) with a voltage of 22-33 kV, as in equation (3), and a voltage lower than 22 kV, as in equation (4).

$$\text{Base}_{\text{TOU}} = 2.6037 + 2.5098 \left( \frac{\text{kWh}_{\text{Peak}}}{\text{kWh}_{\text{Total}}} \right) \quad (3)$$

$$\text{Base}_{\text{TOU}} = 2.6369 + 3.1613 \left( \frac{\text{kWh}_{\text{Peak}}}{\text{kWh}_{\text{Total}}} \right) \quad (4)$$

According to the equation for saving electricity costs from TOD rates to change TOU rates for electricity tariff type 1 residential home can be created, as in equation (5).

$$\varphi = \frac{\text{Base}_{\text{TOD}} - \text{Base}_{\text{TOU}}}{\text{Base}_{\text{TOD}}} \times 100 \quad (5)$$

The result of saving electricity costs found that changing the electricity consumption rate depends on the variables of electricity consumption behavior that differ according to the type of electricity users. The electricity consumers who want to change their electricity usage rate can analyze their electricity consumption behavior and calculate the result from equation (5). It will inform us of the savings in electricity

costs when changing to the TOU rate.  $kWh_{Peak}$  is the electricity consumed for the whole month during the peak period (kWh).  $kWh_{Total}$  is the total electricity consumed for the whole month (kWh).  $Base_{TOD}$  is the base electricity cost per unit of TOD rate (Baht/kWh).  $Base_{TOU}$  is the base electricity cost per unit of TOU rate (Baht/kWh), and  $\phi$  is the percentage of saving electricity costs. The calculation of the error between a measurement from a clamp meter and the proposed system for the experiment. The results were displayed and compared to determine the percentage difference, as in equation (6) [2].

$$\text{Error} = \frac{\text{Measuring}_{Real} - \text{Measuring}_{Exp}}{\text{Measuring}_{Real}} \times 100 \quad (6)$$

## RESULTS AND DISCUSSION

Energy management in the residential sector involves various practices and technologies to optimize energy usage, reduce energy waste, and promote energy efficiency in homes. A vital component is using Home Energy Management Systems (HEMS). These systems, integrated with our IoT-based energy monitoring system, utilize smart devices, sensors, and software to monitor and control energy usage in real-time. By providing insights into energy consumption patterns, HEMS enables homeowners to make informed decisions that can significantly reduce energy waste, thereby promoting energy efficiency in the residential sector. This section presents the results obtained from the proposed system for the experiment with an electrical energy metering system, including Node MCU ESP8266 and AC Digital Power Energy Meter Module PZEM-004T that power energy meter module. It is utilized for voltage (V), current (A), power (W), energy (kWh), frequency (Hz), and power factor measurement of household electricity.

### A. The results of the voltage and current measurement

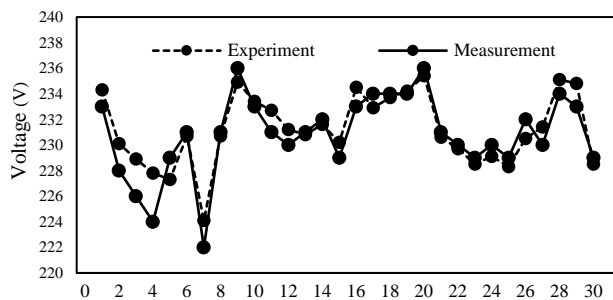
There were two households in the experiment. The energy monitoring system is tested with a randomized measurement process for voltage and current values that test 30 cycles simultaneously. As shown in Table 1, the energy monitoring system tested the household 1. It can store the voltage and current values using an AC digital power energy meter module PZEM-004T and the CM4372 AC/DC clamp meter every 15 minutes. The minimum and maximum voltages were measured with the PZEM-004T module. They were 224.1 V and 235.4 V, respectively, while the CM4372 clamp meter measured voltages 222 V and 236 V, respectively. Moreover, the minimum and maximum current measured with the AC digital power energy meter module PZEM-004T were 1.06 A and 7.85 A, respectively, while the minimum and maximum current measured with the CM4372 AC/DC clamp meter were 1.05 A and 8.5 A, respectively. As shown in Table 2, the household 2 was tested by the energy monitoring system. It can store the voltage and current values using an AC digital power energy meter module PZEM-004T and the CM4372 AC/DC clamp meter every 15 minutes. The minimum and maximum voltages were measured with the PZEM-004T module. They were 225.6 V and 235.4 V, respectively, while the CM4372 clamp meter measured voltages 227 V and 234 V, respectively. Moreover, the minimum and maximum current measured with the AC digital power energy meter module PZEM-004T were 5.26 A and 15.89 A, respectively, while the minimum and maximum current measured with the CM4372 AC/DC clamp meter were 5.6 A and 16.25 A, respectively. The results illustrated that both measuring tools were highly reliable.

**Table 1** The voltage and current measurement of household 1.

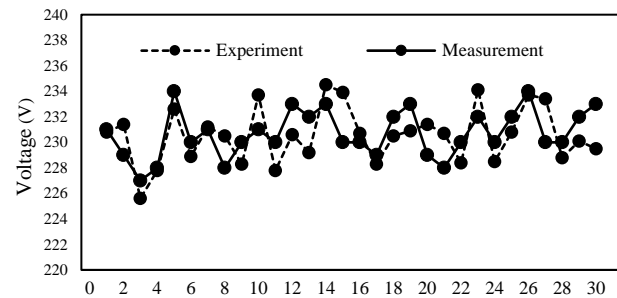
No.	Power Energy Meter Module PZEM-004T		The CM4372 AC/DC Clamp Meter		No.	Power Energy Meter Module PZEM-004T		The CM4372 AC/DC Clamp Meter	
	V	I	V	I		V	I	V	I
1	234.3	4.35	233	4.10	16	234.5	1.25	233	1.2
2	230.1	1.08	228	1.05	17	232.9	1.15	234	1.1
3	228.9	1.35	226	1.24	18	233.7	1.37	234	1.2
4	227.8	4.32	224	4.10	19	234.2	1.18	234	1.1
5	227.3	1.36	229	1.30	20	235.4	1.36	236	1.2
6	230.7	1.60	231	1.50	21	230.6	1.24	231	1.1
7	224.1	5.42	222	5.80	22	229.7	1.25	230	1.1
8	230.7	1.23	231	1.30	23	228.5	3.89	229	3.7
9	234.9	1.06	236	1.15	24	229.1	1.30	230	1.2
10	233.4	1.85	233	1.70	25	228.3	3.54	229	3.2
11	232.7	1.51	231	1.61	26	230.5	7.85	232	8.5
12	231.2	1.14	230	1.13	27	231.4	2.14	230	1.9
13	230.8	1.53	231	1.40	28	235.1	3.76	234	3.4
14	231.6	1.84	232	1.70	29	234.8	5.40	233	5.1
15	230.2	1.28	229	1.20	30	228.5	1.26	229	1.1

**Table 2** The voltage and current measurement of household 2.

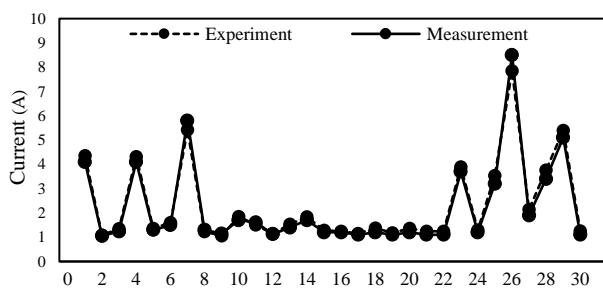
No.	Power Energy Meter Module PZEM-004T		The CM4372 AC/DC Clamp Meter		No.	Power Energy Meter Module PZEM-004T		The CM4372 AC/DC Clamp Meter	
	V	I	V	I		V	I	V	I
1	230.8	12.24	231	11.86	16	230.7	6.42	230	7.8
2	231.4	10.95	229	11.74	17	228.3	13.43	229	14.6
3	225.6	7.46	227	8.31	18	230.5	9.88	232	11.3
4	227.8	9.76	228	10.87	19	230.9	11.25	233	12.5
5	232.6	13.85	234	14.10	20	231.4	8.47	229	7.6
6	228.9	15.02	230	14.50	21	230.7	6.65	228	7.3
7	231.2	10.14	231	11.30	22	228.4	14.73	230	15.2
8	230.5	8.36	228	8.90	23	234.1	9.48	232	10.3
9	228.3	5.26	230	5.60	24	228.5	13.96	230	14.4
10	233.7	11.78	231	13.20	25	230.8	15.14	232	15.5
11	227.8	6.75	230	7.40	26	233.7	10.65	234	11.4
12	230.6	13.56	233	13.20	27	233.4	14.89	230	15.6
13	229.2	10.32	232	12.50	28	228.8	7.32	230	8.1
14	234.5	15.89	233	16.25	29	230.1	6.58	232	7.5
15	233.9	7.41	230	8.60	30	229.5	13.67	233	14.3



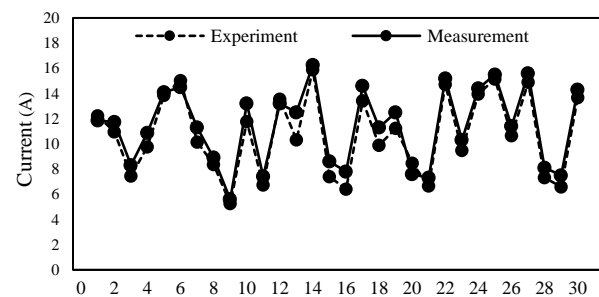
a) Household 1



b) Household 2

**Figure 4** Comparison of voltage measurements between the developed energy monitoring system of experiment and measuring instrument.

a) Household 1



b) Household 2

**Figure 5** Comparison of current measurements between the developed energy monitoring system of experiment and measuring instrument.

The comparison of voltage and current values measured between the power energy meter module PZEM-004T of the experiment and the CM4372 AC/DC clamp meter is shown in Figure 4 and Figure 5. It was found that voltage and current measurements can be made by various factors affecting measurement accuracy, whether it is surrounding environmental conditions such as temperature, humidity, or atmospheric pressure. It can affect measurement error and sensor operation, which can cause the error. One of the key findings of this

research is the importance of regular sensor maintenance for ensuring long-term measurement accuracy. The correct and careful use of current and voltage sensors can significantly reduce measurement error. However, it is crucial to emphasize the need for regular updates and maintenance to keep the sensors performing at their best, thereby ensuring the long-term accuracy of the measurements.

Table 3 shows the voltage and current error percentage compared to the measured value and 30



data collection systems. Household 1 was found to have an average voltage error of 0.487 V, and an average current error of 7.987 A. Household 2 has an average

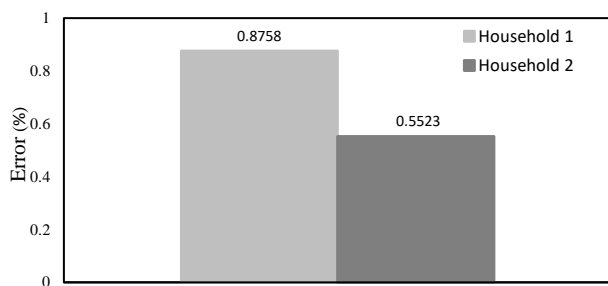
voltage error percentage of 0.773 V and an average current error percentage of 7.880 A.

**Table 3** An error of voltage and current for household 1 and household 2.

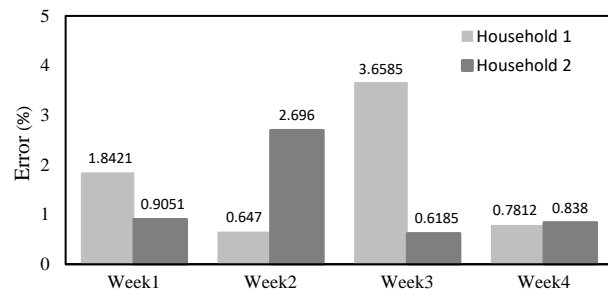
No.	Household 1		Household 2		No.	Household 1		Household 2	
	%Error		%Error			%Error		%Error	
	V	I	V	I		V	I	V	I
1	0.56	6.10	0.09	3.20	16	0.64	4.17	0.30	17.69
2	0.92	2.86	1.05	6.73	17	0.47	4.55	0.31	8.01
3	1.28	8.87	0.62	10.23	18	0.13	14.17	0.65	12.57
4	1.70	5.37	0.09	10.21	19	0.09	7.27	0.90	10.00
5	0.74	4.62	0.60	1.77	20	0.25	13.33	1.05	11.45
6	0.13	6.67	0.48	3.59	21	0.17	12.73	1.18	8.90
7	0.95	6.55	0.09	10.27	22	0.13	13.64	0.70	3.09
8	0.13	5.38	1.10	6.07	23	0.22	5.14	0.91	7.96
9	0.47	7.83	0.74	6.07	24	0.39	8.33	0.65	3.06
10	0.17	8.82	1.17	10.76	25	0.31	10.63	0.52	2.32
11	0.74	6.21	0.96	8.78	26	0.65	7.65	0.13	6.58
12	0.52	0.88	1.03	2.73	27	0.61	12.63	1.48	4.55
13	0.09	9.29	1.21	17.44	28	0.47	10.59	0.52	9.63
14	0.17	8.24	0.64	2.22	29	0.77	5.88	0.82	12.27
15	0.52	6.67	1.70	13.84	30	0.22	14.55	1.50	4.41

**Table 4** Comparison of electrical energy measurements between the developed energy monitoring system of experiment and measuring instrument.

Week	Household 1			Week	Household 2		
	Experiment (kWh)	Measurement (kWh)	Error (%)		Experiment (kWh)	Measurement (kWh)	Error (%)
1	37.3000	38.0000	1.8421	1	117.0500	116.0000	0.9051
2	34.2200	34.0000	0.6470	2	104.7500	102.0000	2.6960
3	42.5000	41.0000	3.6585	3	96.4000	97.0000	0.6185
4	32.2500	32.0000	0.7812	4	104.1200	105.0000	0.8380
Total	146.2700	145.0000	0.8758	Total	422.3200	420.0000	0.5523



a) Weekly average



b) Monthly average

**Figure 6** The error of electrical energy measurements between the experiment and measuring instrument.

### B. The results of measuring energy consumption

Each household's monthly electricity consumption is measured using the electrical energy measurement system developed for the experiment. To verify the accuracy of the information and test the system's performance by measuring the energy value from the prototype measurement system compared with the measuring instrument. This test aims to compare the

system's performance to see if it can accurately measure wireless power with acceptable tolerances. From Table 4, which shows the monthly electric energy consumption of household 1, it was found that the electric energy measured by the developed energy monitoring system was 146.27 kWh/month, and the measuring instrument measured it as 145.00 kWh/month. An error equals 0.8758%. The monthly electric energy consumption of household 2, it was found that the

electric energy value measured by the developed energy monitoring system was 422.32 kWh/month and measured by the measuring instrument was 420.00

kWh/month. An error equals 0.5523%. The error of electrical energy measurements between the experiment and measuring instrument as shown in Figure 6.

**Table 5** The result of electricity cost savings in the household sector.

Household	kWh <sub>Total</sub> (kWh)	kWh <sub>Peak</sub> (kWh)	Base <sub>TOD</sub> (Baht/kWh)	Base <sub>TOU</sub> (Baht/kWh)	kWh <sub>Peak</sub> / kWh <sub>Total</sub>	Φ (%)
1	145.0000	20.0000	3.0816	3.0729	0.1379	0.2807
2	420.0000	160.0000	3.8837	3.8412	0.3809	1.0936

**Table 6** The result of electricity cost savings of electrical energy consumers not exceeding 150 kWh/month.

Electricity consumption	kWh <sub>Total</sub> (kWh)	kWh <sub>Peak</sub> (kWh)	Base <sub>TOD</sub> (Baht/kWh)	Base <sub>TOU</sub> (Baht/kWh)	kWh <sub>Peak</sub> / kWh <sub>Total</sub>	Φ (%)
<150	80.0000	0.0000	1.9927	2.6369	0.0000	-32.3242
kWh/month	90.0000	0.0000	2.2626	2.6369	0.0000	-16.5409
	100.0000	0.0000	2.4785	2.6369	0.0000	-6.3890
	110.0000	0.0000	2.6551	2.6369	0.0000	0.6890
	120.0000	6.0000	2.8024	2.7949	0.0500	0.2654
	130.0000	11.0000	2.9269	2.9043	0.0846	0.7711
	140.0000	17.0000	3.0337	3.0207	0.1214	0.4271
	149.0000	22.0000	3.1175	3.1036	0.1476	0.4458

**Table 7** The result of electricity cost savings of electrical energy consumers exceeding 150 kWh/month.

Electricity consumption	kWh <sub>Total</sub> (kWh)	kWh <sub>Peak</sub> (kWh)	Base <sub>TOD</sub> (Baht/kWh)	Base <sub>TOU</sub> (Baht/kWh)	kWh <sub>Peak</sub> / kWh <sub>Total</sub>	Φ (%)
>150	180.0000	25.0000	3.1663	3.0759	0.1388	2.8532
kWh/month	200.0000	35.0000	3.2918	3.1901	0.1750	3.0901
	220.0000	50.0000	3.3945	3.3553	0.2272	1.1543
	250.0000	65.0000	3.5178	3.4588	0.2600	1.6766
	280.0000	85.0000	3.6146	3.5965	0.3035	0.5003
	300.0000	95.0000	3.6684	3.6379	0.3166	0.8311
	320.0000	105.0000	3.7155	3.6742	0.3281	1.1126
	350.0000	125.0000	3.7760	3.7659	0.3571	0.2684
	380.0000	140.0000	3.8270	3.8015	0.3684	0.6650
	400.0000	150.0000	3.8567	3.8223	0.3750	0.8916
	450.0000	180.0000	3.9195	3.9014	0.4000	0.4624
	500.0000	210.0000	3.9697	3.9646	0.4200	0.1288
	550.0000	235.0000	4.0108	3.9876	0.4272	0.5786
	600.0000	265.0000	4.0450	4.0331	0.4416	0.2952
	650.0000	270.0000	4.0740	3.9500	0.4153	3.0436
	700.0000	280.0000	4.0988	3.9014	0.4000	4.8175

### C. The results of the electricity cost savings

The electricity cost savings effect depends on the amount of electrical units, including the month and the proportion of electricity usage. The analysis of saving electricity when changing the TOU rate of household 1. The rate for general households receiving electricity at 220 volts and using electricity is less than 150 kWh/month.

From Table 5, it was found that it consumed 145 kWh/month. During peak time, 20 kWh/month. The proportion of electricity consumption ( $\text{kWh}_{\text{Peak}}/\text{kWh}_{\text{Total}}$ ) is 0.1379. The percentage of electricity costs saved is

0.2807%. It is possible to reduce electricity bills by changing to the TOU rate.

The electricity cost analysis is saved when changing the TOU rate of household 2. The rate for general households receiving electricity is 220 volts and uses more than 150 kWh/month. From Table 5, it was found that it consumed 420 kWh/month. During peak time, 160 kWh/month. The proportion of electricity consumption ( $\text{kWh}_{\text{Peak}}/\text{kWh}_{\text{Total}}$ ) is 0.3809. The percentage of electricity costs saved is 1.0936%. It is possible to reduce electricity bills by changing to the TOU rate.

Table 6 shows the results of electricity cost savings. In the case study of general households receiving electricity voltage of 220 volts and having electrical

energy consumers not exceeding 150 kWh/month, if considering the total monthly electric energy (kWh) that is in the range of 80 - 100 kWh/month and without energy consumption Electricity during the peak was found not to affect saving electricity bills when changing to the TOU rate. Considering the total monthly electric energy equal to 110 kWh/month and without using electric power during the peak period, it was found that the effect on saving electricity was 0.6890% when changing to the TOU rate. Considering the total monthly electricity consumption in the range of 120 - 149 kWh/month, it was found that electricity costs could be saved. The electricity consumption during the peak period must be more than 5 percent of the total electricity.

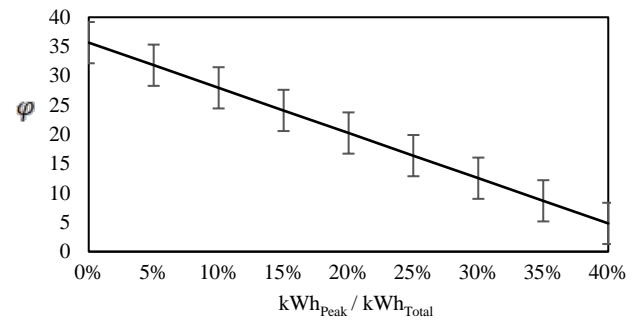
Table 7 shows the results of electricity cost savings. In the case study of a typical household receiving an electricity voltage of 220 V and having electrical energy consumers exceeding 150 kWh/month, if considering the total monthly electricity consumption, it is 180 kWh/month, and the electricity consumption in the peak period is 25 kWh/month. It is about 13% of all units of electricity. It was found that an effect on saving electricity equals 2.8532% when changing to the TOU rate. If the electricity used during the peak period was less than 13% of all units of electricity, it was found that the results in an increase in electricity bill savings of up to 15%.

Electricity cost savings in the household sector can be achieved through various strategies and practices to reduce energy consumption and optimize energy efficiency. Here are some practical ways to save on electricity costs: 1. Install an energy monitoring system to track and analyze household energy consumption in real-time. This visibility helps identify energy-intensive appliances and behaviors to make informed decisions to reduce energy use. 2. Time of Use (TOU) Tariffs: If available, consider switching to a TOU electricity tariff that offers lower rates during off-peak hours. Adjusting energy use to take advantage of lower rates can lead to significant savings, especially for running appliances and charging electric vehicles. 3. Behavioral Changes: Adopt energy-saving habits such as turning off lights when leaving a room, using energy-efficient settings on appliances, and washing clothes in cold water. Implementing these strategies can help households reduce their electricity consumption, lower utility bills, and contribute to a more sustainable environment by reducing energy demand.

#### D. The comparison of electricity bills as TOD and TOU

Considering the total monthly electrical energy is 700 kWh/month, and the electrical energy consumption during the peak is 280 kWh/month or about 40% of the total electrical unit, it was found that the effect on saving electricity is 4.8175% when changing to the TOU rate. Suppose the electricity consumption during the peak period is less than 40% of the total

electricity unit. In this case, it will increase electricity cost savings by up to 35%, as shown in Figure 7.



**Figure 7** The electricity bills saved by electrical energy consumers are 700 kWh/month.

**Table 8** Comparison of electricity bills as TOD and TOU of electrical energy consumers 700 kWh/month.

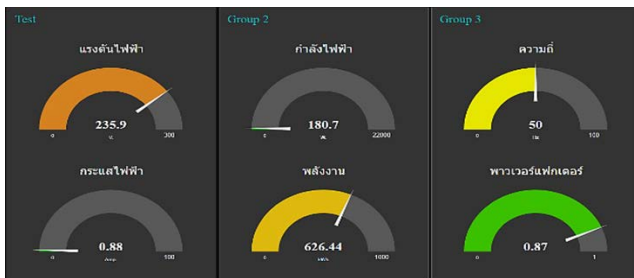
$\text{kWh}_{\text{Peak}}/\text{kWh}_{\text{Total}}$	TOD (Baht)	TOU (Baht)	Error (Baht)
35/700	2869.22	1956.48	912.74
70/700	2869.22	2067.12	802.10
105/700	2869.22	2177.77	691.45
140/700	2869.22	2288.41	580.81
175/700	2869.22	2399.06	470.16
210/700	2869.22	2509.70	359.52
245/700	2869.22	2620.35	248.87
280/700	2869.22	2730.99	138.23

Table 8 compares electricity bills as TOD and TOU of 700 kWh/month electrical energy consumers. Considering the ratio ( $\text{kWh}_{\text{Peak}}/\text{kWh}_{\text{Total}}$ ) of 0.1, it means that  $\text{kWh}_{\text{Peak}}$  is 10% of  $\text{kWh}_{\text{Total}}$ , the TOD electricity bill is 2869.22 Baht and the TOU electricity bill is 2067.12 Baht. Therefore, TOU electricity bills are more economical than TOD electricity bills by 802.10 baht or savings of about 28%. Considering the ratio ( $\text{kWh}_{\text{Peak}}/\text{kWh}_{\text{Total}}$ ) of 0.2, it means that  $\text{kWh}_{\text{Peak}}$  is 20% of  $\text{kWh}_{\text{Total}}$ , the TOD electricity bill is 2869.22 Baht and the TOU electricity bill is 2288.41 Baht. Therefore, TOU electricity bills are more economical than TOD bills by 580.81 baht, or savings of about 20%. Considering the ratio ( $\text{kWh}_{\text{Peak}}/\text{kWh}_{\text{Total}}$ ) of 0.3, it means that  $\text{kWh}_{\text{Peak}}$  is 30% of  $\text{kWh}_{\text{Total}}$ , the TOD electricity bill is 2869.22 Baht and the TOU electricity bill is 2509.70 Baht. Therefore, TOU electricity bills are more economical than TOD electricity bills by 359.52 baht or savings of about 13%.

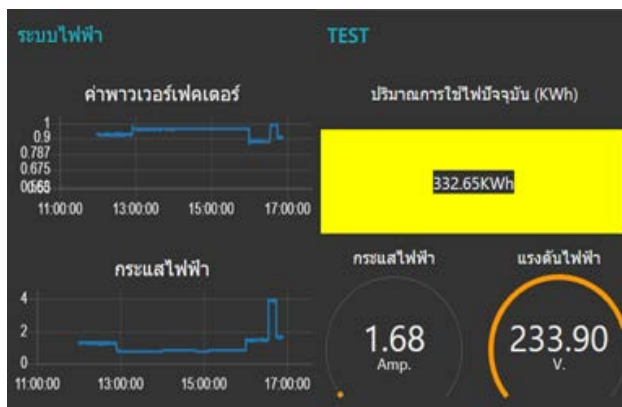
#### E. The display of the real-time data on Node-RED Dashboard

The software consists of storing and displaying data with the cloud server on Raspberry Pi by using Node-RED. The real-time data of power measurement can be transmitted via a wireless system of devices based on the IoT concept. Display of the real-time data on the Node-RED dashboard, including voltage (V),

current (A), power (W), Electricity consumption (kWh), frequency (Hz), and power factor, as shown in Figure 8 and Figure 9.



**Figure 8** The data is shown in a graphical output on the dashboard.



**Figure 9** Display of the real-time data on Node-RED.

## CONCLUSIONS

To develop a real-time energy monitoring system based on smart metering to enhance energy efficiency in the single-phase residential sector. Based on the concept of low-cost IoT devices, this intelligent meter system is designed to monitor household energy consumption. It provides real-time information on a graphical Node-RED Dashboard, making it easy for households to track and manage their energy usage. The research results presented measurements and recorded voltages and currents. This technique employed a facile design and development using a simple and inexpensive IoT configuration. The results found that the system can measure electrical energy by transmitting real-time data through a wireless network. That can store data in the database system and efficiently measure electrical energy. In the electrical energy measurements of households 1 and 2, the mean deviations were 0.8758% and 0.5523 %, respectively. The electricity cost-saving results when changing the electricity tariff from the TOD rate of households 1 and 2 to the TOU rate. It was found that electricity costs can be saved by 0.2807 % and 1.0936 %, respectively. Future research should develop a system that is more compact and user-friendly. Moreover, it would allow users to monitor their homes for theft prevention as if they were bright houses. Standards for all types of electrical devices in the home can be developed. Also, over a long period, monitoring

electric power usage can be used to predict future energy consumption and user behavior.

## REFERENCES

1. PEA. Electricity Tariffs 2023 [Internet]. Bangkok: Provincial Electricity Authority; [cited 2023 June 10]. Available from: <https://www.pea.co.th/electricity-tariffs>.
2. Pudwong S, Vichanpol B, Katkhaw N, Fakkaew W, Lungkadee T. Electricity cost saving simulation of changing to time of use rate (TOU). *J Sci Technol*. 2019;27(6):1147-63.
3. Rupesh M, Anbu Selvan N. Design of IoT based smart energy meter for home appliances. *J Phys Conf Ser*. 2021;1964(5):1-6.
4. Chaibong W, Sonasang S. Applications of energy monitoring using the IoT. *SNRU Journal of Science and Technology*. 2022;14(2):1-9.
5. Kalyan Chakravarthi P, Yuvaraj D. IoT based smart energy meter for smart grids. *International Conference on Devices, Circuits and Systems (ICDCS)*; 2022 April 21-22; Karunya Institute of Technology and Sciences, Coimbatore, India. 2022. p.360-3.
6. Sulthana N, Rashmi N, Prakyathi NY, Bhavana S, Shiva Kumar KB. Smart energy meter and monitoring system using IoT. *International Journal of Engineering Research & Technology (IJERT)*. 2020;8(14):50-3.
7. Jakus D, Vasilj J, Sarajcev P. Advanced energy meter with load control based on ESP8266 module and MQTT protocol. *25th International Conference on Electricity Distribution*; 2019 June 3-6; Madrid, Spain. *CIREC 2019 Proceedings: AIM*; 2019. p.1-5.
8. Govindarajan R, Meikandasivam S, Vijayakumar D. Performance analysis of smart energy monitoring systems in real-time. *Engineering Technology & Applied Science Research*. 2020;10(3):5808-13.
9. Mudaliar MD, Sivakumar N. IoT based real time energy monitoring system using Raspberry Pi. *Internet of Things*. 2020;12:1-20.
10. Khoa NM, Dai LV, Tung DD, Toan NA. An advanced IoT system for monitoring and analysing chosen power quality parameters in micro-grid solution. *Archives of Electrical Engineering*. 2021;70(1): 173-88.
11. Sudame KS, Ali S, Rawate AM. Design of an IoT based energy monitoring system and home automation. *Journal of Emerging Technologies and Innovative Research (JETIR)*. 2020;7(6):1365-75.
12. Samano-Ortega V, Mendez-Guzman H, Martinez-Nolasco J, Padilla-Medina J, Santoyo-Mora M, Zavala-Villalpando J. Electrical energy consumption monitoring system in the residential sector using



- IoT. IEEE Lat Am T. 2023;21(1):158-66.
13. Devireddy Y, Sanke M, Ragi K, Maganti H, Thorlikonda A. Real time energy monitoring and controlling system using IoT. Proceedings of the Second International Conference on Smart Electronics and Communication (ICOSEC). 2021 October 7-9; Trichy, India. 2021. p. 157-61.
  14. Siva Balan RV, Gouri MS, Senthilnathan T, Gondkar S, Gondar RR, Zeema JL, et al. Development of smart energy monitoring using NB-IOT and cloud. Measurement: Sensors. 2023;29:100884.
  15. Himer SE, Ouaisa M, Ouaisa M, Krichen M, Alswailim M, Almutiq M. Energy consumption monitoring system based on IoT for residential rooftops. Computation. 2023;11(4):78.
  16. Priyadharshini SG, Subramani C, Preetha Roselyn J. An IOT based smart metering development for energy management system. International Journal of Electrical and Computer Engineering (IJECE). 2019;9(4):3041-50.



## A study on the behavior of pulling power and flammability of mold walls mixed with high-density polyethylene plastic waste

Thaweesak Rungsaktaweekul<sup>1</sup>, Piyapong Kesawadkorn<sup>1</sup>, Teerin Kongpun<sup>2</sup> and Apised Suwansaard<sup>3\*</sup>

<sup>1</sup>Department of Civil Engineering, Faculty of Engineering, Rajamangala University of Technology Rattanakosin, Wang Klai Kangwon Campus, Prachuap Khiri Khan 77110, THAILAND

<sup>2</sup>Department of Materials Engineering, Faculty of Engineering, Rajamangala University of Technology Rattanakosin, Nakhon Pathom 73170, THAILAND

<sup>3</sup>Department of Civil Engineering, Faculty of Engineering, Rajamangala University of Technology Rattanakosin, Nakhon Pathom 73170, THAILAND

\*Corresponding author: apised.suw@rmutr.ac.th

### ABSTRACT

Currently, materials used in construction have been continuously developed in terms of quality and efficiency, especially fiber reinforcement in mortar, a form of development used in construction. The development aims to enhance concrete's tensile properties and performance for higher flexibility. Most plaster walls are ordinary mortar and have low elasticity, which is a weak point. Therefore, attempts are being made to improve their properties by using a rigid material as a concrete mixture, namely high-density polyethylene plastic, to increase its ability to bear tensile force. This study examines the tensile strength and flammability tests of walls plastered with mortar, with which high-density polyethylene plastic waste is mixed. The tensile strength of mortar plaster walls mixed with high-density polyethylene plastic is tested by replacing at 2.5%, 5%, and 10% proportions and cured at 7, 14, and 28 days. By comparing general mortar and high-density polyethylene plastic mortar, it is found that the general mortar had the highest tensile strength at 28 days of curing. The obtained value is 45 ksc, and the mortar mixed with polyethylene plastic in the amount of 2.5% at 28 days of curing can withstand the strength of 45 ksc. In addition, the general mortar can produce the same tensile strength as mortar mixed with high-density polyethylene plastic. The flammability test shows that general mortar develops red marks after being burned with fire, while the mortar combined with high-density polyethylene plastic develops black marks. However, neither type of wall is in flames nor spread.

**Keywords:** High-density polyethylene plastic waste, Pulling power, Ignition

### INTRODUCTION

Mortar is made from a cement mixture with fine sand and water as a binder. It is trendy for constructing all types of buildings and valuable for plastering the surface of building walls and covering the surface of building structures such as beams and columns to create a neat surface before painting or decorating the surface with other materials. In addition to the benefits of covering walls and structures, mortar can be used for different construction purposes, such as laying bricks or block walls, and as an adhesive for bonding ceramic tiles. Mortar has the highest amount of sand as an ingredient, causing the demand for sand to increase along with the popularity of mortar used in construction [1].

Today's society is interested in environmental conservation. Waste in one industry is used to benefit another sector. The idea for this research is to use waste

from the recycled plastic production process in the construction industry. Because plastic is a material that plays a massive role in our daily lives, the trend of its use is increasing to replace the use of natural resources [2]. Reusing plastic waste by forming it into new products is a prevalent method. The plastic recycling process begins with separating different types of plastic from each other because different types have various properties, such as melting points, density, hardness, softness, and clarity. When each type of plastic is separated, it will be squeezed, flattened, and then bundled into bales to be sent to a plastic recycling factory. Each type of plastic is crushed into small pieces and washed in a large pond during this step. Dust and dirt are removed, and the plastic pieces are dried in the sun or hot air. The paper or film tag attached to the plastic piece will be blown apart and enter the process of melting plastic pieces through an extruder into strips before cutting them into small

pellets and packing them into boxes to go to a plastic molding factory to make new products. When all recycled plastic pellets are used and molded into new products, the new plastic products will have reduced physical properties. Sometimes, factories mix new plastic pellets to give the product better properties. This recycled plastic production process creates waste, including a large amount of solid waste. In 2017, the amount of solid waste throughout the country was 27.40 million tons, an increase from 2016, which had 27.06 million tons, accounting for 1.26 percent or 120,000 tons, while the rate of solid waste generation per person decreased from 1.14 kilograms/person/day in 2016, to 1.13 kilograms/person/day in 2017. The correct waste disposal increased from 9.57 million tons in 2016 to 11.70 million tons in 2017 and increased for use from 5.80 million tons to 8.52 million tons.

Due to the problems mentioned above, the researchers, therefore, had an idea to study the behavior of the tensile strength and flammability of mortar walls mixed with high-density polyethylene plastic waste [3]. The purposes are to examine the possibility of using plastic scraps instead of sand in producing plaster walls and to form a guideline for managing plastic waste for engineering benefits. The reason for choosing plastic waste is to put unused materials to good use and to manage pollution and the environment, reducing the amount of plastic waste that is often difficult to decompose [4].

## MATERIALS AND METHODS

### Materials used for testing

1. Portland cement type 1
2. Clean water

**Table 1** The ratio of mixing mortar and plaster.

Sample	Cement (g)	Sand (g)	HDPE waste (g)	Water (g)
Mortar Sand 100%	125	344	0	88
Mortar HDPE 2.5%	125	335	9	88
Mortar HDPE 5%	125	327	17	88
Mortar HDPE 10%	125	310	34	88

3. Analyzing the mix size and fineness modulus of fine aggregate according to ASTM C136 standard [8].

4. Testing the specific gravity value and absorption of fine aggregate according to ASTM C642 standards [9].

5. Test the flow of mortar (Flow Table) to find the flow rate of cement mortar and cement paste using a flow test table with accessories according to ASTM C230 standards [10].

6. A sample block of mortar was cast to test its tensile strength using a briquette mold measuring 7.5 cm x 2.5 cm x 4.5 cm and 2.5 cm thick according to the ASTM C190 standard [11], as shown in Figure 2.

3. Plastic waste: high-density polyethylene (HDPE) plastic, as shown in Figure 1.

High-density polyethylene (HDPE) has a linear molecular structure. It is cheap, relatively hard but stretchable, and easy to mold. Commonly used to make packaging for cleaning liquids, shampoo, baby powder, and bags with handles, HDPE does not break easily and is resistant to chemicals. In addition, containers made from HDPE also have good properties for preventing moisture transmission [5, 6]. Therefore, this research chose to mix HDPE with mortar to reduce water absorption, increase mortar strength, and help with sound absorption.

4. fine river sand

5. Brick block size 0.07 x 0.19 x 0.39 m

6. Ready-made cement



**Figure 1** High-density polyethylene plastic waste.

### Test procedure

1. Testing the specific gravity of Type 1 Portland cement according to ASTM C188 [7].

2. The proportion of mortar, cement, sand, and water equals 1: 2.75: 0.485. Then, the high-density polyethylene (HDPE) plastic is mixed in the ratio of 2.5%, 5%, and 10% by weight to replace some amount of sand, as shown in Table 1.



**Figure 2** Briquette mold.

7. Density test of mortar mixed with plastic waste according to the standard test method of ASTM C642.

8. Curing 6 mortar blocks of every ratio of each type at the test ages of 7 days, 14 days, and 28 days.

9. Comparing the results of the study of mechanical properties with a tensile tester of concrete test samples at various mixed ratios to find the best and most appropriate properties.

10. Fire test according to the ASTM E119 standard for plaster mortar walls mixed with High-Density Polyethylene (HDPE) plastic [12].

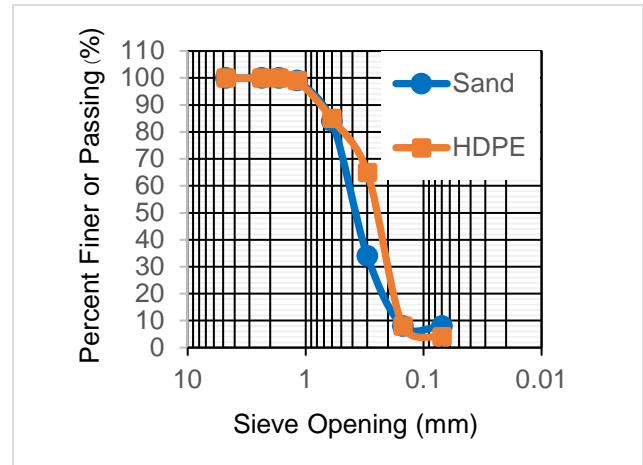
#### Test method

1. Testing the physical properties of cement, fine sand, and HDPE plastic waste.

##### 1.1 Testing the specific gravity of cement

The specific gravity of cement is the ratio of the weight of cement to the weight of water with an equal volume of cement. The specific gravity of Portland cement has a value of approximately 3.00 to 3.20, depending on the composition and fineness of the cement. In general, Portland cement type 1 has a value of approximately 3.15. The specific gravity of the cement indicates its composition and fineness [13].

1.2 Analyzing mix size and the fineness modulus of fine aggregate according to the ASTM C136, as shown in Figure 3 [14].



**Figure 3** Mix size and fineness modulus of fine aggregate.

1.3 Testing the specific gravity and absorption of fine aggregate (Specific Gravity and Absorption of Aggregate) according to the ASTM C642 [15].

1.4 Testing the flow of mortar (Table 2) to find the flow rate of cement mortar and cement paste using a flow test table with accessories according to ASTM C230 standards.

1.5 Density test for mortar mixed with plastic waste (Table 2) according to the ASTM C642 standard [16].

**Table 2** Density, water absorption, and fluidity values of mortar.

Sample	Plastic percentage (%)	Density value (g/cm <sup>3</sup> )	water absorption (%)	Mortar flow (mm)
Reference	0.00	2.04 + 0.09	1.98	101.18 + 0.59
HDPEM2.5	2.50	1.10 + 0.05	6.83	104.23 + 2.68
HDPEM5	5.00	1.69 + 0.03	7.42	102.16 + 0.57
HDPEM10	10.00	1.65 + 0.02	7.91	106.26 + 1.93

##### 2. Testing for tensile strength

The American standard test for tensile strength is the briquette of mortar, which consists of 1 part of cement and 3 parts of standard sand by weight. The sample briquette block used for this test is large at both ends and has a middle cross-section of 1 square inch. The amount of water used in the mix is calculated from the normal consistency of that type of cement.



**Figure 4** Mortar tensile strength test.

After casting the mold and curing according to specified standards, testing was done to determine the tensile strength when the test blocks were of

different ages, namely 7, 14, and 28 days. The tensile force used in the test must be applied uniformly at a rate of approximately 265 -285 kg/min. The average value of the tensile strength obtained must not be less than the values specified in the standard (which are 10, 20, and 25 kilograms per square centimeter) when the test bars are 7, 14, and 28 days old, respectively, as shown in Figure 4 [17].

where

$$F_c = \frac{P}{A} \quad (1)$$

$F_c$  = ultimate tensile strength; the unit is kc.

$P$  = tensile force, the units are kg.

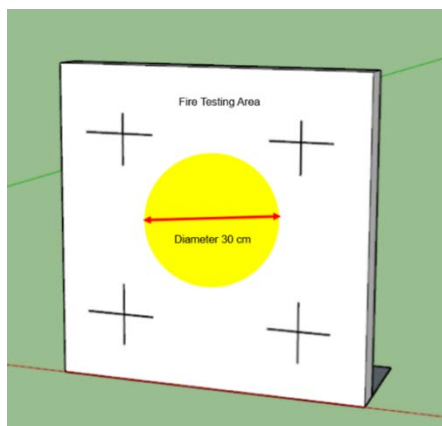
$A$  = Cross-sectional area of the sample bar, the unit is cm<sup>2</sup>.

##### 3. Plastered Wall Flammability Test

Combustion is a chemical reaction in which combustible material oxidizes with oxygen, releasing heat and converting it to oxide compounds or by-products. The complete combustion of fuel includes carbon dioxide and water. Incomplete combustion

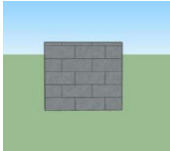



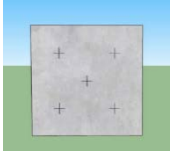





causes wasted fuel and air pollution. Therefore, knowing the principles of the combustion process and how to control complete combustion is very important for energy conservation and environmental protection. In addition, understanding the causes of heat loss in various forms of heat systems and equipment, along with prevention guidelines, will help improve the system's overall thermal energy efficiency to a higher level as well.



**Figure 5** Components of fire testing of plaster walls.

**Table 3** Procedures for fire testing of plaster walls.

No.	Model	Working characteristics
1		
2		
3		
4		

4. Procedure for testing the flammability of plaster walls

4.1 Building a 1 meter x 1 meter concrete block wall [18].

4.2 Plastering the walls with plaster mortar mixed with plastic waste in ratios of 0%, 2.5%, 5%, and 10% by weight instead of some sand.

4.3 Measuring in a circle with a diameter of 30 centimeters, as shown in Figure 5.

4.4 Installing gas torch burning equipment by measuring the plaster mortar wall to a distance of 5 centimeters.

4.5 Burning standard plaster mortar walls and mortar mixed with 2.5, 5, and 10 percent HDPE plastic waste by burning and analyzing the flammability of plaster walls at 30, 60, 90, and 120 seconds.

4.6 Comparing the fire characteristics of a standard mortar plaster wall with a plaster wall mixed with HDPE plastic waste. Details are as shown in Table 3 [19].

## RESULTS AND DISCUSSION

### Test results and discussion

This experimental study investigates investigate the possibility of using plastic waste, including high-density polyethylene (HDPE), for engineering purposes. The research results were obtained by collecting relevant information and conducting experiments in a laboratory.

### Test results

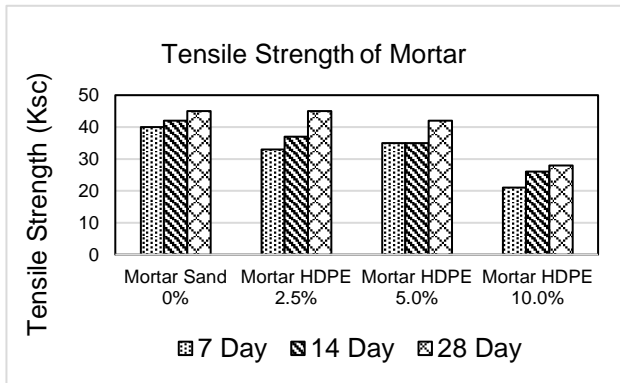
#### 1. Tensile strength test results

The tensile strength properties of mortar mixed with HDPE plastic waste decreased proportionately with increased plastic waste. This is because HDPE plastic particles are of various sizes and shapes, primarily small and delicate. The tensile strength of HDPEM2.5, HDPEM5, and HDPEM10 are equal to 45 ksc, 42 ksc, and 28 ksc, respectively, by the calculation formula (1). However, after 28 days, the tensile strength of HDPEM2.5 containing the lowest HDPE amount is equivalent to that of standard mortar, as shown in Table 4 and Figure 6.

From the test results of the tensile strength of mortar mixed with high-density polyethylene plastic in various amounts, it was shown that when comparing the general mortar with the mortar mixed with polyethylene plastic, the sample of 2.5% plastic mixed at the age of 28 days, was able to bear a tensile strength of 45 ksc, which has the same tensile test value as that of most common mortars. The high-density polyethylene plastic waste in the amount of 2.5% mixed in place of sand does not reduce its strength and helps to reduce the amount of sand used.

**Table 4** Examples of tensile strength test averages.

Sample	Tensile strength (ksc)		
	7 Day	14 Day	28 Day
Mortar Sand 100%	40	42	45
Mortar HDPE 2.5%	33	37	45
Mortar HDPE 5%	35	35	42
Mortar HDPE 10%	21	26	28

**Figure 6** Tensile strength of plaster mortar mixed with HDPE plastic waste.

## 2. Results of the fire test of mortar walls

The flammability test of mortar walls mixed with high-density polyethylene plastic waste was performed with a gas torch by burning for 30, 60, and 120 seconds. The flammability characteristics of standard plastered mortar walls with mortar mixed with high-density polyethylene plastic waste are compared, as shown in Table 5 [20].

**Table 5** Mortar wall flammability test.

Sample	Time		
	30 seconds	60 seconds	120 seconds
Mortar Sand 100%			
Mortar HDPE 2.5%			
Mortar HDPE 5%			
Mortar HDPE 10%			

The flammability test of the wall of mortar mixed with high-density polyethylene plastic in quantities of 2.5%, 5%, and 10%, was done with a burning period

of 30 seconds, 60 seconds, and 120 seconds and with a 5 cm distance from the fire head to the wall. Images were taken, indicating that red stains began to appear during the first 30 seconds of burning. The red stains would expand only slightly until dark stains appeared. The higher the ratio of plastic used in place of sand and the longer the burning time, the more black marks appeared on the wall. However, there was no evidence of ignition or flames in the mortar plaster wall mixed with polyethylene plastic waste in all the ratios.

## Discussion

The number of fine particles passing through sieves 50 and 100 affects fresh concrete's pourability, make-up, and greasiness (Bleeding), where the small particles allow the mortar to mix well. Therefore, the appropriate amount of fine particles is at least 15 percent passing through a No. 50 sieve and at least 5 percent through a No. 100 sieve. An amount greater than 5 percent of the particles to pass through a No. 200 sieve is not recommended because more water is used for mixing, and there is a high rate of change and contraction. The fineness of the aggregate can be seen from the fineness modulus (Fineness Modulus, F.M.) value. The fine aggregate suitable for the concrete mixture is between 2.30 - 3.20, with a lower value indicating more excellent fineness. According to the tests and analyses of the mixed sizes of two types of aggregate, namely sand and HDPE plastic, it is found that the F.M. values of sand and HDPE plastic are equal to 2.75 and 2.39, respectively, which are values within the excellent range [21].

The water absorption value affects the pourability of the mortar, as the dry aggregate absorbs water from the mortar mix, causing the mortar to lose some water and the pouring ability to be lower than designed. On the other hand, if the moisture content of the aggregate exceeds the saturation level, the dry surface will dehydrate the mortar mixture, causing the mortar to become too watery and making the water-to-cement ratio (w/c ratio) higher than designed, resulting in a low strength of the mortar. The experiment suggests that the water absorption value of the mortar mixed with HDPE plastic waste is higher than the standard. The water absorption values of HDPEM2.5, HDPEM5, and HDPEM10 are equal to 6.83%, 7.42%, and 7.91%, respectively, which is higher than standard mortar, which is equal to 1.98%. It can be seen that there is higher water absorption when the amount of HDPE plastic in the mortar increases; this is because the crushed HDPE plastic particles are small and spherical, causing the structure of the mortar to be porous despite the HDPE plastic properties, which have a low water absorption value. As a result of particle characteristics and the ability to absorb water, which is a unique property of each type of plastic, mortar mixed with HDPE plastic has higher water absorption than standard mortar [22].

The density of the material affects the strength and performance of mortar mixed with plastic waste. This is because the density value decreases in proportion to the percentage of plastic replacing sand, which in turn varies with the amount of HDPE plastic waste. The density value of mortar mixed with HDPE plastic waste increases proportionally due to the mixed size of the aggregate, as the aggregate has excellent and weighty particles. The densities of HDPEM2.5, HDPEM5, and HDPEM10 are equal to  $1.10 \text{ g/cm}^3$ ,  $1.69 \text{ g/cm}^3$ , and  $1.65 \text{ g/cm}^3$ , respectively, and affect the mortar's strength properties. The density of mortar mixed with HDPE plastic waste is noted to be lower than that of standard mortar [23].

The mortar flow test is the first step in designing the mix for casting the mortar sample. This gives an idea of the liquidity of the mixture ratio for use. The flow rate value in the test aligned with the standard. It was found that the value went between 100 - 115 percent of the water used, indicating the appropriate amount of water used in casting the mortar samples. The appropriate spread rate of the mortar mixed with HDPE plastic waste was within the specified standards. The flow spread values of HDPEM2.5, HDPEM5, and HDPEM10 mortars equal 104.23 percent, 102.16 percent, and 106.29 percent, respectively.

Briquette mold mortar samples mixed with HDPE plastic waste of size  $7.5 \text{ cm} \times 2.5 \text{ cm} \times 4.5 \text{ cm}$ , thickness 2.5 cm, were tested for tensile strength. Six samples of each type of mixture, at 7, 14, and 28 days of curing, were sampled and tested for the tensile strength exerted on the cross-sectional area of the mortar sample. The results suggest that the mortar mixed with HDPE plastic waste decreases tensile strength properties because HDPE plastic particles are of mixed sizes have small particles and acceptable density. From the tensile strength test at 28 days, the tensile strengths of HDPEM2.5, HDPEM5, and HDPEM10 were 45 ksc, 42 ksc, and 28 ksc, respectively. It should be noted that the HDPEM 2.5 mortar at 28 days (45 ksc) has the same value as standard mortar, showing the efficiency in supporting lateral loads and the cracking behavior of the mortar that will be used in construction. Another facet of the experiment showed that replacing sand with high-density polyethylene plastic waste could increase the tensile strength, as shown in Table 4. Still, it is recommended that the amount not exceed 10% to comply with the mortar tensile strength standards. (Cement mortar samples aged 28 days must not be less than  $25 \text{ kg/cm}^2$  (ksc). The trend indicates that replacing high-density polyethylene plastic waste decreases the tensile strength [24].

Comparing the fire characteristics of standard mortar plaster walls with mortar mixed with HDPE plastic waste, it was found that the flames on the standard mortar plaster walls did not change their original color from the gas torch, but the flame characteristics of the mortar wall mixed with HDPE

plastic waste had a spreading characteristic. The color of the flame turned orange. This is because the mixture is explosive and easily creates heat around the walls, resulting in the color change. As the proportion of plastic waste increased, the walls got more serious burns and were left with more black stains on the surface. Various proportions of sand replacement and the duration of the fire test at the same distance did not affect the flammability time or the damage from burning on the cement surface [25].

## CONCLUSIONS

The study's findings indicate that the inclusion of HDPE plastic waste has an impact on both the tensile strength and flammability of mortar walls. The selection of HDPE plastic was based on its high density, chemical resistance, and heat resistance, which make it well-suited for the intended uses. The research suggests the potential for using different types of plastic waste to further investigate their effects on the tensile strength and flammability of plastered mortar walls. This approach aligns with efforts to enhance the physical and mechanical properties of cement while promoting environmentally friendly construction materials by reducing natural sand usage and plastic waste in the environment.

## ACKNOWLEDGEMENT

This dissertation was accomplished with the help and advice of Asst. Prof. Dr. Maneerat Khemkhao, Asst. Prof. Dr. Teerin Kongpun and Asst. Prof. Dr. Apised Suwansaard, who kindly provided advice in conducting research and testing tools to study the behavior of tensile strength and flammability of plaster mortar walls mixed with high-density polyethylene plastic waste. The appreciation also goes to the civil engineering department of the faculty of engineering, Rajamangala University of Technology Rattanakosin, for its facility to use tools and equipment in this experiment. I would like to thank civil engineering students who helped with the testing until the research was completed successfully.

## REFERENCES

1. Bhogayata A, Arora N. Feasibility study on using metalized plastic waste in concrete. In: Proceedings of Conference on International Congress and Exhibition. 2018 Jul 1; Springer; 2017. p. 328-37.
2. Batayneh M, Marie I, Asi I. Use of selected waste materials in concrete mixes. Waste Manage. 2007; 27(12):1870-6.
3. Badache A, Benosman A, Senhadji Y, Mouli M. Thermo-physical and mechanical characteristics of sand-based lightweight composite mortars



- with recycled high-density polyethylene (HDPE). *Constr Build Mater.* 2018;163:40-52.
4. Apised S, Teerin k, Maneerat k. Properties of Mortar Composites from Plastic Waste. *Journal of Applied Science and Engineering.* 2021;25(1): 59-70.
  5. Menten D, Nagy G, Szab T, Hornyk E, Fiser B, Viskolcz B, et al. Combustion behavior of plastic waste - A case study of P.P., HDPE, PET, and mixed PES-EL. *J Clean Prod.* 2023;402:136850.
  6. Chen Y, Awasthi A, Wei F, Tan Q, Li J. Single-use plastics: production, usage, disposal, and adverse impacts. *Sci Total Environ.* 2021;752:141772.
  7. Pichetsilpa K. A Guideline for Building Wall System to Improve Thermal Performance [dissertation]. Bangkok: Chulalongkorn University; 2002.
  8. ASTM C136-06, Standard Test Method for Sieve Analysis of Fine and Coarse Aggregates. West Conshohocken, PA: ASTM International; 2006.
  9. ASTM C642-13, Standard Test Method for Density, Absorption, and Voids in Hardened Concrete. West Conshohocken, PA: ASTM International; 2013.
  10. ASTM C230/C230 M-14, Standard specification for flow table for use in tests of hydraulic cement. West Conshohocken, PA: ASTM International; 2014.
  11. ASTM C190, Standard test method for Tensile Strength of hydraulic cement mortars. West Conshohocken, PA: ASTM International; 1985.
  12. Rongviriyapanich O. Chemical physical and mechanical properties of oven-dried mortar after fire exposure [dissertation]. Bangkok: Chulalongkorn University; 2012.
  13. Nibudey N, Nagarnaik B, Parbat K, Pande M. A model for compressive strength of PET fiber reinforced concrete. *American Journal of Engineering Research (AJER).* 2013;2(12):367-72.
  14. Posee V, Suhaya H, Abedeen D. Heat transfer of non-load-bearing interlocking block with mixture of Para Rubber wood fly ash. *J Res Unit Sci Technol Environ.* 2013;4(1):1-6.
  15. Panthapulakkal S, Sain M. Injection-molded short hemp fiber/glass fiber-reinforced polypropylene hybrid composites - Mechanical, water absorption and thermal properties. *J Appl Polym Sci.* 2007; 103:2432-41.
  16. Chen C, Yang Y, Zhou Y, Xue C, Chen X, Wu H, et al. Comparative analysis of natural fiber reinforced polymer and carbon fiber reinforced polymer in strengthening of reinforced concrete beams. *J Clean Prod.* 2020;263(2):121572.
  17. Hung CC, Chang JN, Wang HY, Wen FL. Effect of adding waste polyethylene and GGBFS on the engineering properties of cement mortar. *Appl Sci.* 2022;12:12665.
  18. Chumnandee K. A comparison of insulation installation on the inside and outside of walls for cooling energy efficiency [dissertation]. Bangkok: Chulalongkorn University; 2011.
  19. Qamar F, Thomas T, Ali M. Improvement in lateral resistance of mortar-free interlocking wall with plaster having natural fibres. *Constr Build Mater.* 2020;234:117387.
  20. Garas G, Allam M, Mamdouh K. Straw bale fire test on cement plaster mixes. *WIT Trans Built Env.* 2009;108:51-9.
  21. Suwan T, Wattanachai P. Properties and internal curing of concrete containing recycled autoclaved aerated lightweight concrete as aggregate. *Adv Mater Sci Eng.* 2017;8:1-11.
  22. Rupasinghe N, Sathiparan N. Mechanical behavior of masonry strengthened with coir fiber reinforced hydraulic cement mortar as surface plaster. *Journal of Structural Engineering & Applied Mechanics.* 2019;2(1):12-24.
  23. Yatim M, Mohammadhossein H. Evaluation of the effective mechanical properties of concrete composites using industrial waste carpet fiber. *Springer Link INAE Lett.* 2017;2:1-12.
  24. Meng B, Xu J, Lou C, Gu C, Peng G. Effect of water content on tensile properties of cement mortar. In: 2018 International Conference on Civil and Hydraulic Engineering; 2018 Nov 23-25; p. 189-98.
  25. Triantafillou T, Karlos K, Kefalou K, Argyropoulou E. An innovative structural and energy retrofitting system for URM walls using textile reinforced mortars combined with thermal insulation. Mechanical and fire behavior, *Constr Build Mater.* 2017;133:1-13.





## The fabrication of wood alternative material from cassava rhizome and cassava peel pulp

Nichapha Minaboon<sup>1</sup>, Prachoom Khamput<sup>2</sup>, Kongpop Watcharasawe<sup>3</sup> and Attapole Malai<sup>3\*</sup>

<sup>1</sup>Department of Facility Management, Faculty of Architecture and Design, Rajamangala University of Technology Rattanakosin, Nakhon Pathom 73170, THAILAND

<sup>2</sup>Department of Civil Engineering, Faculty of Engineering, Rajamangala University of Technology Thanyaburi, Pathum Thani 12110, THAILAND

<sup>3</sup>Department of Civil Engineering, Faculty of Engineering, Rajamangala University of Technology Rattanakosin, Nakhon Pathom 73170, THAILAND

\*Corresponding author: attapole.mal@rmutr.ac.th, prachoom\_k@rmutt.ac.th

### ABSTRACT

The increasing demand for wood alternative material in construction and furniture. Corresponds to global efforts to reduce pressure on forests, necessitating the exploration of alternative materials to wood. The agricultural industry can not only supply raw materials from non-wood plants but also waste material and byproducts. The aim of this research was to explore and manufacture wood alternatives using cassava rhizomes and cassava peels, thereby valorizing agricultural waste. The research methodology involved blending milled rhizomes and cassava peels with urea-formaldehyde resin followed by a hot-pressing process to form the final product. The samples size for this study was 450x450x10 mm were made using 6-10 percent urea-formaldehyde resin by weight of the composite materials aiming to achieve a sheet density about 600 kg/cu-m. Three distinct ratios of Cassava rhizome to cassava peel pulp were examined as potential wood substitutes. All test results of sample were compared with the industrial standards outlined in Thai Industrial Standard. The study found that wood substitutes created from Cassava rhizome and Cassava peel pulp combined with urea-formaldehyde resin could meet the set standards. Cassava rhizome improves important properties like density, moisture content, thickness swelling, formaldehyde content, modulus of rupture, and modulus of elasticity according to TIS 876-2547 standards. However, adding peel pulp tends to reduce these qualities. There is no significant change in the density of the wood-alternative materials. However, a 10% urea formaldehyde content improves the mechanical properties. The study found that wood substitutes created from Cassava rhizome and Cassava peel pulp combined with urea-formaldehyde resin could meet the set standards. Moreover, the production cost of these wood substitute materials was lower than the prevailing market prices. This study disseminates knowledge from research that utilizes cassava rhizomes and peels to create sheet like wood substitute materials. Using modern methods and appropriate technologies, cassava rhizomes and peels can be transformed into a diverse range of wood substitute products, and capable of effectively competing with wood and other materials in the future.

**Keywords:** Cassava rhizome, Cassava peel pulp, Wood-alternative material

### INTRODUCTION

The demand for wood panels in buildings and furniture increases and with global concerns over forest conservation, so worldwide need to find different materials that can replace wood [1-3, 5-7]. This aligns with a growing need for living space, driving the demand for building and furniture materials [2]. With increasing global demand for environmentally friendly products, forests are under significant pressure as they are a primary source of renewable materials [3]. Agricultural waste materials have the potential to be recycled into practical natural wood substitutes which can help generate income and employment opportunities within

the local community through the production of these materials [4]. However, they generally possess a lower density compared to wood [5]. This offers the advantage of producing low-density composites. Therefore, the use of alternative materials in panel manufacturing is only feasible to a certain extent in conjunction with wood. Alternatively, greater quantities of adhesives are necessary to achieve the desired mechanical strength level of the panels [1]. Urea-formaldehyde (UF) resin is widely used as an adhesive in the manufacture of wood-alternative materials due to its excellent bonding performance and cost-effectiveness. Products like particleboard, medium-density fiberboard (MDF), and hardwood plywood are commonly fabricated with

UF resin as a binder, providing them with significant mechanical strength and durability [6]. The ratio of urea to formaldehyde in UF resins significantly impacts the performance and properties of wood alternative products. A balanced ratio optimizes the adhesive's durability, water resistance, and mechanical strength while simultaneously minimizing formaldehyde emissions [7].

Cassava, or *Manihot esculenta*, thrives in tropical and subtropical regions and is cultivated for its starchy root known as the cassava rhizome. Rich in starch and carbohydrates, it serves as a crucial food source for millions globally [8]. The "Cassava peel pulp" is the waste left after peeling and processing the cassava root for human or industrial use. It consists of cassava peels and leftover root parts and is known for its high fiber and carbohydrate content. Traditionally, people have used it as animal feed because it is nutritious [9]. Researchers have recently uncovered new potential uses for cassava, including biofuel production and as a raw material for eco-friendly, wood-alternative products. These discoveries show how important it is to use all parts of the cassava plant, turning waste into valuable materials that can help with sustainable development and protect the environment. Cassava, scientifically known as *Manihot esculenta*, holds a crucial role in Thailand's agriculture. Thailand is the world's largest exporter of cassava products, making a significant impact on the global cassava market [10]. The main processing of cassava revolves around its rhizome, or root, which is rich in starch. This starch finds wide applications in various industries, including food, feed, and biofuel production. Due to extensive cassava processing, Thailand generates a large amount of cassava peel pulp as a byproduct. In the past, these peels were considered waste or used as inexpensive animal feed. However, recently, there is growing recognition of their potential to be transformed into valuable products [11]. By utilizing cassava peel pulp, which is abundant in carbohydrates and fiber, as a raw material for eco-friendly wood substitutes, Thailand aligns with the concept of a circular economy. This approach turns waste into wealth and promotes environmental sustainability [12]. The diverse uses of cassava emphasize the importance of this resource, showcasing the benefits of both economic value addition and waste management in Thailand's cassava industry.

This study is focused on the exploration and fabrication of wood substitute materials from cassava rhizomes and cassava peel pulp, which includes conducting physical and chemical properties tests, studying fiber morphology of samples, physical test and evaluating their mechanical properties. All observed properties are associated with the industry standard TIS 876-2547 [13]. chemical properties. This research is marking the first venture into this specific field of study.

## MATERIALS AND METHODS

The use of wood and alternative materials, either alone or blended with wood fibers or chips, in panel production has been widely researched over recent decades. These materials have been utilized as raw inputs in fiberboard or particleboard manufacturing, often combined with different adhesives in varying quantities. Panels produced from these combinations were assessed based on their mechanical and physical properties, including internal bond strength, modulus of elasticity, modulus of rupture, thickness swelling, and water absorption.



**Figure 1** Characteristics of wood substitute materials from rhizomes and cassava peel.

**Table 1** The symbols representing the samples tested.

Sample symbol	Cassava rhizome (%)	Cassava peel (%)	Urea formaldehyde (%)
R1P0-6	100	0	6
R1P0-8	100	0	8
R1P0-10	100	0	10
R0P1-6	0	100	6
R0P1-8	0	100	8
R0P1-10	0	100	10
R6P4-6	60	40	6
R6P4-8	60	40	8
R6P4-10	60	40	10

Note: R= Cassava rhizome, P= Cassava peel

In research on the development of substitutes for natural wood from waste materials in cassava fields, there is a study of the types and quantities of adhesives as well as the conditions required to produce wood substitute materials. Test methods are available for evaluating chemical properties, fiber morphology, and enlarged images of cassava rhizomes and peels. Additionally, the produced wood-based panels are tested for density, moisture content, thickness swelling, modulus of rupture, and modulus of elasticity. It was tested according to the industrial standard TIS 876-2547 as well as studying the economic cost of forming sheets using urea formaldehyde in the amounts of 6, 8, and 10% as the adhesive. The fibers from cassava rhizome and cassava pulp were evaluated for their

morphological characteristics following established standards. Fiber length was measured using the ISO 16065-1 standard, while the coarseness of the fibers was determined using the ISO 23713 standard. The produced sheet has a size of 450x450x10 mm, and the specified sheet density is 600 kg/cu-m. It was tested for chemical, physical, and mechanical properties according to the industrial standard TIS 876-2547. The preliminary molding experiments results showed that using cassava stock at concentrations below 60% hinders the proper formation of the workpiece. This is likely due to the lack of sufficient bonding, which affects the material's stability and cohesion. The wood substitute used in the study had 3 mixing ratios: cassava stock: cassava peel 100: 0, 0: 100, and 60: 40. Properties of substitute materials derived from rhizomes and cassava peels used as wood alternatives as to shown in Figure 1. Table 1 displays the symbols representing the samples that were utilized for testing and discussion.

## RESULTS AND DISCUSSION

This research is a study of the development of substitutes for natural wood from waste materials in cassava fields. The wood substitute materials were used to study the physical and mechanical properties, as

well as the economic costs. The research results can be summarized as follows:

### *Chemical properties test results*

The results of the study on chemical properties and fiber size of cassava rhizomes and cassava peels. The study delved into the compositional characteristics of cassava by examining samples of waste material sourced from cassava fields, including both rhizomes and peels.

These samples were dried at 105°C for 24 hours to assess their chemical properties, specifically the cellulose and lignin content. Following the drying process, they were finely ground and the cellulose and lignin were extracted using the detergent method. Several studies have investigated using cassava waste like rhizomes and peels to extract cellulose and nanocellulose.

Widiarto et al. extracted these from cassava peels, resulting in nanofibers with unique properties [14]. Pasquini et al. extracted cellulose whiskers from cassava bagasse a byproduct of cassava starch production using them to reinforce natural rubber [15]. These studies show the potential of cassava waste for making cellulose and nanocellulose useful in various industries. Table 2 presents the results of the chemical property tests conducted on rhizomes and cassava peels.

**Table 2** Test results of chemical properties of rhizomes and cassava peels.

Chemical Properties		Testing method	Cassava rhizome	Cassava peels
- Chemical Properties	% as received	[16]	5.63	3.69
- Ash content	% as pulp	[17]	24.28	16.35
- Acid-insoluble Lignin	% as pulp	[18]	56.80	35.01
- Holocellulose	% as pulp	[19]	24.56	11.23

The results of the chemical composition of cassava rhizome and cassava pulp showed that the cassava rhizome contained 5.63% of ash while the cassava pulp contained 3.69% of ash. Cassava rhizomes contained 24.28% of acid-insoluble lignin, while cassava pulp contained 16.35% of acid-insoluble lignin. Cassava rhizomes contained 56.80% holocellulose, while cassava pulp contained 35.01% holocellulose. Cassava rhizomes

contained 24.56% of cellulose, while cassava pulp contained 11.23% of cellulose.

In conclusion, cassava is a plant that has high holocellulose, cellulose, and lignin contents suitable for hot pressing processing due to the amount of the above 3 substances mixed with the filler (binder). It will make the wood panels have the strength to hold together in sheets suitable for forming synthetic wood sheets used in the general market.

**Table 3** Fiber morphology test results of cassava rhizome and cassava peel samples.

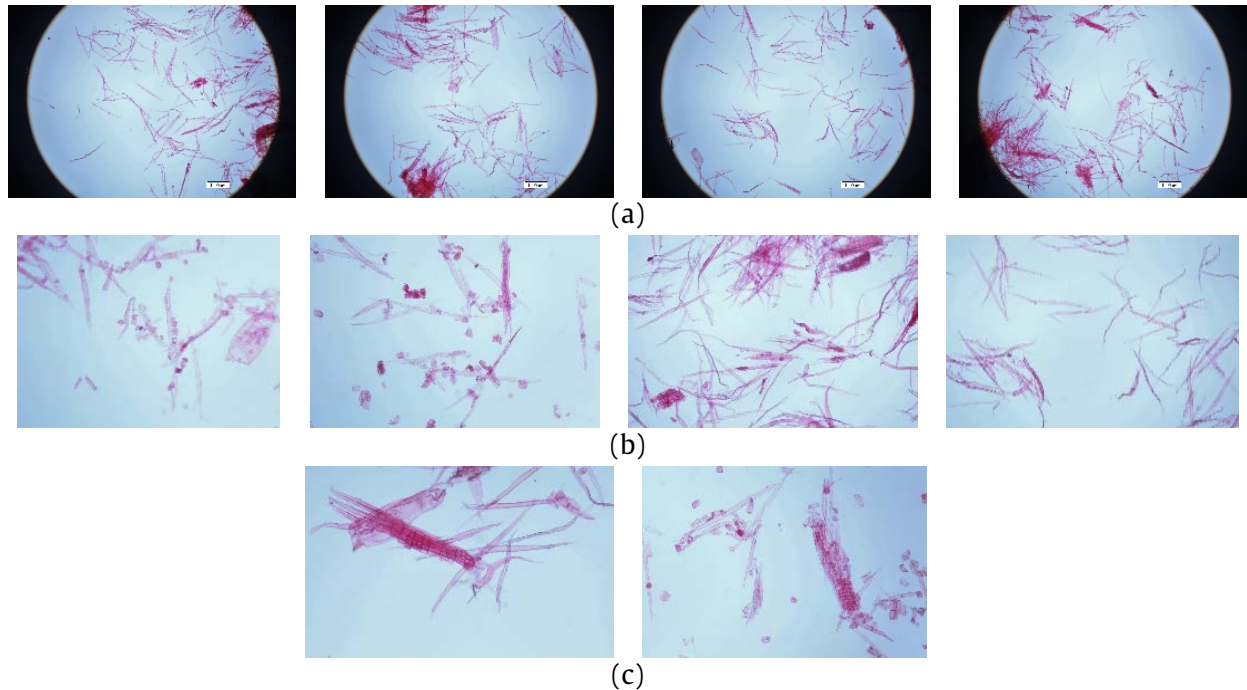
Pulp properties	Unit	Testing method	Cassava rhizome	Cassava peels
Pulp yield				
(Soda pulp AA20% H-factor 1300)	% as received	-	27.79	13.68
Pulp Reject	% as receive	-	1.816	0.003
Length-weighted Fiber Length	mm	[20]	0.659	0.496
Fines	% as pulp	[20]	44.90	73.60
Fiber width	µm	[20]	35.25	35.15
Fiber coarseness	Mg/m	[21]	0.133	0.701



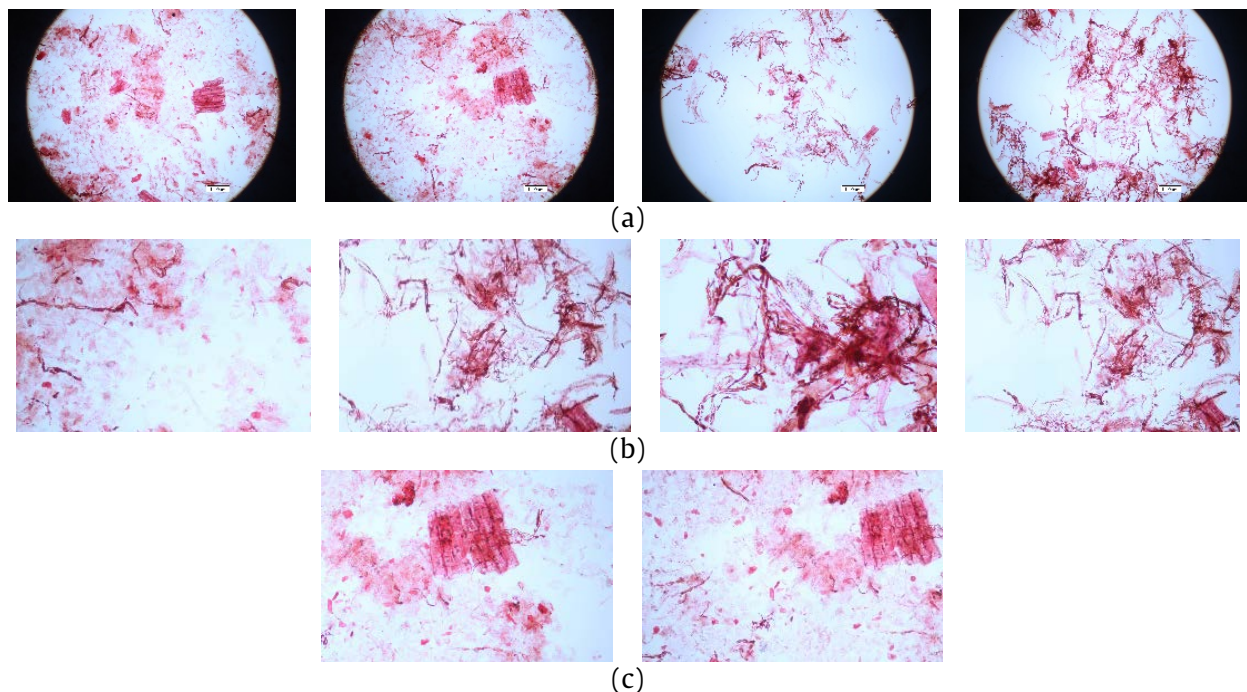
### *Fiber morphology test results of cassava rhizome and cassava peel samples*

The fibers from cassava rhizome and cassava pulp were analyzed for fiber morphology, utilizing specific standards. The ISO 16065-1 standard was

employed to measure fiber length [20], while the ISO 23713 standard was used to gauge the coarseness of the fiber length [21]. Table 3 exposed test results reveal the fibrous morphology of samples derived from cassava rhizomes and cassava peels.



**Figure 2** Enlarged images of cassava rhizome pulp: (a) at 4x magnification, (b) at 10x magnification, (c) at 20x magnification.



**Figure 3** Enlarged images of cassava peel pulp: (a) at 4x magnification, (b) at 10x magnification, (c) at 20x magnification.

Based on analysis with ISO 16065-1, which is a standard for measuring fiber length found that cassava rhizome contained fiber length at 0.659 mm, while cassava peel contained fiber length at 0.496 mm.

The analysis of ISO16065-1, which is a standard for measuring fiber length found that the fines of cassava rhizome have 44.90%, while the fines of cassava peel have 73.60%.



The analysis of ISO 16065-1, which is a standard for measuring fiber length found that fiber width of cassava rhizome is at 35.25  $\mu\text{m}$ , while fiber width of cassava peel is at 35.15  $\mu\text{m}$ . The analysis of ISO 23713 which is the length measurement of fiber coarseness found that fiber coarseness of cassava rhizome weighs 0.133 mg/m, while fiber coarseness of cassava peel weighs 0.701 mg/m. Figure 2 illustrates cassava rhizome pulp, and Figure 3 demonstrates the pulp of cassava peel in magnifications of 4, 10, and 20 times.

#### Physical test results

The produced wood-based panels were tested for physical properties in terms of density, moisture content and thickness swelling in accordance with the standard of flat pressed particleboard industry TIS 876-2547.

#### Density test results

The density of a fabricated wood-alternative material refers to its mass per unit volume. These materials are often designed to mimic the appearance and function of wood but may be composed of various substances like plastics, resins, recycled wood fibers, and other additives. The density of these materials can vary widely depending on their composition and the manufacturing process used. The key points related to the density of wood-alternative materials are composition, manufacturing process and application-specific.

In this study, the density test at moisture content between 6-9% for a sample size 450x450x10 mm, which is the proportion of mass with moisture to the volume of specimen at moisture content. The samples are first weighed, and their thickness is measured at the diagonal intersection point. Measurements of b1 and b2 are taken at two points parallel to the sample's edge, along lines passing through the center of opposing edges. Density is then calculated using Equation (1):

$$\rho = \frac{m}{b_1 \cdot b_2 \cdot t} \quad (1)$$

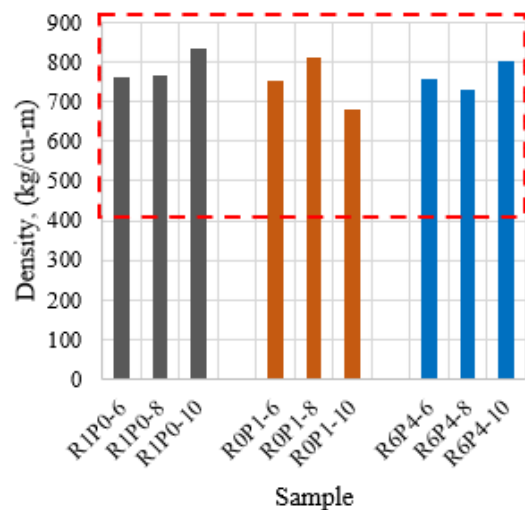
where

$\rho$  = density ( $\text{kg}/\text{m}^3$ )  
 $m$  = mass (kg)  
 $t$  = thickness (m)  
 $b_1$  and  $b_2$  = dimension of edges (m)

The adhesive content can pass the specified standard value, which is the density value of 400-900  $\text{kg}/\text{cu-m}$  because the property of cassava rhizome and cassava peel can absorb water well according to the standard criteria as shown in Figure 4.

#### Moisture content test results

Moisture content (MC) of wood refers to the amount of water present in the wood, expressed as a percentage of the weight of the oven-dry wood.



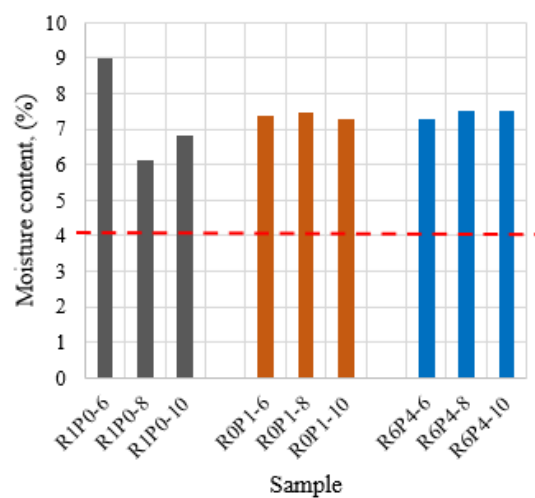
**Figure 4** Test results pertaining to the densities of the three distinct sample groups.

It is a critical parameter in many aspects of wood science, processing, and utilization because the physical and mechanical properties of wood can change significantly with variations in moisture content. The moisture content test measures the weight of moisture in the sample dimensions 450x450x10 mm relative to its dry weight. This contains baking the sample in an oven at  $103 \pm 2^\circ\text{C}$  for 24 hours. The moisture ratio is calculated using Equation 2.

$$w = ((m_v - m_s) / m_s) \times 100 \quad (2)$$

where

$w$  = moisture content (%)  
 $m_s$  = dry mass (g)  
 $m_v$  = humid mass (g)



**Figure 5** Moisture content between the quantity of adhesive in each ratio.

Figure 5 shown the wood substitute materials from cassava rhizome and cassava peel, all ratios pass the standard criteria, which has a moisture content value between 4 -1 3%. It was found that the ratio of cassava rhizome: cassava peel, R1P0-6 (100:0, UF 6%),

has a highest moisture content, and the ratio of cassava rhizome: cassava peel, R1P0-8 (100:00, UF 8%) has a lowest moisture content. It can be determined that every component of wood-based panels from cassava rhizome and cassava peel, when physically tested, it was found that it was in the standard criteria.

### Thickness Swelling test results

Thickness Swelling (TS) refers to the increase in thickness of a material when it absorbs moisture. This term is often associated with wood-based materials, such as particleboard, fiberboard, and plywood, but can also apply to other porous materials.

When these materials come into contact with water or high humidity, they can absorb the moisture, causing the individual fibers or particles to expand. This results in an increase in the thickness of the material, known as thickness swelling. Thickness swelling can be a concern in construction and manufacturing, as it may lead to changes in the dimensions and properties of the material. It may cause warping, deformation, and loss of mechanical strength, potentially affecting the functionality and appearance of the product. In this study, the Thickness Swelling test was conducted on an average of 5 samples, which were submerged in clean water with pH  $7 \pm 1$ , at a temperature of  $20 \pm 1$  °C and must remain submerged in  $25 \pm 5$  mm of water for 24 hours. The percentage of thickness swelling was determined using Equation 3:

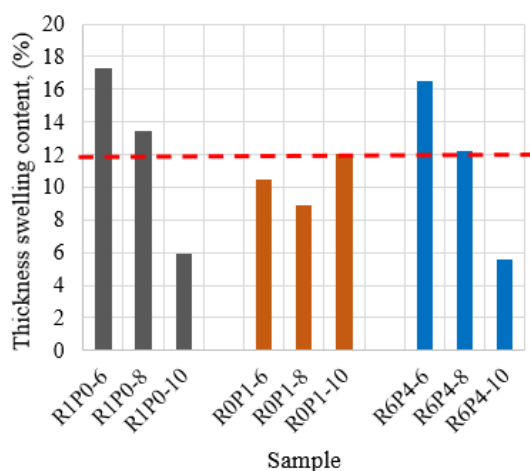
$$G_t = \frac{(t_2 - t_1)}{t_1} 100 \quad (3)$$

where

$G_t$  = thickness swelling 24h (%)

$t_1$  = initial thickness (mm)

$t_2$  = final thickness after 24h (mm)



**Figure 6** Thickness swelling result between the amount of adhesive in each ratio.

The physically of wood-based panels from cassava rhizome and cassava peel in every component found that it passed the standard criteria for 4 components and did not pass the standard criteria for 5 components.

Sheets that contain a minimum of 6% urea-formaldehyde E2 have higher properties than sheets that use a large amount of it. High-density test strips had low swelling and moisture content but had high mechanical properties, with 10% urea-formaldehyde E2 adhesive having the highest density as shown in Figure 6. It was found that four formulations met the specified standards: R1P0-10, R1P1-6, R1P1-8, and R6P4-10. Generally, increasing the amount of urea-formaldehyde in the mixture results in reduced swelling.

### Mechanical properties test results

The produced wood-based panels were tested for mechanical properties, Modulus of rupture (MOR), Modulus of elasticity (MOE), Tensile strength perpendicular to the surface value, and Formaldehyde content in accordance with the standard of flat pressed particleboard industry TIS 876 -2547.

### Modulus of rupture and modulus of elasticity

The Modulus of Rupture is a measure of a material's tensile strength. It represents the maximum stress that a material can withstand before failure in bending. The Modulus of Elasticity, also known as Young's Modulus, describes how a material deforms under stress. It's a measure of the material's stiffness in the elastic region (i.e., the range where deformation is reversible). MOR is related to the material's strength, specifically its resistance to bending until failure. MOE, on the other hand, is related to the material's stiffness and its ability to resist deformation within the elastic range.

In static bending tests for determining modulus of elasticity (MOE) and modulus of rupture (MOR), rectangular samples with a width ( $b$ ) of  $50 \pm 1$  mm are utilized. The length ( $l$ ) equals 20 times the nominal thickness plus 50 mm. Specimens are conditioned until reaching a constant weight at a relative moisture of  $(65 \pm 5)$  % and a temperature of  $20 \pm 2$  °C. Constant weight is attained when two consecutive weighing, separated by at least 24 hours, show a difference of no more than 0.1% from the initial sample weight.

Modulus of elasticity in bending strength (MOE) is then computed using Equation 4, with the mean value derived from samples taken from the same panel.

$$MOE = ((l^3 \cdot (F_2 - F_1)) / (4 \cdot b \cdot t^3 \cdot (a_2 - a_1))) \quad (4)$$

$l$  = distance between the support centers (mm);

$b$  = sample width (mm)

$t$  = sample thickness (mm)

$F_2 - F_1$  = force increase, Newton, in the rectilinear section of the force-arrow curve,

where  $F_1$  should be about 10% and  $F_2$  about 40% of the rupture force;

$a_2 - a_1$  = increase of corresponding arrow  $F_2 - F_1$ .

The MOR value of each sample, given in N/mm<sup>2</sup>, is calculated by Equation 5. Each set of samples taken from the same panel gives the mean value to MOR:

$$\text{MOR} = (3 \cdot F_{\max} \cdot l_1) / (2 \cdot b \cdot t^2) \quad (5)$$

$F_{\max}$  = Rupture force (N)

$l_1$  = distance between support centers (mm)

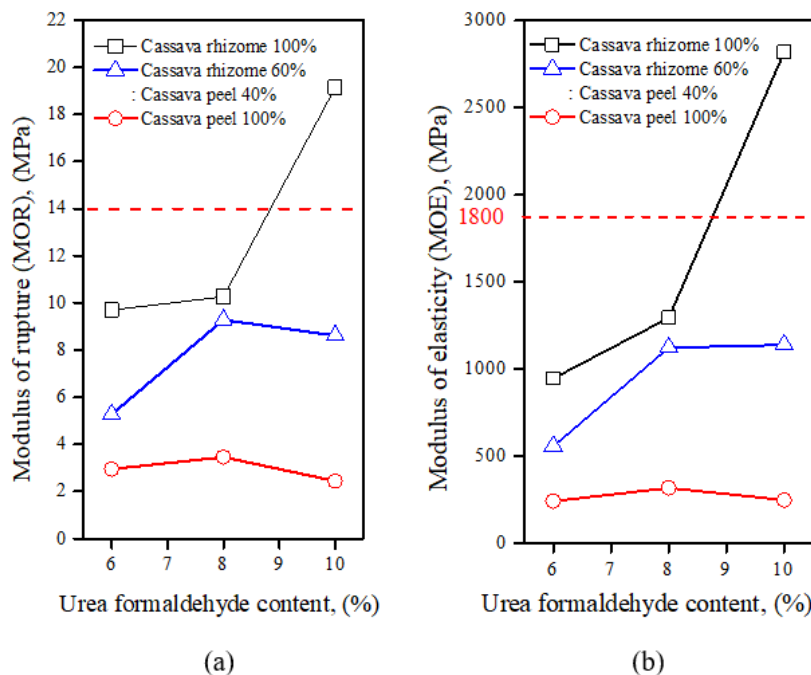
$b$  = sample width (mm)

$t$  = sample thickness (mm)

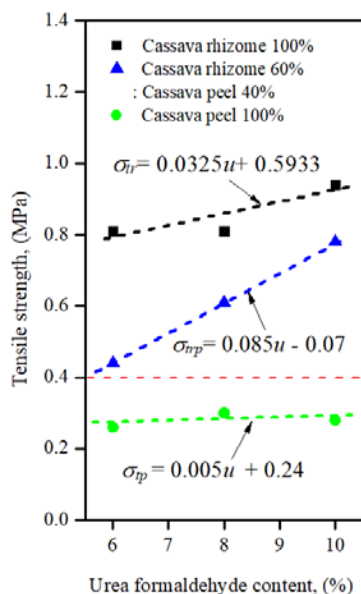
Figure 7 illustrates the variation in Modulus of Rupture and Modulus of Elasticity of a sample with different urea formaldehyde content levels. The black curve represents the sample containing pure cassava

rhizome, the red curve illustrates the sample containing pure cassava peel, and the blue curve depicts a mixture of 6 parts cassava rhizome to 4 parts cassava peel. The sample with pure cassava rhizome exhibited the highest MOR and MOE values, in contrast to the sample containing pure Cassava peel, which had the lowest values. Cassava rhizome used as a pure material with 10% urea formaldehyde is the only ingredient that meets the criteria specified in TIS 876-2547.

The modulus of rupture and modulus of elasticity are higher when cassava rhizome is the primary ingredient. In contrast, using cassava peel as a composite material yields lower test results.



**Figure 7** The sample with different urea formaldehyde content levels: (a) Variation in Modulus of Rupture (MOR), (b) Modulus of Elasticity (MOE).



**Figure 8** Tensile strength of samples varied in relation to urea formaldehyde content.

### Tensile strength test results

The dumbbell-shaped specimens were prepared following ASTM D3500 [22] standards, with dimensions set at a length of 400 mm, a width of 48 mm, and a narrowed middle section width of 25 mm to ensure typical tensile failure mode occurrence.

Tensile strength and urea-formaldehyde (UF) content are vital factors in the fabrication of wood-alternative materials. Tensile strength refers to the ability of the material to withstand pulling or stretching forces without breaking. UF resin is a common adhesive used in the production of wood-alternative products like particleboard and medium-density fiberboard (MDF). Urea-formaldehyde resin offers strong bonding properties, making it suitable for binding wood fibers and other lignocellulosic materials together.

Figure 8 exposed the tensile strength of the samples varied in correlation with the urea-formaldehyde content. The fabrication of wood-alternative materials

utilizing pure cassava rhizome resulted in the highest tensile strength. This was followed by a mixture comprising 6 parts cassava rhizomes to 4 parts cassava peel, with pure cassava peel exhibiting the lowest tensile strength among the tested compositions. The research findings align with studies on agricultural materials combined with formaldehyde [23 -25].

The tensile strength of wood-alternative materials fabricated from cassava rhizome and cassava peel is determined by Equations 6 to 8:

$$\sigma_{tr} = 0.0325u + 0.5933 \quad (6)$$

$$\sigma_{tp} = 0.085u - 0.07 \quad (7)$$

$$\sigma_{tp} = 0.005u + 0.24 \quad (8)$$

where

$\sigma_{tr}$  is tensile strength of materials from pure cassava rhizome.

$\sigma_{tp}$  is tensile strength of materials from a mixture comprising 6 parts cassava rhizomes to 4 parts cassava peel.

$\sigma_{tp}$  is tensile strength from pure cassava peel.

$u$  is urea formaldehyde content ( $6\% \leq u \leq 10\%$ )

**Table 4** Formaldehyde content test results.

Property	Unit	Testing Result
Formaldehyde Emission (After corrective 6.5%MC.)	Mg/100g ODB	15.76

**Table 5** Criteria and methods formaldehyde quantity.

Quality level	Criteria	Methods
1	Not over 8 mg/100g	[26]
	Not over 0.5 mg/1 (E0)	[27]
	Over 0.5 mg/1 - 1.5g/1 (E1)	[27]
2	Over 8 mg/100 g - 30 mg/100 g	[26]
	Over 1.5 mg/1 - 5.0 mg/1 (E2)	[27]

Note: E0 E1 E2 means Formaldehyde Emission quantity  
Source: The industrial standard TIS. 876-2547

#### Formaldehyde content test results

In this research, the sheet material was tested for formaldehyde content by using 10% of urea-formaldehyde E2 at a sheet thickness of 10 mm and a specified density of 600 kg/cu-m in accordance with the standard of flat pressed. The formaldehyde content test generated a result of 15.76 mg/100g, as presented in Table 4. The testing method for formaldehyde content used in this research is outlined in Table 5. When compared with criteria and formaldehyde content test method by using the Perforator by BS EN 120 found that wood-based panels at the ratio of cassava rhizome: cassava peel R1P0-10 had met the standard of flat pressed particleboard industry TIS 876 -2547. The test result

showed that the formaldehyde content of wood-based panels at the ratio of cassava rhizomes: cassava peel R1P0-10 is in the 2nd quality level with a criteria of formaldehyde content which is over 8 mg/100 g to 30 mg/100 g using Perforator by BS EN 120.

#### Results of studies on economic costs

Based on the cost estimate from an economic analysis of the production of wood-based panels from cassava rhizome and cassava peel the ratio of cassava rhizome: cassava peel as 100:0, UF 10% which is a mixture ratio that meets physical and mechanical properties according to industrial standard. The economic cost analysis consists of the cost of tools and equipment, chemicals and raw materials, electricity, labor and other materials used in the production of wood-based panels from cassava rhizome and cassava peel with a width of 450 mm, a length of 450 mm and a thickness of 10 mm. The total cost of producing wood-based panels of this study concluded that wood-based panels from cassava rhizome and cassava peel using urea formaldehyde is 42.68 baht/sheet, which was lower than the market price when compared to the price of construction materials.

**Table 6** Cost of manufacturing tools and equipment for Cassava Rhizome and Peel Pulp Wood-Alternative Material.

Manufacturing tools and equipment	Price (Thai baht)
1. Hydraulic hot press equipment	85,000
2. Hot press assembly machinery set	30,000
3. Biomass shredding device	45,000
4. Grinder for cassava rhizomes and peels	4,500
5. Equipment for mixing and spraying glue	20,000
6. Circular saw table	15,000
7. Air pump	8,000
8. Balance	4,500
9. Urea-formaldehyde adhesive e2	2,000
10. Other	2,000
Total cost price	216,000

Note: All of the price is the purchasing price in 2022.

Table 6 illustrates that the production cost of wood substitute panels made from cassava rhizomes and bark is significant, involving an initial investment of around 216,000 baht. With a lifespan of 10 years, there are also enduring maintenance expenses amounting to 25,000 baht annually.

## CONCLUSION

Agricultural waste materials offer a sustainable alternative for wood-based panel production, as they



originate from renewable sources and can replace wood chips and fibers partially or entirely. These materials share physical and mechanical properties similar to wood, which facilitates their integration into industrial manufacturing processes for wood panels. Their compatibility with traditional methods provides a practical solution for reducing reliance on wood resources while promoting environmentally friendly practices.

This paper details the fabrication of wood-alternative material using pure cassava rhizome, pure cassava peel pulp, and a blend of cassava rhizome with cassava peel pulp, all bound together with urea formaldehyde. The test results demonstrated that the mixture R1P0-10, consisting solely of cassava rhizome with 10% urea formaldehyde as a binder, successfully met the standards of the TIS 876-2547 test. The characteristics of the sample boards can be summarized as follows.

1. Cassava rhizome contributes to enhancing the desirable properties in accordance with TIS 876-2547, while cassava peel pulp tends to reduce those properties.

2. In the range of 6-10% urea formaldehyde content, there is no noticeable increase or decrease in the sample density of the wood-alternative materials. However, when the urea formaldehyde content reaches 10%, it leads to an enhancement in the mechanical properties of the product. This observation underscores the importance of optimizing the urea formaldehyde concentration to achieve desired structural characteristics in the fabrication of wood-alternative materials.

3. In this study, it was discovered that pure cassava peel is a material that does not enhance tensile strength to meet the standard. Therefore, this material should be discarded prior to the fabrication of artificial wood panels.

Therefore, composites made from cassava rhizome should present a highly competitive alternative to traditional wood-based composites, potentially becoming a significant agricultural product in the future. Cassava rhizome is a wood substitute and an agricultural waste. It has properties similar to natural wood but has not yet been used in industrial applications. Its utilization could help reduce waste and decrease pollution from incineration.

### ACKNOWLEDGEMENT

This research project was supported by the cluster administration and the research program in research management of the National Science and Technology Development Agency, the fiscal year 2015. The research team would like to thank the cluster administration and the research program in research management of the National Science and Technology Development Agency for providing support in conducting this research. We would like to express our gratitude to Rajamangala University of Technology Rattanakosin

for providing the facilities necessary to conduct this research.

### REFERENCES

1. Neitzel N, Hosseinpourpia R, Walther T, Adamopoulos S. Alternative materials from agro-industry for wood panel manufacturing-a review. *Materials* [Internet]. 2022;15(13):4542. Available from: <https://doi.org/10.3390/ma15134542>.
2. UNFPA. Population Data Portal [Internet]. 2022. Available from: <https://pdp.unfpa.org/>.
3. Ceccherini G, Duveiller G, Grassi G, Lemoine G, Avitabile V, Pilli R, et al. Abrupt increase in harvested forest area over Europe after 2015. *Nature*. 2020;583(7814):72-7.
4. Aoonchittichai W. Wood - Substitute Composite. Bangkok: Wood Industry Development Group, Forest Research and Development Office, Royal Forest Department; 2012.
5. Müller C, Schwarz U, Thole V. On the utilization of agricultural residues in the wood-based panel industry. *Eur J Wood Wood Prod* [Internet]. 2012;70(5):587-94. Available from: <https://doi.org/10.1007/s00107-011-0589-0>.
6. Pizzi A, Mittal KL. Principles of polymer networking and gel theory in thermosetting adhesive formulations. In: Pizzi A, Mittal KL, editors. *Handbook of adhesive technology*, revised and expanded. 2nd ed. Boca Raton: CRC Press; 2003.
7. Dunky M. Urea-formaldehyde (UF) adhesive resins for wood. *Int J Adhes Adhes* [Internet]. 1998;18(2):95-107. Available from: [https://doi.org/10.1016/S0143-7496\(97\)00054-7](https://doi.org/10.1016/S0143-7496(97)00054-7).
8. Montagnac JA, Davis CR, Tanumihardjo SA. Nutritional value of cassava for use as a staple food and recent advances for improvement. *Compr Rev Food Sci Food Saf* [Internet]. 2009;8(3):181-94. Available from: <https://doi.org/10.1111/j.1541-4337.2009.00077.x>.
9. Aro SO. Potential contribution of cassava peels to dietary fiber intake of Nigerians. *Food Nutr Sci*. 2010;1(1):1-5.
10. Srzednicki G. Cassava: A versatile and sustainably produced crop. In: *Cassava*. Cham: Springer; 2018. p. 1-6. Available from: <https://doi.org/10.5772/intechopen.72166>.
11. Sriroth K, Piyachomkwan K, Wanlapatit S, Oates CG. Cassava starch technology: the Thai experience. *Starch-Stärke* [Internet]. 2000;52(12):439-49. Available from: [https://doi.org/10.1002/1521-379X\(200012\)52:12<439::AID-STAR439>3.0.CO;2-E](https://doi.org/10.1002/1521-379X(200012)52:12<439::AID-STAR439>3.0.CO;2-E).

12. Sricharoenchaikul V, Atong D. Development of fuel briquettes from biomass lignin mixtures. *Mater Sci Forum*. 2008;587:133-8.
13. Thai Industrial Standards Institute (TISI). Medium density fiberboard industrial standards. TIS.876-2547. Bangkok: Ministry of Industry; 2004.
14. Widiarto S, Pramono E, Suharso R, Rochliadi A, Arcana IM. Cellulose nanofibers preparation from cassava peels via mechanical disruption. *Fibers*. 2019;7(5):44. Available from: <https://doi.org/10.3390/FIB7050044>.
15. Pasquini D, de Morais Teixeira E, da Silva Curvelo AA, Belgacem MN, Dufresne A. Extraction of cellulose whiskers from cassava bagasse and their applications as reinforcing agent in natural rubber. *Ind Crops Prod*. 2010;32(3):486-90. Available from: <https://doi.org/10.1016/j.indcrop.2010.06.022>.
16. TAPPI T211 om-07. Ash in wood, pulp, paper and paperboard: combustion at 525°C. Test method T 211 om-22. Technical Association of the Pulp and Paper Industry; 2009.
17. TAPPI T222 om-02. Acid insoluble lignin in wood and pulp. Norcross: TAPPI Press; 2002.
18. Wies FA. Diseases of the retina. *Yale J Biol Med*. 1946;19(1):137.
19. Updegraff DM. Semimicro determination of cellulose in biological materials. *Anal Biochem*. 1969;32(3):420-4. Available from: [https://doi.org/10.1016/S0003-2697\(69\)80009-6](https://doi.org/10.1016/S0003-2697(69)80009-6).
20. ISO 16065-1. Determination of fiber length by automated optical analysis-part 1; polarized light method. Geneva: International Organization for Standardization; 2001.
21. ISO 23713. Specifies a method for determining fiber coarseness using polarized light. Geneva: International Organization for Standardization; 2005.
22. American Society for Testing and Materials. Standard test methods for structural panels in tension. D3500-90. ASTM; 2003.
23. Antov P, Savov V, Krišťák Ľ, Réh R, Mantanis GI. Eco-friendly, high-density fiberboards bonded with urea-formaldehyde and ammonium lignosulfonate. *Polymers*. 2021;13(2):220. Available from: <https://doi.org/10.3390/polym13020220>.
24. Hematabadi H, Behrooz R, Shakibi A, Arabi M. The reduction of indoor air formaldehyde from wood-based composites using urea treatment for building materials. *Constr Build Mater*. 2012;28(1):743-6. Available from: <https://doi.org/10.1016/j.conbuildmat.2011.09.018>.
25. Zhang J, Chen H, Pizzi A, Li Y, Gao Q, Li J. Characterization and application of urea-formaldehyde-furfural co-condensed resins as wood adhesives. *BioResources*. 2014;9(4):6267-76. Available from: <https://doi.org/10.15376/biores.9.4.6267-6276>.
26. BS EN 120:1984 re 1992. Standard addition recovery test: wood-based panels determination of formaldehyde content extraction method called the perforator method. London: British Standards Institution; 1992.
27. JIS A 5908:2003. Japanese industrial standard particle board. Tokyo: Japanese Standard Association; 2003.



## Phytochemical screening and toxicity assessment of compounds isolated from the leaves of *Mangifera indica* L. for the control of *Spodoptera litura* (Lepidoptera; Noctuidae)

Poonnanan Phankaen<sup>1</sup>, Vasakorn Bullangpoti<sup>2</sup>, Wanchai Pluempanupat<sup>3</sup>, Chatwadee Saiyaitong<sup>4</sup>, Parinthorn Temyarasilp<sup>5\*</sup> and Nutchaya Kumrungsee<sup>6\*</sup>

<sup>1</sup>Valaya Alongkorn Rajabhat University under the Royal Patronage Sa Kaeo, Valaya Alongkorn Rajabhat University under the royal patronage Pathum Thani, Pathum Thani 13180, THAILAND

<sup>2</sup>Animal Toxicology and Physiology Speciality Research Unit, Department of Zoology, Faculty of Science, Kasetsart University, Bangkok 10900, THAILAND

<sup>3</sup>Center of Excellence for Innovation in Chemistry and Special Research Unit for Advanced Magnetic Resonance, Faculty of Science, Department of Chemistry, Kasetsart University, Bangkok 10900, THAILAND

<sup>4</sup>Institute of Research and Development, Rajamangala University of Technology Thanyaburi, Pathum Thani 12110, THAILAND

<sup>5</sup>Chemistry Program, Faculty of Science and Technology, Valaya Alongkorn Rajabhat University under the royal patronage Pathum Thani, Pathum Thani 13180, THAILAND

<sup>6</sup>Biology Department, Faculty of Science and Technology, Rajamangala University of Technology Thanyaburi, Pathum Thani 12110, THAILAND

\*Corresponding author: parinthorn@vru.ac.th, Nutchaya\_k@rmutt.ac.th

### ABSTRACT

This study aimed to analyze the phytochemical composition and antioxidative capabilities of mango leaves (*Mangifera indica* L., Nam Dok Mai), indigenous to Sa Kaeo Province, Thailand. Various solvents with differing polarities, including *n*-hexane, DCM, ethyl acetate, and MeOH, were utilized for leaf extraction. The findings revealed the existence of eight groups of phytochemical compounds: alkaloids, flavonoids, coumarins, saponins, tannins, terpenoids, steroids, and cardiac glycosides. The MeOH crude extract exhibited the highest concentration of total phenolic compounds at 409.88 ± 0.02 mg GAE/g. Furthermore, the MeOH crude extract demonstrated the strongest antioxidant activity, with an IC<sub>50</sub> value of 0.52 ± 0.02 µg/ml, as determined by the DPPH method. High-performance liquid chromatography (HPLC) was employed to identify gallic acid and mangiferin in the MeOH crude extract. Laboratory tests were conducted using the topical application method to evaluate the toxicity of the *M. indica* leaf crude extract on 2nd instar *Spodoptera litura* larvae. The MeOH crude extract exhibited high efficacy, with an LD<sub>50</sub> value of 10.58 µg per larvae within 24 hours. Gallic acid and mangiferin were identified as the primary active ingredients, with LCD<sub>50</sub> values of 1.19 µg per larvae and 1.90 µg per larvae, respectively, within 24 hours. Additionally, the impact on detoxification enzymes (24 hours post-treatment) was assessed in surviving 2nd instar *S. litura* larvae using the topical application method. The MeOH extract treatment resulted in 1.31-fold inhibition of carboxylesterase (CE), 1.31-fold inhibition of glutathione-S-transferase (GST), and 1.32-fold inhibition of acetylcholinesterase (AChE).

**Keywords:** *Spodoptera litura*, *Mangifera indica*, Phytochemicals, Biocides, Detoxification enzymes

### INTRODUCTION

The tobacco caterpillar, *Spodoptera litura* (Lepidoptera: Noctuidae), is a destructive insect that causes damage to more than 180 agricultural crops, including cotton, maize, sunflower, rice, cereal, and vegetables [1, 2]. Currently, conventional insecticides such as organophosphates, carbamates, deltamethrin, cypermethrin, chlorpyrifos, and prophenofos are being utilized to manage herbivorous insects like *S. litura*. However, the prolonged use of these insecticides

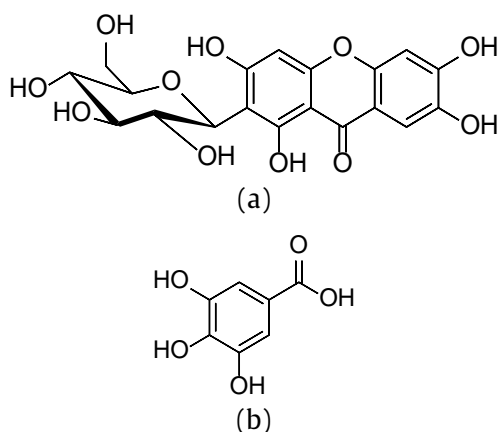
can lead to the development of resistance in insects. Additionally, using these chemicals poses risks to the ecosystem and non-target organisms. Therefore, developing natural insecticides promptly and reducing chemical contamination in the environment is crucial to exploring new strategic approaches for monitoring this insect.

Plant-derived phytochemicals, including extracts from *Piper ribesoides*, and *Acorus calamus*, as well as allelochemicals such as pinocembrin, pinostrobin,



methyl cinnamate, chrysin, pachypophyllin, and galangin, have been used to prevent lepidopteran insects such as *Spodoptera exigua* and *S. litura* [3-5]. Furthermore, plants possess a variety of secondary metabolites, such as alkaloids, phenolics, terpenoids, and polyacetates, which serve as biological defenses against herbivorous insects. These compounds exhibit a range of activities, including repelling insects, acting as antitumor agents, attracting food sources, and displaying antimicrobial properties [6].

Mango, scientifically known as *Mangifera indica* L., is a popular fruit that is widely cultivated in subtropical and tropical regions, including Thailand. In fact, Thailand is one of the world's top five exporters of the fresh mango variety Nam Dok Mai [7]. The leaves of *M. indica* have also been found to contain various secondary substances, such as phenolic acids, flavonoids, terpenoids, and carotenoids [8]. These extracts from *M. indica* have shown potential biological activities, including anti-allergic, antidiabetic, and antioxidant properties [9-10]. This study is the first to investigate the properties of *S. litura* larvae in Thailand, a major agricultural center known for its mango production and export. However, the production of mangoes also generates agro-industrial waste in the form of mango leaves and unripe fruits. Hence, the objective of this study is two-fold: to explore the potential utilization of mango waste as a biopesticide and to assess the larval eradication capabilities of *M. indica* extract and its allelochemicals against *S. litura* larvae through acute toxicity tests. Additionally, the study aims to examine the biochemical reactions triggered by the *M. indica* extract, particularly the activity of detoxification enzymes and neuronal enzymes such as carboxylesterase, glutathione-*S*-transferase, and acetylcholinesterase.



**Figure 1** Chemical Structures of (a) Mangiferin and (b) Gallic Acid.

Mangiferin (figure 1a) is a major component found in many species of mangoes. It is a phytochemical that has been found to have various biological activities, including anti-inflammatory, anti-oxidative, immune-modulatory, anti-obesity, anti-bacterial, anti-viral, anti-depression, and anti-diabetic properties [11-14]. It also

modulates the expression of key enzymes involved in inhibiting lipolysis and promoting fatty acid oxidation in the liver [15, 16]. Additionally, mangiferin has shown larvicidal activity against *Culex pipiens* L. [17].

Gallic acid (figure 1b) is a well-known polyphenol with antioxidant potential, making it an effective bioactive element in treating gastrointestinal diseases and oral health problems [18]. Furthermore, gallic acid exhibits the same larvicidal activity against *Culex pipiens* L. as mangiferin [19].

## MATERIALS AND METHODS

### Plant extraction

The leaves of *M. indica* were washed and dried in the shade. These samples were collected from Sa Kaeo province, Thailand in June 2022. A hot-air oven (Memmert UM300 oven) was used to dry the samples. Subsequently, a commercial blender (Zhejiang HC-2000Y) was used to powder the dried samples. A total of 257 g of *M. indica* leaf powder was obtained. For extraction, maceration was performed using different organic solvents (*n*-hexane, dichloromethane (DCM), ethyl acetate, and methanol (MeOH)) in a sequential 7-day process. Each extract was filtered through a suction filter connected to a vacuum pump. The resulting solutions were concentrated using a rotary evaporator (BÜCHI R-215). The percentage yield of each extract was calculated. The crude plant extracts were then stored at 4°C until further use in phytochemical detection and biological assays.

### Phytochemical screening

This study aims to identify the phytochemicals in Nam Dok Mai mangoes from Sa Kaeo and compare them with those cultivated in other regions.

**Alkaloids:** 0.20 g of crude extract was dissolved in 1 mL of a 10% ammonia solution and then extracted with 3 mL of DCM. The DCM was evaporated until it became dry, and the remaining residue was dissolved in 3 mL of diluted H<sub>2</sub>SO<sub>4</sub>. Mayer's reagent was added to the test tube, and the presence of alkaloids was indicated by observing an opalescent or yellow precipitate [18].

**Flavonoids:** A crude extract weighing 0.20 g was dissolved in 1 mL of 50% MeOH by heating. Then, magnesium metal and 5-6 drops of concentrated HCl were added to the solution. In this experiment, red represents flavanols, while orange represents flavone [18].

**Anthraquinone:** A total of 0.20 g of crude extract was dissolved in 4 mL of DCM and then heated in a steam bath for 5 minutes. The hot extract was filtered and allowed to cool. Afterward, an equivalent volume of 10% ammonia solution was added to the filtrate. When shaken, the upper aqueous layer turned a bright pink color, indicating the presence of anthraquinone [18].



**Coumarins:** A test tube with 0.2 g of crude extract was covered with filter paper. Then, a drop of 10% NaOH was added to the paper, and the mixture was heated in a water bath for 5 minutes. Next, the filter paper was examined under a 365 nm UV light, revealing a greenish-blue spot. This observation confirms the presence of coumarins [18].

**Saponins:** The crude extract (0.2 g) was vigorously shaken with 10 mL of deionized water for 5 minutes until it foamed. If the foam remains in the test tube after resting for 10 minutes, it indicates the presence of saponins [18].

**Tannins:** A few drops of a 5% FeCl<sub>3</sub> solution were added to the 0.2 g of crude extract. The presence of a green color indicated the presence of gallotannins [18].

**Terpenoids:** The crude extract weighing 0.2 g was mixed with 2 mL of DCM. Then, 3 mL of concentrated H<sub>2</sub>SO<sub>4</sub> was added to create a layered effect. The appearance of a red-brown color at the interface confirmed the presence of terpenoids [18].

**Steroids:** A total of 0.2 g of crude extract was dissolved in 5 mL of DCM. Then, 1 mL of acetic anhydride was added to the mixture. Next, 1 mL of concentrated H<sub>2</sub>SO<sub>4</sub> was carefully added to the side of the test tube, forming a distinct layer. The presence of steroids was indicated by the green color observed at the bottom of the test tube [18].

**Cardiac Glycosides:** A brown ring appeared between layers when a solution of glacial acetic acid (4.0 mL) containing 1 drop of 2.0% FeCl<sub>3</sub> was mixed with 0.2 g of crude extract and 1 mL of concentrated H<sub>2</sub>SO<sub>4</sub>. This brown ring represents the presence of cardiac steroidal glycosides [18].

#### *The contents of total phenolics, total flavonoids, and total tannin determination*

The Folin-Ciocalteu method was used to determine the total content. A 0.02 mL portion of a 2.0 mg/mL extract solution was combined with 0.2 mL Folin-Ciocalteu reagent and 2.0 mL of distilled water. After 3 minutes, 1.0 mL of sodium carbonate was added. The mixture was then incubated at room temperature for 20 minutes. The absorbance at 765 nm was measured using a microplate reader. The total phenolic content was calculated using a gallic acid standard curve. A stock standard solution of gallic

acid at a concentration of 1.0 mg/mL was prepared by dissolving gallic acid in distilled water. The results were reported as milligrams of gallic acid equivalent (mg GAE) per gram of extract [20].

The total flavonoid content of the extracts was determined using a modified version of the method described by Arvouet-Grand, Vennat, Pourrat, and Legret. Quercetin was prepared in MeOH to create the standard solutions. To measure the flavonoid content, 1.0 mL of sample (1.0 mg/mL) was mixed with 1 mL of 2% AlCl<sub>3</sub> in MeOH. The mixture was then incubated at room temperature for 10 minutes. The absorbance was measured at 415 nm using a microplate reader, with a blank sample consisting of 1 mL sample solution mixed with 1 mL of MeOH without AlCl<sub>3</sub>. A calibration line was created by plotting the absorbance against the quercetin concentration. The flavonoid content is expressed as quercetin equivalents (mg QE) per gram of extract [20].

Tannins were determined using the Folin-Denis method. An extract of approximately 0.1 mL was added to a volumetric flask with a total volume of 10.0 mL. This flask contained 7.5 mL of distilled water, 0.5 mL of Folin-Denis reagent, and 1.0 mL of 35% Na<sub>2</sub>CO<sub>3</sub>. The mixture was then diluted to a final volume of 10.0 mL with distilled water. After shaking the mixture, it was left at room temperature for 30 minutes. A standard solution of tannic acid was prepared in the same manner. The absorbance of both the assay and standard solution was measured at 700 nm against a blank using a microplate reader. The tannin content is as milligrams of tannic acid equivalent (mg TAE) per gram of the extract [20].

#### *DPPH radical-scavenging activity*

To evaluate the antioxidant activity of 2,2-diphenyl-1-picryl-hydrazyl (DPPH), we employed it as a free radical. Different concentrations of DPPH were prepared to ascertain IC<sub>50</sub>. The total volume in each well of the 96-well plate was 100 µL, comprising 90.0 µL of the DPPH solution and 10.0 µL of the crude extract solution. Using a microplate reader, the mixture was thoroughly blended and incubated at 37°C for 30 minutes to measure the absorbance at 517 nm. A negative control using a DPPH solution and a reference standard using Trolox were implemented. The DPPH scavenging activity percentage was calculated using equation (1).

$$\text{Inhibition (\%)} = \frac{(\text{Absorbance of control} - \text{Absorbance of sample}) \times 100}{\text{Absorbance of control}} \quad (1)$$

where the absorbance of the control represents the overall radical activity without an inhibitor, while the absorbance of the sample reflects the activity found in the sample extract [21].

#### *HPLC analysis of gallic acid and mangiferin*

The HPLC analysis of *M. indica* leaf extracts was characterized and identified using reverse phase

HPLC (HPLC 1100 Agilent). The separation was conducted on a Varian column (250 x 4.6 mm) with a C<sub>18</sub> guard column. Elution was performed on an isocratic system using a mixture of acetonitrile in 0.2% orthophosphoric acid (10:90, v/v). The flow rate was set at 1.2 mL/min, and the temperature was maintained at 40°C. The diode array detector was set to a wavelength of 242 nm, and the injection volume was 10 µL.

### *Insect maintains*

*S.litura* larval egg colonies were obtained from the National Center for Genetic Engineering and Biotechnology, Bangkok. The colonies were maintained in controlled laboratory conditions at  $26 \pm 2^\circ\text{C}$ , with a relative humidity of 60% to 75% and a photoperiod of 14 hours of light to 10 hours of darkness until the larvae hatched. Subsequently, the larvae were transferred to a new plastic box (25 x 15 cm) and were fed a modified artificial diet based on Pengsook [3]. This diet included commercial green bean powder (100 g; Raithip®), agar (10 g), ascorbic acid (1 g), sorbic acid (1 g) methylparaben (1.5 g), yeast (8.0 g), mixed vitamins (15 mL), formaldehyde (1 mL), and distilled water (600 mL). Pupae were then transferred to a net cage (45 x 40 cm, 45 cm high) for adult emergence, with wax paper sheets provided for moth oviposition. The adults were fed honey solutions consisting of a 30% sugar solution via cotton swabs. Daily, the egg colonies were collected and briefly immersed in a 10% formaldehyde solution (for 10 seconds) to prevent bacterial infection.

### *Larval bioassay*

The isolated compounds, mangiferin, and gallic acid, were utilized in this study. Leaf extract and active ingredients from *M. indica* were prepared using acetone. The solutions were applied topically to the 2<sup>nd</sup> instar *S. litura* larvae at a rate of 2  $\mu\text{L}$  per larva, with larvae prepared in three replicates ( $n = 90$ ). The larvae were transferred to a petri dish containing an artificial diet after exposure. The treated insects were maintained under laboratory conditions as described above. The acute toxicity of the compounds was assessed after 24 and 48 hours. Mortality was determined based on  $\text{LD}_{50}$  values using the STATPLUS program (Probit Analysis, version 2019).

### *Detoxification enzyme analysis*

**Enzyme source:** The enzyme source was prepared from *S. litura* larvae that survived for 24 hours. Nobsathian outlined the procedure for extracting the enzymes [22]. The larvae were homogenized in a microtube with a phosphate buffer (100 mM, pH 7.2) and triton x-100 (0.5%). After homogenization, the mixture was centrifuged at 12,000 rpm ( $4^\circ\text{C}$ ) for 15 minutes. The resulting supernatants were collected and stored at  $-20^\circ\text{C}$  for biochemical assays.

**General Esterase: Carboxylesterase (CE)** activity was determined using a modified procedure based on the method described by Nobsathian [22] and Kumrungsee [23]. To begin, 50  $\mu\text{L}$  samples of the enzyme were collected from the enzyme source and pre-incubated at  $30^\circ\text{C}$  for 30 minutes. A substrate homogenate was then prepared: para nitrophenyl acetate (10 mM, 50  $\mu\text{L}$ ) and phosphate buffer (50 mM, 3.0 mL). Next, the enzyme-substrate mixture was transferred to the 96-well microreader plates. CE

activity was measured at 400 nm for 3 minutes at  $25^\circ\text{C}$ . The enzyme activity was assessed in triplicates.

**Glutathione-S-transferase (GST):** To prepare GST, an enzyme solution (20  $\mu\text{L}$ ) was collected. The substrate solution consisted of 0.1 M phosphate buffer (pH 7.2, 1150  $\mu\text{L}$ ) with the addition of 1-chloro-2,4-dinitrobenzene (150 mM, 10  $\mu\text{L}$ ). The homogenized enzyme and substrate were mixed well. The enzyme activity was measured using a microplate reader in kinetic mode at an absorbance of 340 nm, at a temperature of  $25^\circ\text{C}$  for a duration of 3 minutes. Three biological replicates were analyzed.

**Acetylcholinesterase (AChE):** AChE activity was determined using the modified Ellman procedure [24]. The homogeneous substrate consisted of 100 mM phosphate buffer (pH 7.2; 50  $\mu\text{L}$ ), 5,5'-dithiobis (2-nitrobenzoic acid) with 0.1 M ethylenediamine tetraacetic acid and 100 mM acetylthiocholine-iodide. The enzyme solution was collected from the enzyme source and preincubated at  $30^\circ\text{C}$  for 30 minutes. The enzyme and substrate mixture solutions were homogenized, and the AChE reaction was measured at a wavelength of 412 nm. The enzyme activity was calculated using an extinction coefficient of  $1.36 \times 10^4 \text{ M}^{-1} \text{ cm}^{-1}$ . Three biological replicates were performed.

## RESULTS AND DISCUSSION

### *Plant extracts*

*M. indica* leaves were extracted using organic solvents in the following sequence: *n*-hexane, DCM, ethyl acetate, and MeOH. The extract with the highest amount was obtained using MeOH. The percentages of yield and their corresponding characteristics are listed in Table 1.

### *Phytochemical screening*

The preliminary phytochemical examination of *M. indica* leaf extracts was conducted using various solvents, as shown in Table 2. The results revealed the presence of flavonoids, coumarins, tannins, terpenoids, steroids, and cardiac glycosides in the whole-leaf extract. However, alkaloids and saponins were only found in the MeOH extract. Notably, anthraquinones were not found in any leaf extracts.

The variation in the phytochemical constituents of different extracts may be due to the use of different extraction solvents. This can affect the extraction of various bioactive compounds. An examination of the phytochemicals in *M. indica* extract reveals the presence of pharmacological constituents such as tannins, saponins, cardiac glycosides, flavonoids, steroids, and alkaloids. This research supports previous findings by Pintu [25], who also found tannins, alkaloids, steroids, glycosides, and flavonoids in *M. indica* leaf extract. However, this research differs from the finding of Olasehinde [26], who reported that steroids were not present in the leaf extracts obtained using water and ethanol. The content

of plant compounds in mango cultivars can vary depending on factors such as acid synthesis, degradation,

utilization, partitioning, and external factors like temperature, light, fertilization, and water supply [27].

**Table 1** Characteristic of *M. indica* leaf extracts and yield obtained from organic solvents through maceration.

Solvents used for extraction	Characteristics	Yield <sup>a</sup> of crude extract (%w/w)
<i>n</i> -hexane	Dark green and sticky	2.0241
DCM	Dark green and sticky	3.0600
Ethyl acetate	Dark green and sticky	2.9662
MeOH	Dark green and sticky	4.0084

<sup>a</sup>Yield of extracts was calculated as  $W/W_0 \times 100$  ( $W$  = Total weight of dried extract;  $W_0$  = Weight of the specimen of *M. indica* L. leaf after extractions).

**Table 2** Preliminary Phytochemical Screening of *M. indica* leaf extracts.

Phytochemical constituents	Solvent extract <sup>a</sup>			
	<i>n</i> -hexane	DCM	Ethyl acetate	MeOH
Alkaloids	-	-	-	+
Flavonoids	+	+	+	+
Anthraquinones	-	-	-	-
Coumarins	+	+	+	+
Saponins	-	-	-	+
Tannins	+	+	+	+
Terpenoids	+	+	+	+
Steroids	+	+	+	+
Cardiac Glycosides	-	-	+	+

<sup>a</sup> (+): presence, (-): absence of phytochemical

**Table 3** Contents of total phenolics, total flavonoids and total tannins in leaf extracts of *M. indica*.

Extracts	Total phenolics (mg GAE/g)	Total flavonoids (mg QE/g)	Total tannins (mg TAE/g)
<i>n</i> -hexane	9.63±0.00 <sup>a</sup>	250.93±0.08 <sup>a</sup>	7.82±0.00 <sup>a</sup>
DCM	22.59±0.00 <sup>b</sup>	284.24±0.03 <sup>b</sup>	18.46±0.00 <sup>a</sup>
Ethyl acetate	150.95±0.02 <sup>d</sup>	172.21±0.02 <sup>c</sup>	123.76±0.02 <sup>b</sup>
MeOH	409.88±0.02 <sup>c</sup>	158.77±0.03 <sup>c</sup>	336.34±0.02 <sup>c</sup>

Values (averages of three replicates) labeled with different letters indicate significant differences at  $p < 0.05$ .

#### Determination of total phenolics, total flavonoids and total tannins content

The total phenolic content was determined using the Folin-Ciocalteu method, which involves quantification of a blue chromophore formed through UV-Vis spectrophotometry at 765 nm. The results in Table 3 indicate the phenolic content in various extraction solvents. The content was expressed as milligrams of gallic acid equivalent per gram of extract (mg GAE/g). The total phenolic content ranged from 9.63 to 409.88 mg GAE/g in leaves, with the highest value observed in MeOH leaf extract (409.88±0.02 mg GAE/g), while the lowest content was found in the leaf extract using *n*-hexane (9.63±0.00 mg GAE/g).

The total flavonoid content was measured using aluminum chloride, based on forming acid-stabilized complexes between flavonoids and aluminum chloride,

with an absorption peak at 415 nm. The total flavonoid content was expressed in milligrams of quercetin equivalents per gram of extract (mg QE/g). As shown in Table 3, the total flavonoid content ranged from 158.77 to 284.24 mg QE/g. The DCM leaf extract found the highest content of 284.24(0.03 mg QE/g), while the lowest content of 158.77±0.03 mg QE/g was found in the MeOH leaf extract.

Total tannin content was determined using Folin-Denis with sodium carbonate. The Folin-Denis reagent reacts with tannins, forming a mixture of blue oxides that can be measured using UV-VIS spectrophotometry at an absorption peak of 700 nm. The total tannins were expressed in milligrams of tannic acid equivalent per gram of extract (mg TAE/g). As shown in Table 3, the total tannin content ranged from 7.82 to 336.34 mg GAE/g. The MeOH leaf extract had the highest tannin content extract (336.34±0.02mg TAE/g),

while the *n*-hexane leaf extract had the lowest ( $7.82 \pm 0.00$  mg TAE/g).

#### DPPH radical-scavenging activity

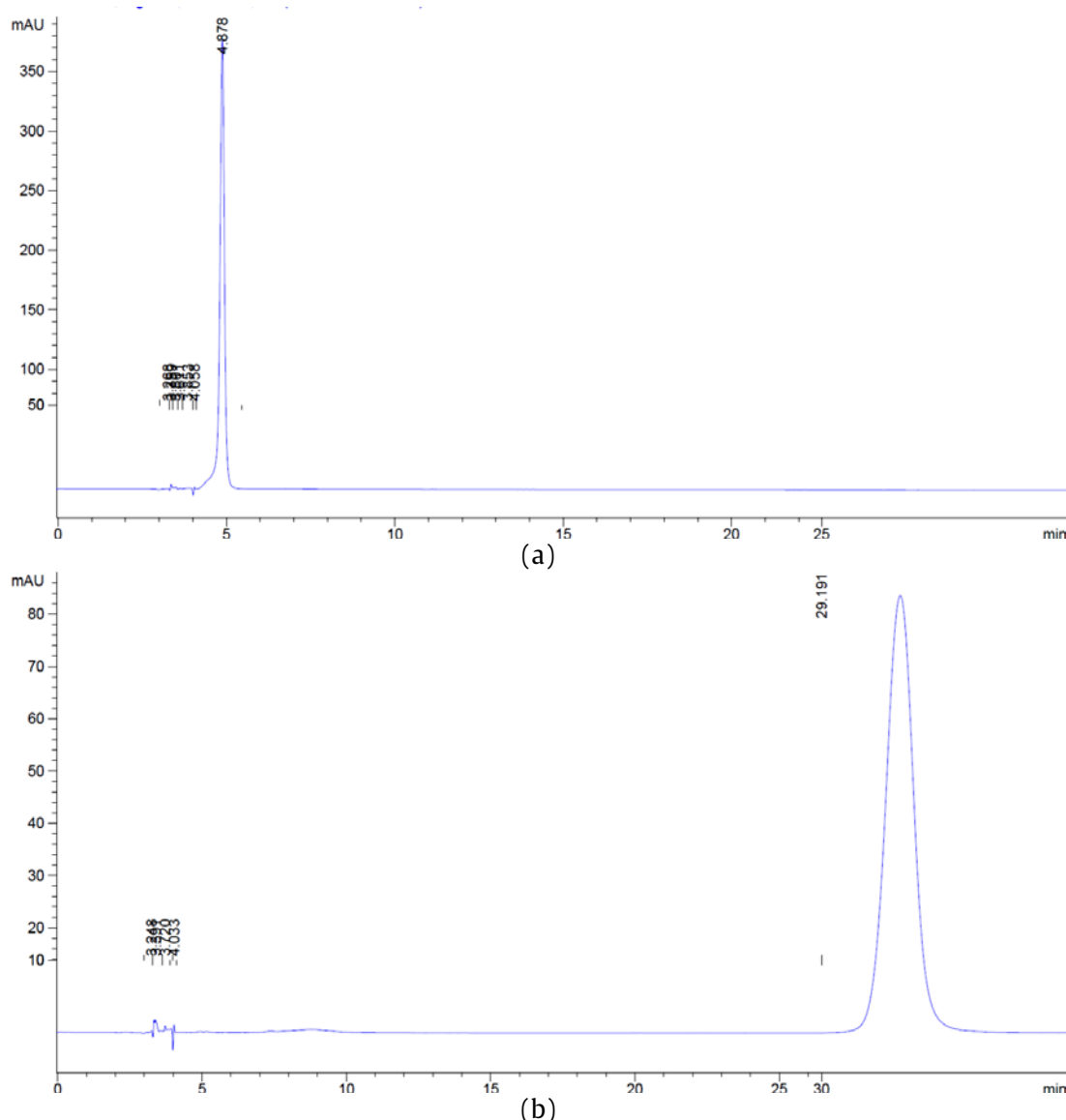
The antioxidant activities of *M. indica* extract were assessed using the DPPH assay. This DPPH method is based on the reduction of purple DPPH radicals through electron acceptance from antioxidants, resulting in the formation of reduced DPPH (DPPH-H). The color of the solution changes from purple to yellow upon

reduction, which can be measured at 520 nm using UV-VIS Spectrophotometry. The concentration of each extract required to inhibit 50% of the DPPH radicals ( $IC_{50}$ ) was determined and compared to the antioxidant standard (Trolox). The results presented in Table 4 demonstrate that the MeOH extraction exhibited the highest antioxidant activity ( $0.52 \pm 0.02$   $\mu\text{g/mL}$ ), followed by ethyl acetate ( $13.84 \pm 0.10$   $\mu\text{g/mL}$ ), DCM ( $184.52 \pm 0.03$   $\mu\text{g/mL}$ ) and *n*-hexane ( $1141.41 \pm 0.01$   $\mu\text{g/mL}$ ), respectively.

**Table 4** Scavenging activity expresses as median inhibitory concentration ( $IC_{50}$ ), in the DPPH test with leaf extracts of *M. indica*.

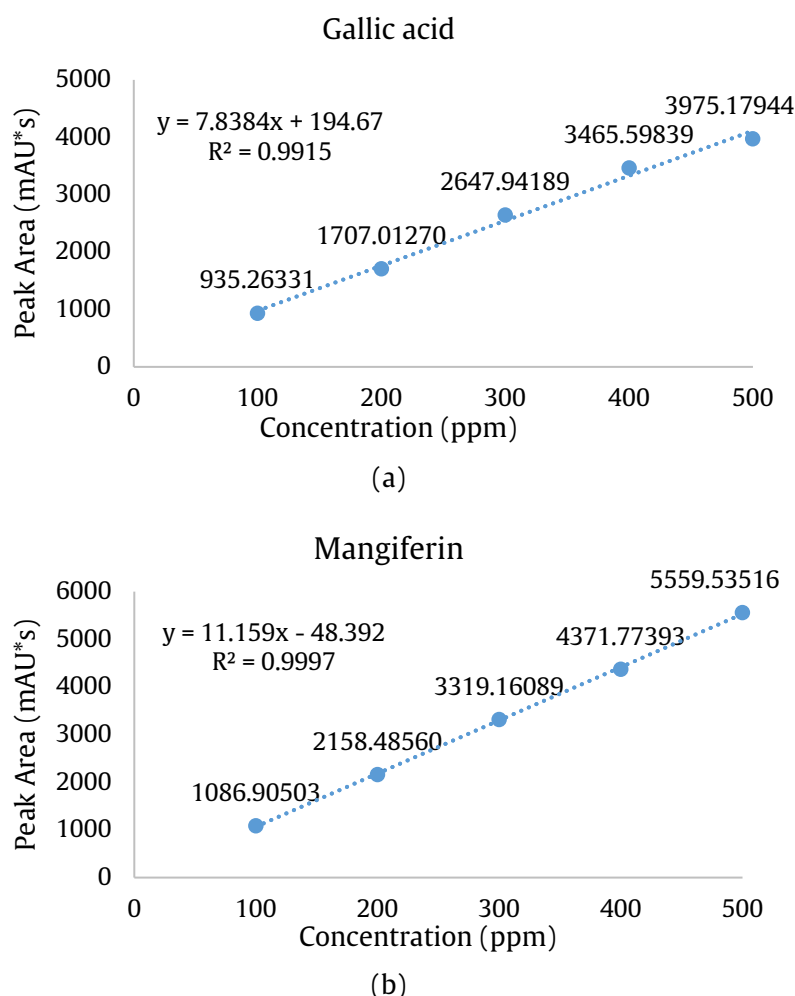
Extract	DPPH radical scavenging assay; $IC_{50}$ ( $\mu\text{g/mL}$ )
<i>n</i> -hexane	$1141.41 \pm 0.01^d$
DCM	$184.52 \pm 0.03^c$
Ethyl acetate	$13.84 \pm 0.10^b$
MeOH	$0.52 \pm 0.02^a$

Values (averages of three replicates) labeled with different letters indicate significant differences at  $p < 0.05$ .

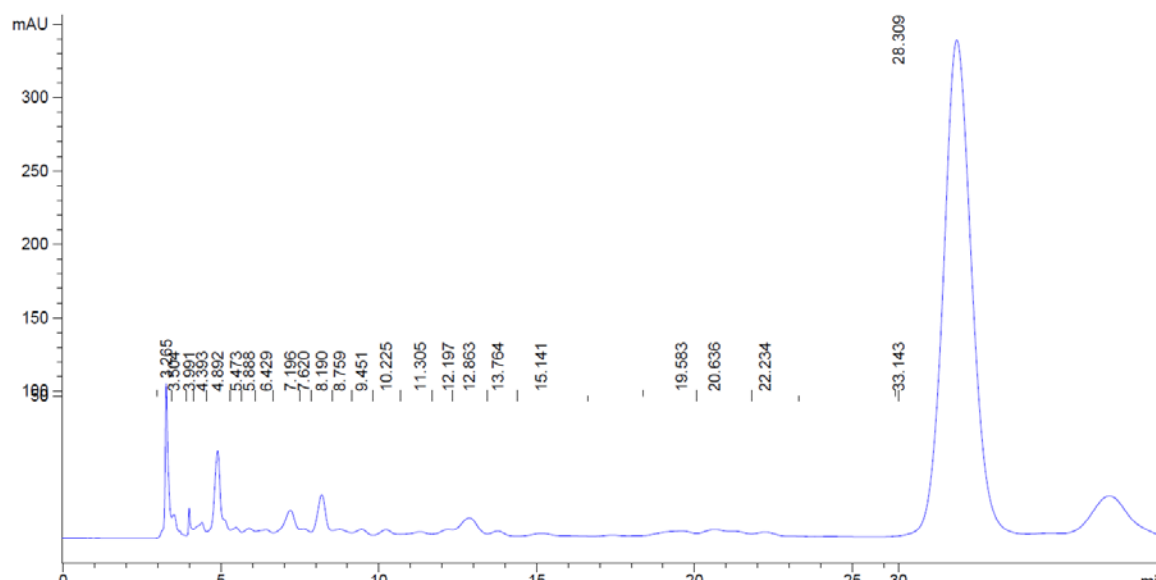


**Figure 2** (a) HPLC chromatogram of standard of gallic acid and (b) mangiferin.





**Figure 3** Calibration curve of (a) gallic acid and (b) mangiferin.



**Figure 4** HPLC chromatogram of crude *M. indica* leaf MeOH extract.

According to Fitmawati [28], the wild mango demonstrated the highest antioxidant activity in terms of total antioxidant activity of mangoes by DPPH assay. In this study, the MeOH leaf extract of the wild mango exhibited the highest antioxidant activity ( $0.52 \pm 0.02$   $\mu\text{g/mL}$ ). Additionally, Fitmawati found that the wild

mango displayed significant antioxidants in both its leaf ( $0.88$   $\mu\text{g/mL}$ ) and bark ( $33.24$   $\mu\text{g/mL}$ ).

#### HPLC analysis of gallic acid and mangiferin content

The chromatogram in Figure 2 demonstrates the elution of gallic acid at 4.88 minutes and mangiferin

at 29.19 minutes. Both gallic acid and mangiferin showed a linear response within the 100–500 mg/L concentration range. The linearity was confirmed with a correlation coefficient ( $R^2$ ) of 0.9915 and 0.9997 for gallic acid and mangiferin, respectively. The calibration curve can be seen in Figure 3. Figure 4 presents the chromatograms of gallic acid and mangiferin contents in the MeOH extract. The analysis of the crude extracts revealed

several peaks with different retention times ( $R_t$ ) and peak areas. Two peaks were observed at approximately 4.9 and 28 minutes, which correspond closely to the standard gallic acid and mangiferin peaks, respectively. Consequently, the HPLC analysis results indicated that the MeOH extract contained 8.9978 mg/g of gallic acid and 188.0275 of mangiferin, as shown in Table 5.

**Table 5** HPLC analysis of gallic acid and mangiferin content in the crude leaf extract MeOH fraction from *M. indica*.

Compound	Retention time ( $R_t$ )		Area (mAU*s)	Content (mg/g)
	Standard	MeOH fraction		
Gallic acid	4.878	4.892	899.95129	8.9978
Mangiferin	29.191	29.309	20933.60	188.0275

**Table 6** The insecticidal properties of *M.indica* leaf extract and isolated compounds after treatment with 2<sup>nd</sup> *S.litura* at 24 and 48 hours h via topical.

Compound	Time (h)	LD <sub>50</sub> ( $\mu\text{g}/\text{cm}^2$ ) <sup>a</sup>	LCL-UCL ( $\mu\text{g}/\text{cm}^2$ ) <sup>b</sup>	Chi square	P-value
<i>n</i> -hexane extract	24	21.53	12.49–62.65	1.05	0.79
	48	0.86	0.80–1.40	2.87	0.41
DCM extract	24	11.10	4.65–55.09	15.88	0.00
	48	0.69	0.41–0.98	7.43	0.06
Ethyl acetate extract	24	11.79	9.56–15.29	2.62	0.45
	48	6.63	5.34–8.42	0.74	0.86
MeOH extract	24	10.58	7.26–18.71	0.96	0.81
	48	0.88	0.49–1.28	3.19	0.36
Mangiferin	24	1.90	0.96–7.41	0.76	0.94
	48	0.77	0.30–2.18	0.54	0.97
Gallic acid	24	1.19	0.36–3.90	0.79	0.94
	48	0.55	0.22–1.21	0.39	0.98

<sup>a</sup>LD<sub>50</sub>: Lethal Dosage means the compound kills 50% of the exposed larvae, expressed in  $\mu\text{g}/\text{cm}^2$

<sup>b</sup>Lower Confidence Limit–Upper Confidence Limit ( $\mu\text{g}/\text{cm}^2$ )

#### Acute toxicity

The larvicidal killing potential of the *M. indica* leaf extracts was determined by applying them topically and measuring the LD<sub>50</sub> after 24 hours. The MeOH extract had the highest LD<sub>50</sub> of 10.58  $\mu\text{g}$  per larvae, followed by DCM, ethyl acetate, and *n*-hexane. The specific LD<sub>50</sub> values can be found in Table 6.

This study found that gallic acid and mangiferin, when isolated, showed LD<sub>50</sub> values of less than 2  $\mu\text{g}$  per larvae at 24 and 48 hours after topical application. These results suggest these substances may have highly toxic and larvicidal properties when applied topically. A previous study also reported that *Alpinia galanga*, a plant extract, effectively controlled *S. litura* larvae with LD<sub>50</sub> values of 1.68 and 1.25  $\mu\text{g}$  per larvae after 24 and 48 hours [3]. Moreover, a previous report highlighted the insecticidal efficacy of gallic acid in inhibiting the growth of the oriental fruit fly, *Bactrocera dorsalis* [29].

#### Impact on detoxification enzyme activity general esterase

The extract from *M. indica* leaves showed inhibition of MeOH (1.31-fold), followed by the *n*-hexane extract (0.98-fold), DCM, and ethyl acetate extracts (both 0.91-fold) against *S. litura*. Additionally, mangiferin and gallic acid exhibited 2.56-fold and 1.27-fold inhibition of CE activity, respectively (Table 7).

#### Glutathione-S-Transferase (GST)

After exposure to insects, the enzyme reaction was inhibited 1.23-fold by the MeOH extract. Mangiferin exhibited the highest inhibitory activity, with a 1.28-fold increase. However, the *n*-hexane extract caused a 0.94-fold increase in GST levels, which varied (Table 7).

#### Acetylcholinesterase (AChE)

The leaf extract of *M. Indica* in MeOH showed a 1.31-fold inhibition of AChE, while gallic acid exhibited the highest inhibitory activity with 3.98-fold increase.

However, the *n*-hexane extract caused a 0.99-fold increase in the AChE reaction (Table 7).

Conventional pesticides leave residues in the environment, soil, air, and water, and they negatively impact insect development through detoxification enzymes. However, botanical insecticides offer a safer alternative [30]. Plant extracts, including secondary metabolites, play a crucial role in controlling growth, exterminating larvae, and preventing insect feeding [5]. The metabolism of detoxification enzymes relies on xenobiotic compounds' hydrophilicity and catalytic activity, leading to their elimination through the

excretory system. Insects possess cytochrome P450 mono-oxygenase (P450s), a versatile agent for detoxifying foreign compounds such as allelochemicals, common pesticides, and pollutants. Other foreign enzymes like glutathione-*S*-transferase (GST), carboxylase (CE), and acetylcholinesterase Ares (AChE) also play a significant role as key metabolites, inducing or neutralizing plant toxins [31–33]. Although the MeOH extract, which contains mangiferin and gallic acid, was isolated in the present phytochemical study, these compounds inhibited CE levels in *S. litura*.

**Table 7** Detoxification enzyme reactions after *M. indica* leaf extracts and allelochemical application on 2<sup>nd</sup> instar *S. litura* larvae after 24 hours.

Compound	Carboxylesterase		Glutathione- <i>S</i> -transferase		Acetylcholinesterase	
	reaction <sup>a</sup>	CF <sup>b</sup>	reaction <sup>a</sup>	CF <sup>b</sup>	reaction <sup>a</sup>	CF <sup>b</sup>
Control	0.0563 <sup>c</sup>	–	0.2529 <sup>bc</sup>	–	0.1916 <sup>e</sup>	–
<i>n</i> -hexane extract	0.0572 <sup>c</sup>	0.98	0.2680 <sup>c</sup>	0.94	0.1940 <sup>e</sup>	0.99
DCM extract	0.0620 <sup>c</sup>	0.91	0.2275 <sup>abc</sup>	1.11	0.1740 <sup>c</sup>	1.10
Ethyl acetate extract	0.0621 <sup>c</sup>	0.91	0.2276 <sup>ab</sup>	1.10	0.1540 <sup>bc</sup>	1.24
MeOH extract	0.0430 <sup>a</sup>	1.31	0.2063 <sup>a</sup>	1.23	0.1457 <sup>d</sup>	1.32
Mangiferin	0.0220 <sup>b</sup>	2.56	0.1974 <sup>ab</sup>	1.28	0.1741 <sup>a</sup>	1.10
Gallic acid	0.0445 <sup>b</sup>	1.27	0.2085 <sup>a</sup>	1.21	0.0482 <sup>b</sup>	3.98

<sup>a</sup>Mean values within a column followed by the same letter were not significantly different ( $P < 0.05$ ) by Tukey's test. Carboxylesterase (CE) measured as *p*-nitrophenol/min/mg esterase in nM. Glutathione-*S*-transferase (GST) measured as glutathione conjugated product/min/mg in nM. Acetylcholinesterase (AChE) measured as  $\mu$ M/min/mg of protein.

<sup>b</sup>Correction factor (CF) of detoxification enzyme activities calculated as enzyme activity in controls / enzyme activity in treatments.

In contrast, the extracts of *n*-hexane, DCM, and ethyl acetate induce the activity of CE in *S. litura* by 0.91 to 0.98-fold after exposure. CE is a hydrolase enzyme that is widely distributed in organisms, including bacteria and animals. It hydrolyzes water-soluble small molecules of ester and acylglycerol bonds in insects, making it an important detoxification enzyme involved in the development of insecticides [34, 35]. Similarly, the MeOH extract and its isolated compounds inhibit the levels of GST in *S. litura*. GST is an enzyme found in the metabolism of both eukaryotes and prokaryotes, and it is involved in the processing of endogenous and foreign substances. Although this study demonstrates that other parts of *M. indica* induce GST activity in *S. litura* after exposure, it remains unclear whether *M. indica* itself induces GST activity. GST also catalyzes glutathione peroxidase and plays a role in regulating cellular mechanisms [36]. Almost all fractions of *M. indica*, except the *n*-hexane extract, exhibit larvicidal properties by inhibiting the AChE reaction in *S. litura*. AChE is an essential enzyme in both vertebrates and invertebrates and is used in biochemical sensors to induce the AChE pathway or recurrent excitation. ChE inhibitors are useful for treating neurological symptoms

caused by acetylcholine (Ach) deficiency. However, it is necessary to have an inducer of AChE inhibition in order to block inappropriate Ach neurotransmitters [36]. Therefore, pest strategies need to be economically and ecologically addressed in order to reduce the harm caused by conventional chemical compounds. Plant extracts contain allelochemicals and active metabolites, which are toxic compounds that protect plants against herbivorous organisms. This indicates that phytochemicals can be applied to insects and have a phytochemical effect that is effective against specific or multiple target sites through a biochemical pathway.

## CONCLUSIONS

This study aimed to analyze the phytochemical composition and antioxidative capabilities of mango leaves (*M. indica* L., Nam Dok Mai), indigenous to Sa Kaeo Province, Thailand. Leaf extraction was performed using different solvents with varying polarities: *n*-hexane, DCM, ethyl acetate, and MeOH. The results revealed the presence of eight groups of phytochemical compounds: alkaloids, flavonoids, coumarins, saponins, tannins, terpenoids, steroids, and cardiac glycosides. The MeOH crude extract exhibited the highest

concentration of total phenolic compounds at 409.88  $\pm$  0.02 mg GAE/g. Moreover, the MeOH crude extract demonstrated the strongest antioxidant activity with an IC<sub>50</sub> value of 0.52  $\pm$  0.02  $\mu$ g/ml, as determined by the DPPH method. High-performance liquid chromatography (HPLC) was employed to identify gallic acid and mangiferin in the MeOH crude extract. To assess the toxicity of the *M. indica* leaf crude extract on 2nd instar *S. litura* larvae, laboratory tests were conducted using the topical application method. The MeOH crude extract exhibited high efficacy, with an LD<sub>50</sub> value of 10.58  $\mu$ g per larvae within 24 hours. Gallic acid and mangiferin were identified as the primary active ingredients, with LCD<sub>50</sub> values of 1.19  $\mu$ g per larvae and 1.90  $\mu$ g per larvae, respectively, within 24 hours. Additionally, using the topical application method, the impact on detoxification enzymes (24 hours post-treatment) was evaluated in surviving 2nd instar *S. litura* larvae. The MeOH extract treatment resulted in a 1.31-fold inhibition of carboxylesterase (CE), a 1.31-fold inhibition of glutathione-S-transferase (GST), and a 1.32-fold inhibition of acetyl-cholinesterase (AChE).

Mango leaves contain beneficial substances that can effectively 2nd instar *S. litura* larvae. This makes them a potential source for developing insecticide products. Furthermore, it is recommended that other active botanical compounds found in *M. indica* for their insecticidal properties be investigated further in the future.

## ACKNOWLEDGEMENT

This research was supported by Fundamental Fund (FF) from Thailand Science Research and Innovation. Thanks to Department of Zoology and Department of Chemistry, Faculty of Science, Kasetsart University including Science Center, Faculty of Science and Technology, Valaya Alongkorn Rajabhat University under the Royal Patronage for supporting and using analytical equipment in this research.

## REFERENCES

1. Sujatha M, Lakshminarayana M. Resistance to *Spodoptera litura* (Fabr.) in Helianthus species and backcross derived inbred lines from crosses involving diploid species. Euphytica. 2007;155: 205-13.
2. Jafir M, Ahmad JN, Arif MJ, Ali S, Samina JNA. Characterization of *Ocimum basilicum* synthesized silver nanoparticles and its relative toxicity to some insecticides against tobacco cutworm, *Spodoptera litura* Feb (Lepidoptera; Noctuidae). Ecotox Environ Safe. 2021;218:112278.
3. Pengsook A, Bullangpoti V, Koul O, Nobsathian S, Saiyaitong C, Yooboon T, et al. Antifeedant activity and biochemical responses in *Spodoptera exigua* Hübner (Lepidoptera: Noctuidae) infesting broccoli, *Brassica oleracea* var. alboglabra exposed to *Piper ribesoides* Wall extracts and allelochemicals. Chem Biol Technol Agric. 2022;9(17):1-10.
4. Wiwattanawanichakun P, Saehlee S, Yooboon T, Kumrungsee N, Nobsathian S, Bullangpoti V. Toxicity of isolated phenolic compounds from *Acorus calamus* L. to control *Spodoptera litura* (Lepidoptera: Noctuidae) under laboratory conditions. Chem Biological Technol Agric. 2022;9(10):1-10.
5. Ayil-Gutiérrez AB, Sánchez-Teyer LF, Vazquez-Flota F, Monforte-González M, Tamayo-Ordóñez Y, Tamayo-Ordóñez MC, et al. Biological effects of natural products against *Spodoptera* spp. Crop Prot. 2018;114:195-207.
6. Miresmailli S, Isman MB. Botanical insecticides inspired by plant-herbivore chemical interactions. Trends Plant Sci. 2014;19(1):29-35.
7. Schulze K, Spreer W, Keil A, Ongprasert S, Müller J. Mango (*Mangifera indica* L. cv. Nam Dokmai) production in Northern Thailand-Costs and returns under extreme weather conditions and different irrigation treatments. Agric Water Manag. 2013; 126:46-55.
8. Kato-Noguchi H, Kurniadie D. Allelopathy and allelopathic substances of mango (*Mangifera indica* L.). Weed Biol Manag. 2020;20:131-8.
9. El-Gied AAA, Joseph MR, Mahmoud IM, Abdelkareem AM, Al Hakami AM, Hamid ME. Antimicrobial activities of seed extracts of mango (*Mangifera indica* L.). Adv Appl Microbiol. 2012;2(04):571-6.
10. Lauricella M, Lo Galbo V, Cernigliaro C, Maggio A, Palumbo Piccionello A, Calvaruso G, et al. The anti-cancer effect of *Mangifera indica* L. peel extract is associated to  $\gamma$ H2AX-mediated apoptosis in colon cancer cells. Antioxidants. 2009;8(10):422.
11. Ganogpichayagrai A, Palanuvej C, Ruangrunsi N. Antidiabetic and anticancer activities of *Mangifera indica* cv. Okrong leaves. J Adv Pharm Technol Res. 2017;8(1):19-24.
12. Imran M, Arshad MS, Butt MS, Kwon JH, Arshad MU, Sultan MT. Mangiferin: a natural miracle bioactive compound against lifestyle related disorders. Lipids Health Dis. 2017;16(1):84.
13. Telang M, Dhulap S, Mandhare A, Hirwani P. Therapeutic and cosmetic applications of mangiferin: A patent review. Expert Opin Ther Pat. 2013;23(12):1561-80.
14. Zhao Y, Wang W, Wu X, Ma X, Qu R, Chen X, et al. Mangiferin antagonizes TNF- $\alpha$ -mediated inflammatory reaction and protects against



- dermatitis in a mice model. *Int Immuno-pharmacol*. 2017;45:174-9.
15. Guo F, Huang C, Liao X, Wang Y, He Y, Feng R, et al. Beneficial effects of mangiferin on hyperlipidemia in high-fat-fed hamsters. *Mol Nutr Food Res*. 2011; 55(12):1809-18.
  16. Niu Y, Li S, Na L, Feng R, Liu L, Li Y, et al. Mangiferin decreases plasma free fatty acids through promoting its catabolism in liver by activation of AMPK. *PLoS One*. 2012;7(1):e30782.
  17. Mahmoud E, Doaa RAH, Shaimaa MF, Mohamed AEA, Mansour S. Larvicidal activity of pentagalloyl glucose and mangiferin isolated from the waste of mango kernel against *Culex pipiens* L. *Waste Biomass Valori*. 2021;13:83-93.
  18. Masibo M, He Q. Major mango polyphenols and their potential significance to human health. *Compr Rev Food Sci F*. 2008;7:309-19.
  19. Junaid RS, Pati MKI. Qualitative tests for preliminary phytochemical screening: An overview. *Int J Chem Stud*. 2020;8(2):603-8.
  20. Kavitha CCI, Indira G. Quantitative estimation of total phenolic, flavonoids, tannin and chlorophyll content of leaves of *Strobilanthes Kunthiana* (Neelakurinji). *J Med Plants Stud*. 2016;4(4):282-6.
  21. Athilah FAF, Afnani A, Nurul AHZ, Noor AM. Total phenolic, total flavonoids content and antioxidant activity of *Mangifera* sp. leaf extracts. *J Agrobiotechnology*. 2020;11(1S):69-78.
  22. Nobsathian S, Saiyaithong C, Koul O, Pluempanupat W, Bullangpoti V, Kumrungsee N. The insecticidal potential of *Piper ribesoides* (Piperaceae) extracts and isolated allelochemicals and their impact on the detoxification enzymes of *Spodoptera exigua* (Lepidoptera: Noctuidae). *Phytoparasitica*. 2021;49:659-73.
  23. Kumrungsee N, Pluempanupat W, Koul O, Bullangpoti V. Toxicity of essential oil compounds against diamondback moth, *Plutella xylostella*, and their impact on detoxification enzyme activities. *J Pest Sci*. 2014;87:721-9.
  24. Ellman GL, Courtney DK, Andreas V, Featherstone RM. A new and rapid colorimetric determination of acetylcholinesterase activity. *Biochem Pharmacol*. 1961;7:88-95.
  25. Pintu KD, Arna P. Effects of aqueous young leaves extract of *Mangifera indica* on gm (-) microorganisms causing gastro-intestinal disorders. *AJPSKY*. 2014; 4(1):23-27.
  26. Olasehinde GI, Sholotan KJ, Openibo JO, Taiwo OS, Bello OA, Ajayi JB, et al. Phytochemical and antimicrobial properties of *Mangifera indica* leaf extracts. *CJPS*. 2018;6(1):55-63.
  27. Osorio DMS, Vallarino JG. From central to specialized metabolism: An overview of some secondary compounds derived from the primary metabolism for their role in conferring nutritional and organoleptic characteristics to fruit. *Front Plant Sci*. 2019;10:835.
  28. Fitmawati F, Resida E, Kholifah SN, Roza RM, Almurdani M, Emrizal Z. Antioxidant (gallic acid and quercetin) profile of Sumatran wild mangoes (*Mangifera* spp.): a potential source for antidegenerative medicine. *Food Res*. 2020;9:220.
  29. Shivashankar S, Sumathi M. Gallic acid induces constitutive resistance against *Bactrocera dorsalis* infestation in mango fruit by its dual action. *Pestic Biochem Physiol*. 2022;188:105268.
  30. Campos EVR, Proença LFP, Oliveira JL, Bakshi M, Abhilash PC, Fraceto LF. Use of botanical insecticides for sustainable agriculture: Future perspectives. *Ecol Indic*. 2019;105:483-95.
  31. Hwei Chen C. Chapter seventh - Detoxifying metabolism: Detoxification enzymes. *Xenobiotic Metabolic Enzymes: Bioactivation and Antioxidant Defence*: Springer Cham; 2020. p. 71-81.
  32. Lu K, Song Y, Zeng R. The role of cytochrome P450-mediated detoxification in insect adaptation to xenobiotics. *Curr Opin Insect Sci*. 2021;43:103-7.
  33. Ramsey JS, Rider DS, Walsh TK, De M, Vos KH, Gordon J, et al. Comparative analysis of detoxification enzymes in *Acyrtosiphon pisum* and *Myzus persicae*. *Insect Mol Biol*. 2010;19(S2):155-64.
  34. Nazarian Z, Arab SS. Discovery of carboxylesterases via metagenomics: Putative enzymes that contribute to chemical kinetic resolution. *Process Biochem*. 2022;121:439-54.
  35. Mao K, Ren Z, Li W, Cai T, Qin X, Wan H, et al. Carboxylesterase genes in nitenpyram-resistant brown planthoppers, *Nilaparvata lugens*. *Insect Sci*. 2021;28:1049-60.
  36. Board PG, Menon D. Glutathione transferases, regulators of cellular metabolism and physiology. *Biochim Biophys Acta*. 2013;1830(5):3267-88.



## Synthesis of biocompatible hydroxyapatite from quail eggshell, oyster shell, and periwinkle snail shell

Phurinart Suandork<sup>1</sup> and Marchin Hongsuwong<sup>2\*</sup>

<sup>1</sup>Patumwan Demonstration School, Bangkok 10330, THAILAND

<sup>2</sup>Ekamai International School, Bangkok 10110, THAILAND

\*Corresponding author: marchin252@gmail.com

### ABSTRACT

This study focuses on the synthesis of hydroxyapatite (HA,  $\text{Ca}_{10}(\text{PO}_4)_6(\text{OH})_2$ ) from calcium carbonate ( $\text{CaCO}_3$ )-rich quail eggshells, oyster shells, and periwinkle snail shells (*Filopaludina bengalensis*) through the use of the wet precipitation method. The methodology involved calcining the shell waste to convert  $\text{CaCO}_3$  to calcium oxide ( $\text{CaO}$ ), undergoing hydration, and reacting with phosphoric acid ( $\text{H}_3\text{PO}_4$ ) to synthesize HA. The results indicated that periwinkle snail shells had the highest percent yield of HA at 92.12%, followed closely by quail eggshells at 92.01%, and oyster shells at 73.65%. For producing  $\text{CaO}$ , oyster shells provided the highest percent yield of  $\text{CaO}$  at 103.72%, followed by quail eggshells at 98.6% and periwinkle snail shells at 92.09%. The synthesized HA exhibited high biocompatibility, which is crucial for its potential applications in medical fields such as bone replacement and regeneration. The X-ray diffraction (XRD) analysis confirmed the successful synthesis of high-quality HA, with characteristic peaks indicative of excellent crystallinity and purity and near identity to the standard XRD pattern of HA of ICDD 9-432 and the XRD pattern of successfully synthesized HA in other studies, indicating high biocompatibility. The research highlights the potential of recycling food waste, specifically shell waste, into valuable biomaterials. This not only addresses environmental concerns but also supports sustainable practices in the food industry. Moreover, the study contributes to advancements in biomaterials for medical applications, emphasizing the viability of utilizing organic waste for high-value products. By transforming food waste into useful medical materials, this research offers promising solutions for waste management and resource utilization, particularly within Thailand's ecological and industrial framework.

**Keywords:** Hydroxyapatite synthesis, Seashells, Calcium carbonate, X-ray diffraction, Calcium oxide

### INTRODUCTION

It is estimated that a third of human-produced foods are wasted globally, which accounts for around 1.3 billion tons of food wasted annually [1]. The average human wastes 65 kg of food on average per year, with dairy and eggs contributing to 7% of total food waste weight, leading to the wasting of essential nutrients such as calcium, choline, riboflavin, zinc, and vitamin B12 [2].

In Thailand, eggs are a prevalent food source, with more than 15,000 million eggs being consumed per year. The estimated waste generated from the eggshells is around 90,000 tons per year [3]. Similarly, oyster shells generate a staggering 18.86 million tons of waste globally [4]. Shell waste produced from the rapidly increasing production and consumption of eggs and oysters is posing serious environmental threats in countless countries around the world, which require immediate action. It is suggested that these shell wastes be efficiently recycled and transformed into practical materials for sustainable advancement [5].

One solution is to utilize these shells, particularly eggshells, as an alternative source of biocompatible material to synthesize substitutive substances and materials in the medical field, since these shells are rich in valuable minerals such as calcium [6]. Eggshells and oyster shells contain high contents of calcium carbonate ( $\text{CaCO}_3$ ), with eggshells at 93-97% and oyster shells at approximately 96% [7-9].

Quail eggs were selected for this study due to their substantial consumption and production in Thailand. In 2016, a particular supermarket franchise in Thailand reported a monthly consumption of 350,000 quail eggs, while the production of quail eggs for international export was approximately 125,000,000 eggs per year [10]. Quail shells consist of 96% or more  $\text{CaCO}_3$  [11], which is considered a sufficient amount for hydroxyapatite synthesis [12]. Similarly, oyster shells were chosen due to their substantial  $\text{CaCO}_3$  content and their high production and consumption rates in Thailand [9]. Oysters are a popular food widely consumed in Thailand, with the marine shellfish culture

statistics survey by the Department of Fisheries, Ministry of Agriculture and Cooperatives reporting a production of 17,903.26 Tons of oysters with a total commercial value of over 749 million baht in the 2019 Department of Fisheries [13]. Additionally, periwinkle snail shells (*Filopaludina bengalensis*) contain 96%  $\text{CaCO}_3$  [14]. In summary, these three materials (quail eggs, oyster shells, and periwinkle snail shells) were selected due to their high demand and popularity of consumption in Thailand, as well as the presence of  $\text{CaCO}_3$  in their shells, making them suitable for hydroxyapatite synthesis. Furthermore, producing hydroxyapatite from these shell wastes contributes to reducing household and industrial waste from food shells, as they are currently not efficiently utilized to their maximum capacity.

$\text{CaCO}_3$  is the least expensive variation and the most common type of calcium. For medical uses and applications,  $\text{CaCO}_3$  is generally used as a supplement or fundamental material for creating other commercial or medical consumables [15]. With more sophisticated materials and procedures, the compound  $\text{CaCO}_3$  found in eggshells and snail shells is also popularly used as a calcium precursor in the methodology of the synthesis and production of HA, which is a proficient material for various medical and dental applications such as bone replacement, bone regeneration, and therapy [6].

Hydroxyapatite (HA) is an inorganic material that contains calcium (Ca), phosphate ( $\text{PO}_4^{3-}$ ), and hydroxide ( $\text{OH}^-$ ) in its standard apatite lattice structure with the chemical formula structure of  $\text{Ca}_{10}(\text{PO}_4)_6(\text{OH})_2$  [16]. It is a key component of human bone, which comprises approximately 60% HA, 30% proteins, and 10% water, respectively [17]. HA is a biocompatible ceramic with no toxicity, and numerous studies have demonstrated its similarities in composition, bioactivity, biocompatibility, osteoconductive, and chemical stability to the inorganic components of human bones and teeth [18, 19]. These close analogies to organic bone components have led to the development and production of synthetic HA via various methods. HA has the unique property of biologically interacting with organic materials, including chemically bonding with living tissues [16]. Due to its biocompatibility and osteoconductive nature, HA is widely used in orthopedics, dentistry, maxillofacial surgery, and orthopedic surgery. It is typically employed as a bone tissue replacement, for bone defect restoration, and as a coating substance for metallic implants [20]. Given its numerous applications and variations, synthetic hydroxyapatite can be manufactured utilizing different techniques and methodologies. A variety of methods may be employed for the synthesis of synthetic hydroxyapatite, such as high-temperature processes (combustion and pyrolysis), wet methods (chemical precipitation, hydrolysis, sol-gel, hydrothermal, emulsion, and sonochemical), and dry methods (solid-state and mechanochemical) [21].

Saeri et al. [22] proposed the precipitation method due to its simplicity, with water being the sole by-product. This method involves the process of sintering, which can have a substantial influence on the morphology and size of the synthesized HA. Saeri et al. [22] also used field emission electron microscopy (FESEM), XRD, and Raman spectroscopy methods to verify and examine as well as show the morphology and size of particles that the samples produced after each step.

Azis et al. [23] conducted a similar study on the synthesis of hydroxyapatite from duck eggshells by using a similar method, which was the precipitation method. In their study, the duck eggshells were converted into precipitate calcium carbonate (PCC) by undergoing calcination, hydration, and carbonation. Then, it was added with  $(\text{NH}_4)_2\text{HPO}_4$  in various Ca/P molar ratios (1.67, 1.77, 1.87) and stirring speeds (200, 250, 300 rpm) in a basic environment of pH 10-11. The most proficient conditions are the molar ratio of 1.77 and a stirring speed of 200 rpm. Then, the characteristics of the synthesized hydroxyapatite were analyzed by X-ray Diffraction (XRD).

Kareem & Eyiler (2024) [24] characterize the wet precipitation method as low cost, low operating temperature, enabling control of the morphology and the mean size of the powder, as well as not requiring an organic solvent, which is why the method was selected and used.

Regarding the feasibility, Ibrahim et al. [25] state that HA does not only offer economic benefits but also contributes to global waste management processes. They also found that HA has economic gain to be had via using HA in biodiesel production, which would reduce the cost in various departments of production.

This study focuses on the synthesis of HA utilizing three distinct organic sources: quail eggshells, oyster shells, and the periwinkle snail shells taxonomically classified as *Filopaludina bengalensis*. The research methodology employs a wet precipitation technique for HA production due to its balance of simplicity, cost-effectiveness, environmental friendliness, the production of high-quality HA, and profound scalability for potential industrial-scale production, encompassing a series of processes from initial shell preparation to final product obtainment [26]. The primary objective of this study is to synthesize and conduct a comparative analysis of HA derived from these three shell types, evaluating their respective compositions and properties in relation to human osseous tissue. By ascertaining which shell source yields HA most analogous to human bone, this research endeavor contributes to potential advancements in the medical industry, with particular emphasis on the field of biomaterials. This study investigates the synthesis of HA from the three understudied materials, proposing potential uses for these materials which contain abundant availability and high cost-effectiveness while maintaining the



essential properties of high crystallinity and biocompatibility, as alternatives compared to the conventional methods. Moreover, this study explores the viability of repurposing food waste byproducts in Thailand, specifically concentrating on shells from consumed aquatic species. This approach not only addresses waste management concerns but also aligns with sustainable practices in the Thai food industry. Through comprehensive analysis and comparison, this research aims to enhance the current understanding of biomaterial synthesis while concurrently promoting environmental sustainability. The findings may potentially facilitate innovative applications in medical science and offer valuable insights into the efficient utilization of organic waste materials within the context of Thailand's unique ecological and industrial landscape.

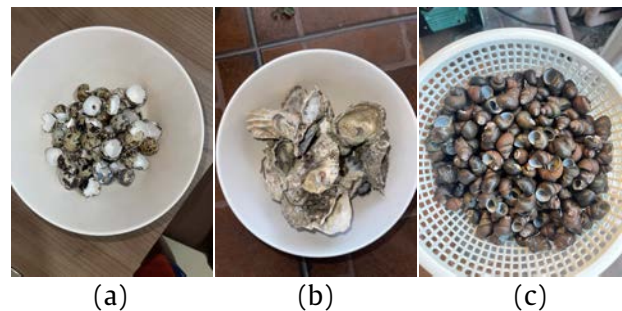
This study offers a novel approach and valuable contribution to the field of hydroxyapatite synthesis by utilizing three specific types of shells (quail eggshells, oyster shells, and periwinkle snail shells) studied together. The combination of these shells has not been extensively explored in research before, providing a new perspective on hydroxyapatite synthesis and valorizing shell waste into usable biomaterials for potential biomedical applications with low-cost and accessible materials. Moreover, this research contributes to the growing knowledge of quail eggshells, oyster

shells, and periwinkle snail shells, highlighting their potential usability in hydroxyapatite synthesis.

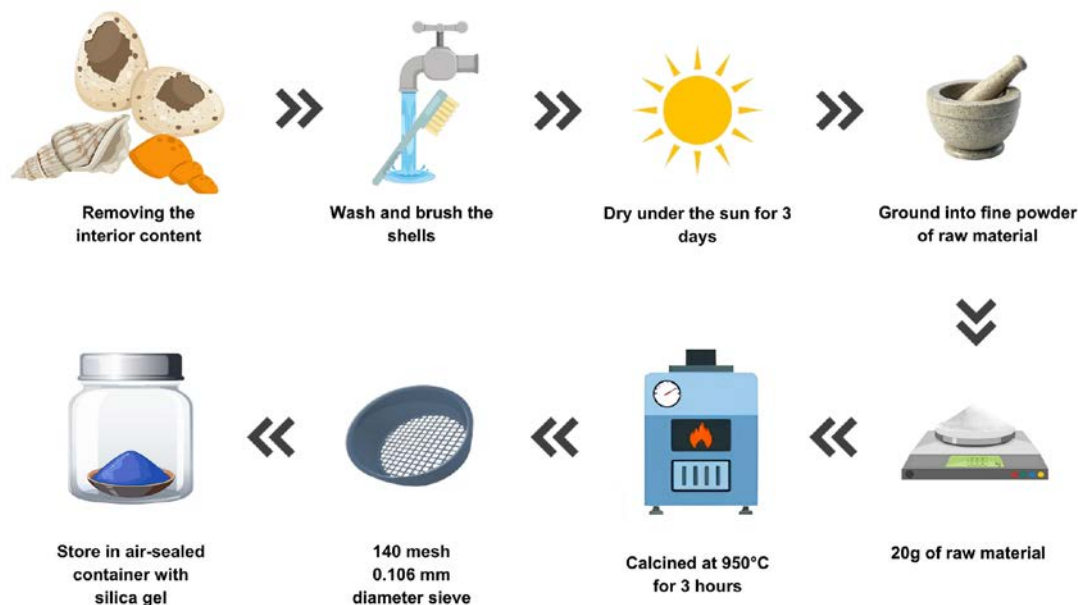
## MATERIALS AND METHODS

### Materials

Quail eggshell, oyster shell, and periwinkle snail shell waste were procured from a supermarket in Bangkok, Khlong Toei market, as shown in Figure 1. Other materials also include distilled water, laboratory-grade  $H_3PO_4$  from RCI Labscan Limited, laboratory-grade ethanol (95%), weighing machine, VELP AREC T. heating magnetic stirrer, SH-2 magnetic stirrer, Whatman filter paper No. 1, AS29 Oilless vacuum pump, and calcination furnace.



**Figure 1** (a) Quail eggshell, (b) oyster shell, (c) periwinkle snail shell.

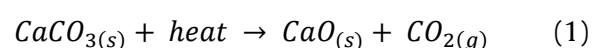


**Figure 2** Diagram of preparation of CaO Precursor.

### CaO precursor preparation

Prior to all the steps that require operating on the laboratory bench or table, the surfaces of the operating areas were sterilized with ethanol. Figure 2. shows the process of preparing CaO precursor, initiating with the contents of quail eggshells, periwinkle snail shells, and oyster shells being extracted. The shells were then thoroughly washed, brushed, and cleansed of dirt and membrane. These three shell materials were

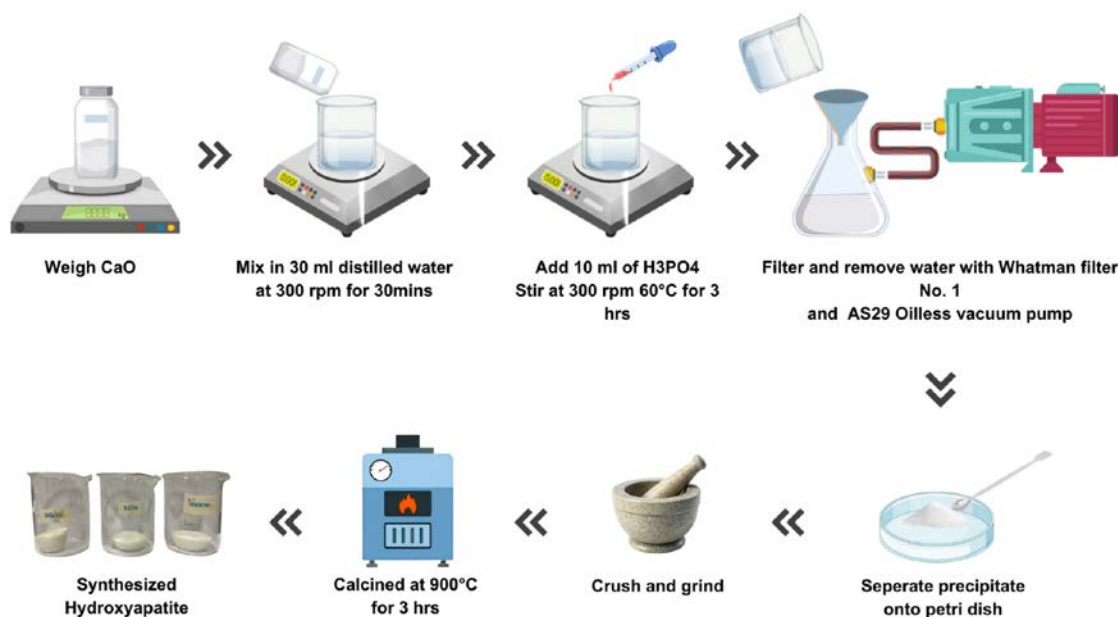
subsequently sun-dried for 3 days. After drying, the shells were ground into 20 g of fine powder of raw material using a mortar and were calcined in a furnace at 950°C for 3 hours. This sintering process transformed the raw material powder with  $CaCO_3$  from the shell waste into CaO, serving as a calcium precursor, as represented by Eq. (1):





The samples were then sieved through a 140-mesh screen with an aperture of 0.106 mm. Finally, they were weighed and stored in a container with silica

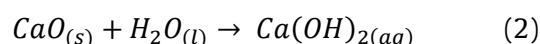
gel to absorb moisture and prevent phase alteration of the substance.



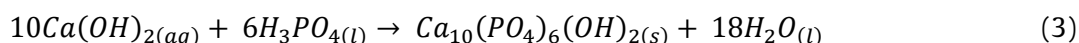
**Figure 3** Illustration of hydroxyapatite synthesis process.

#### *Synthesis of hydroxyapatite*

Figure 3 demonstrates the process of Then, the CaO precursor, approximately 10 g, was weighed in the laboratory using an analytical balance. Each sample was then mixed with 30 mL of distilled water and stirred using a magnetic stirrer for 30 minutes at 300 rpm. The CaO reacted with distilled water to form calcium hydroxide,  $\text{Ca}(\text{OH})_2$ , according to Eq. (2):



The precipitation method was conducted by adding 10 mL of  $\text{H}_3\text{PO}_4$  to each solution of  $\text{Ca}(\text{OH})_2$ . Each mixture was then stirred at 300 rpm and  $60^\circ\text{C}$  for 3 hours. Its pH was measured with litmus paper. The reaction can be represented by Eq. (3):



After cooling, the solution was filtered using airtight connection to a flask. The flask was connected to an AS29 oil-free vacuum pump to remove the water content, leaving hydroxyapatite as the residue or the precipitate. The HA precipitate was carefully removed from the filter paper onto a petri dish, and it was crushed and grinded into fine powder before being sintered in a furnace at the temperature of  $900^\circ\text{C}$  for 3 hours.

#### *Characterization of hydroxyapatite*

The crystal structure of hydroxyapatite powder was characterized by X-ray diffraction, as 1 g of HA samples from the three types of shell were analyzed by the EMPYREAN PANalytical X-ray diffractometer - SC with the XRD patterns recorded in the  $2\theta$  range  $5^\circ - 90^\circ$ .

## RESULTS AND DISCUSSION

#### *Calculate the amount yielded according to calculations made*

Before commencing the laboratory experiment, chemical equilibrium equations were developed to

determine the theoretical quantities of reactants ( $\text{CaCO}_3$ ), intermediates ( $\text{CaO}$  and  $\text{Ca}(\text{OH})_2$ ), and the expected yield of the product (HA). In this study, the process began by preparing 20 g of crushed, fine powder of the raw material of three different shell types: quail eggshells, oyster shells, and periwinkle snail shells. However, the raw material of the three shell types contains approximately 96% calcium carbonate ( $\text{CaCO}_3$ ) [9, 11, 13]. Thus, 20 g of raw material is equivalent to 19.2 g of  $\text{CaCO}_3$ , which represents the actual starting material for the whole process of the synthesis of HA. In each step of the chemical reactions, the theoretical yield of the producing essential compounds ( $\text{CaO}$ ,  $\text{Ca}(\text{OH})_2$ , and  $\text{Ca}_{10}(\text{PO}_4)_6(\text{OH})_2$ ) will be calculated and elucidated.

#### *Decomposition of calcium carbonate ( $\text{CaCO}_3$ )*

The process began with the calcination of eggshell, oyster shell, and periwinkle snail shell to eliminate organic compounds from the shell waste and to convert calcium carbonate ( $\text{CaCO}_3$ ) to calcium oxide ( $\text{CaO}$ ). The molar mass of  $\text{CaCO}_3$  is 100 g/mol, while the molar mass of  $\text{CaO}$  is 56 g/mol. According to Eq.

(4), the moles of a compound are defined by the mass of the compound divided by the molar mass of the compound. Since the process in this study starts with 19.2 g of  $\text{CaCO}_3$ , to calculate the moles of  $\text{CaCO}_3$ , divide 19.2 g of  $\text{CaCO}_3$  by 100 g/mol of  $\text{CaCO}_3$ , which equals 0.192 mol of  $\text{CaCO}_3$ .

$$n(\text{moles}) = \frac{m(\text{mass})}{M(\text{molar mass})} \quad (4)$$

According to Eq. (1), the reaction shows a 1:1 stoichiometric ratio between  $\text{CaCO}_3$  and  $\text{CaO}$ ; therefore, 0.192 mol of  $\text{CaCO}_3$  produces 0.192 mol  $\text{CaO}$ . According to Eq. (5), the mass of the substance can be calculated by multiplying the moles of the compound by the molar mass of the compound. To calculate the mass of  $\text{CaO}$  produced, multiply 0.192 mol  $\text{CaO}$  by 56 g/mol of  $\text{CaO}$ , which equals 10.75 g of  $\text{CaO}$ . In short, 19.2 g of  $\text{CaCO}_3$  will theoretically yield 10.75 g of  $\text{CaO}$  from the decomposition of  $\text{CaCO}_3$  during the calcination process.

$$m(\text{mass}) = n(\text{moles}) \times M(\text{molar mass}) \quad (5)$$

In this stage, the percent yield of  $\text{CaO}$  from the sintering process at the temperature of  $950^\circ\text{C}$  for 3 hours is shown in Table 1. The major changes in this process include the color transformation and mass reduction. For the former occurrence, there are color changes of the quail eggshell from brown to white, oyster shells from gray to white, and periwinkle shells from brown to cream white, in which all of the color alterations represent the organic decomposition in each sample. For the latter occurrence, it is apparent that the results of the production of  $\text{CaO}$  from the calcination process is relatively efficient, as the percent yield of  $\text{CaO}$  for quail eggshell, oyster shell, and periwinkle shell were 98.6, 103.72 and 92.09 percent which is calculated from the following Eq. (6).

$$\text{Percent yield} = \frac{\text{Experimental mass}}{\text{Theoretical mass}} \times 100 \quad (6)$$

The slight mass reduction can be due to the release of carbon and organic compounds during the sintering process, which causes the compounds to shrink [27]. The  $\text{CaO}$  production from oyster shells has the highest percent yield as a result of the oyster's prominent crystalline structures and the natural shell's content of  $\text{CaCO}_3$  [28, 29]. However, the mass of  $\text{CaO}$  and thus the experimental yield of  $\text{CaO}$  from oyster shells are slightly higher than the theoretical yield. The excessive amount of such can be due to the rare impurities presented in the oyster shells, which were not removed during the calcination. As a result, the resulting mass of the sintered  $\text{CaO}$  also contains the mass of other compounds, which suggests that higher temperatures and periods of calcination, such as  $1000^\circ\text{C}$  for 10 h or  $1200^\circ\text{C}$  for 1 h, are required [30]. Due to the limitation of the capability of the calcinating machine, which reaches the highest temperature of only  $950^\circ\text{C}$ , the impurities remain, which causes the

excessive mass and experimental yield of  $\text{CaO}$  from the oyster shells. Another explanation is that there were experimental errors, such as the inaccuracy of the weighing instrument, which led to plausibly false data and abnormal results. Nonetheless, these  $\text{CaO}$  compounds will be the fundamental materials for producing hydroxyapatite compounds via the precipitation method.

#### *Hydration of calcium oxide (CaO)*

In this reaction, the formation of calcium hydroxide ( $\text{Ca(OH)}_2$ ) occurs from the dissolution of calcium oxide ( $\text{CaO}$ ) in 30 ml distilled water ( $\text{H}_2\text{O}$ ) and stirred at 300 rpm for 30 minutes.  $\text{CaO}$  was the limiting reactant, while distilled water is the excess reactant.

According to Eq. (2), the reaction shows a 1:1 stoichiometric ratio between  $\text{CaO}$  and  $\text{Ca(OH)}_2$ , therefore, 0.192 mol  $\text{CaO}$  produces 0.192 mol  $\text{Ca(OH)}_2$ . The molar mass of  $\text{Ca(OH)}_2$  is 74 g/mol. Using Eq. (5), the mass of  $\text{Ca(OH)}_2$  produced is calculated by multiplying 0.192 mol of  $\text{Ca(OH)}_2$  by 74 g/mol of  $\text{Ca(OH)}_2$ , which equals 14.21 g of  $\text{Ca(OH)}_2$ . This indicates that the mixture of 10.75 g of  $\text{CaO}$ , previously produced from the decomposition of 19.2 g of  $\text{CaCO}_3$ , and 30 ml distilled water will subsequently yield 14.21 g of  $\text{Ca(OH)}_2$ .

#### *Synthesis of hydroxyapatite ( $\text{Ca}_{10}(\text{PO}_4)_6(\text{OH})_2$ )*

In the final stage of the synthesis of hydroxyapatite, the hydroxyapatite compound is the product of the precipitation method between  $\text{Ca(OH)}_2$  and phosphoric acid, a phosphorus precursor selected because of its cost-effectiveness with the production of water as the sole by-product of the reaction, with a mixing duration of 3 hours.

According to Eq. (3), the stoichiometry indicates that 10 mol of  $\text{Ca(OH)}_2$  react with 6 mol of  $\text{H}_3\text{PO}_4$  to produce 1 mol of HA and 18 mol of  $\text{H}_2\text{O}$ . Stoichiometrically, if 10 mol of  $\text{Ca(OH)}_2$  requires 6 mol of  $\text{H}_3\text{PO}_4$ , then 0.115 mol of  $\text{H}_3\text{PO}_4$  should be used, as 0.192 mol of  $\text{Ca(OH)}_2$  is cross multiplied with 6 mol of  $\text{H}_3\text{PO}_4$  and divided by 10 mol of  $\text{Ca(OH)}_2$ . Therefore, 11.27 g of  $\text{H}_3\text{PO}_4$  (calculated from 0.115 mol  $\text{H}_3\text{PO}_4 \times 98 \text{ g/mol } \text{H}_3\text{PO}_4$ ) or 6.98 ml of  $\text{H}_3\text{PO}_4$  (the density of the  $\text{H}_3\text{PO}_4$  used in this study is 1.685 g/ml) should be used. However, as  $\text{Ca(OH)}_2$  is designated as the limiting reactant while  $\text{H}_3\text{PO}_4$  is designated as the excess reactant, the amount of  $\text{H}_3\text{PO}_4$  used in this study is 10 ml, which does not affect the result or the property of the synthesized HA as the pH level is being regulated and the solution remained basic, as confirmed by using litmus paper, despite the addition of the excess  $\text{H}_3\text{PO}_4$ .

Onto the calculation of HA theoretical yield. Firstly, moles of HA must be determined. According to Eq. (3), the reaction shows a 10:1 stoichiometric ratio between  $\text{Ca(OH)}_2$  and HA; therefore, 0.192 mol of  $\text{Ca(OH)}_2$  produces 0.0192 mol of HA, calculated from cross-multiplying 0.192 mol  $\text{Ca(OH)}_2$  with 1 mol HA and being divided by 10 mol  $\text{Ca(OH)}_2$ . As the molar

mass of HA ( $\text{Ca}_{10}(\text{PO}_4)_6(\text{OH})_2$ ) is 1004 g/mol, using Eq. (5), the mass of HA produced can be determined by multiplying 0.0192 mol HA by 1004 g/mol HA, which equals 19.28 g of HA. Ultimately, this indicates that the mixture of previously produced 14.21 g  $\text{Ca}(\text{OH})_2$  and 10 ml  $\text{H}_3\text{PO}_4$  will theoretically yield 19.28 g of HA, which originated from the initial substance of 20 g of raw material of the shell waste or 19.2 g of  $\text{CaCO}_3$ .

Table 1 demonstrates the quantified relationship between the final product of the HA solid compound, the initial starting compound of  $\text{CaCO}_3$ , and the intermediate compound of CaO for better effectiveness of comparison of different masses of products, as well as the percent yield of the resulting HA compounds.

Comparing the experimental yield of HA to the theoretical yield of HA, it is perceptible that there are losses of compound mass in the process of hydration and synthesis of HA. For quail eggshell and periwinkle shell, the percent yield of HA is slightly lower than the percent yield of CaO, signifying that there is slight weight loss during the transformation from CaO to  $\text{Ca}(\text{OH})_2$  or the transformation from  $\text{Ca}(\text{OH})_2$  to HA, in which the slight reduction will be explained later on. More importantly, for oyster shells, the percent yield of HA is markedly lower than its percent yield of CaO, signifying a lot more weight loss compared to the other two groups. This is due to the difference in the crystallinity in the shell types and the calcium-deficient structure in oyster shell composition [31]. To elucidate,

the crystal structure of calcium carbonate ( $\text{CaCO}_3$ ) in the three shell types has two main crystalline forms: calcite and aragonite. The shells of periwinkle snail quail eggs contain only 10% or less aragonite and 90%, and their main crystal structure is 90% or almost pure calcite in periwinkle snail shells and quail eggshells, respectively [11, 32]. Meanwhile, the composition of the crystal structure of  $\text{CaCO}_3$  in the oyster shells is different, as it contains 72.3% calcite and 27.7% aragonite [33]. Aragonite is less stable and more soluble compared to calcite, in which its higher solubility and less ordered structure, when mixed with distilled water during the hydration and  $\text{H}_3\text{PO}_4$  during the synthesis, can contribute to a calcium-deficient structure. As the composition of the oyster shells contains more aragonite, the larger portion of the crystalline structure in the oyster shell group with higher solubility and less stability can immensely affect and reduce the final mass and experimental yield of the synthesized HA product from the oyster shells, compared to the periwinkle snail shells and egg shells [34, 35].

Moreover, the weight loss in all shell types can be caused by the loss of HA compounds during the process of separating, grinding, and purifying HA precipitates after they were filtered. Nevertheless, the efficiency of production of HA compounds for all types of shell is greater than 50%, which marks the valuable success of the hydroxyapatite synthesis. [36, 37].

**Table 1** Mass and percentage yield of CaO and HA from different  $\text{CaCO}_3$  sources.

Sample Type	Mass (g)			Percent Yield	
	$\text{CaCO}_3$	CaO	HA	CaO	HA
Theoretical Value	19.2	10.75	19.28	100	100
Quail eggshell	19.2	10.6	17.74	98.6	92.01
Oyster snail shell	19.2	11.15	14.2	103.72	73.65
Periwinkle shell	19.2	9.9	17.76	92.09	92.12

Overall, the entire process of the production of synthesized hydroxyapatite is derived from the initial compound of  $\text{CaCO}_3$ . For all types of shells, the initial quantity was 20 g of raw material or 19.2 g of  $\text{CaCO}_3$ , and the theoretical yield of synthesized HA compound was 19.28 g. The experimental yield of HA compounds was 17.74 g for quail eggshell, 14.20 g for oyster shell, and 17.76 g for periwinkle shell, as represented in Table 1. Regarding percent yield of HA, calculated from Eq. (6), the periwinkle shell had the highest percentage yield of 92.12%, followed by the quail eggshell with a slightly lower percent yield of 92.01%; meanwhile, the oyster shell had a considerably lower percent yield of 73.65% compared to the other two sample types. Quail eggshell and oyster snail shell have marginally lower percent yield compared to the experimental yield, while CaO has drastically lower percent yield. The lower experimental yield of all

samples was affected by the experimental errors during different processes of separation and purification of the solutions, where  $\text{CaCO}_3$ , CaO, and HA compounds may be lost throughout various procedures, mainly during the separation of HA precipitate from the filter paper, as accumulation of leftover HA compound on the filter paper can account for the considerable amount of weight loss and yield difference.

In addition, the reasons for the dramatic difference in percent yield in CaO are possibly due to similar reasons as to the weight loss and HA production efficiency from various CaO sample sources [27, 36].

#### *Thermal analysis*

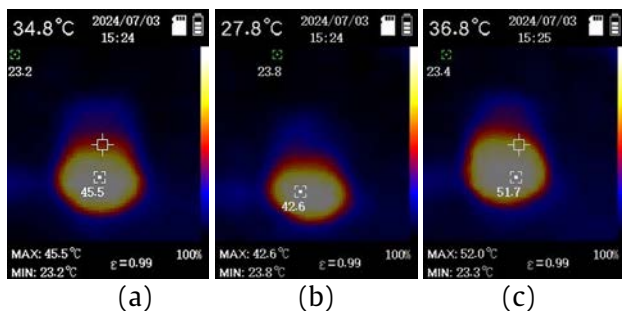
Figure 4 reveals the exothermic nature of the reactions involving oyster shells, periwinkle snail shells, and quail eggshells during the synthesis process. These images provide valuable insights into the heat



release patterns and maximum temperatures reached for each material. Oyster shells exhibited the lowest peak temperature (42.6°C), suggesting a more moderate heat release during the reaction. Quail eggshells showed an intermediate thermal profile, reaching a maximum of 45.5°C. Periwinkle snails demonstrated the highest exothermic activity, with temperatures peaking at 51.7°C.

The varying thermal profiles can be attributed to differences in the chemical composition and structural characteristics of each shell type. Oyster shells, primarily composed of calcium carbonate in the form of calcite, tend to have a more stable crystal structure, which may contribute to their lower heat release [37]. In contrast, quail eggshells, while also rich in calcium carbonate, typically contain a higher proportion of organic matter and a more porous structure, potentially leading to more rapid decomposition and higher heat generation during the reaction [38].

The higher exothermic activity observed in periwinkle snail shells could result in faster reaction rates and potentially affect the crystallinity and particle size of the resulting hydroxyapatite. This increased thermal energy might promote better crystallization and could influence the final product's properties [39].



**Figure 4** Thermal images showing the exothermic reaction during hydroxyapatite synthesis from different shell sources: (a) quail eggshell, (b) oyster shell, and (c) periwinkle shell.

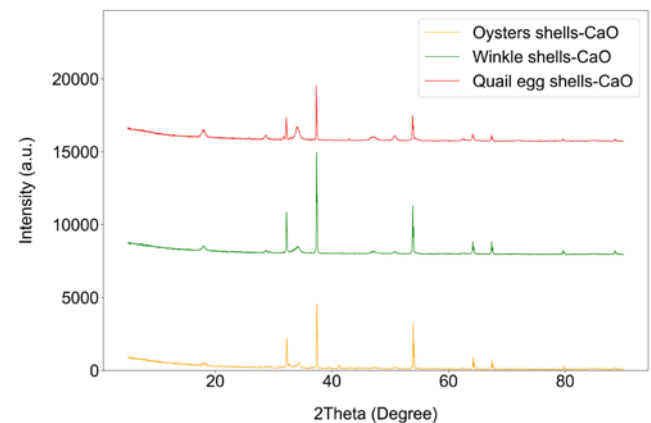
#### XRD characterization

Figure 5 illustrates the XRD patterns of the calcium oxide (CaO) samples, which were gathered from calcined quail eggshells, oyster shells, and periwinkle snail shells. Typical characteristic peaks of CaO can be observed at  $2\theta$  values of approximately 37.4° and 53.8°, and all three samples exhibit pronounced peaks at these positions. The calcination process was conducted at 950°C for 3 hours and successfully converted  $\text{CaCO}_3$  to CaO across all shell types. Subtle variations in peak intensities among the three sources suggest slight differences in crystallinity or purity.

The characterization of the CaO samples closely aligns with the findings and results reported by Meshkatsadat (2023) [40], who observed diffraction peaks ( $2\theta$ ) at approximately 32°, 37°, 53°, 64°, and 67°. This correlation further confirms the successful

conversion of  $\text{CaCO}_3$  to CaO during the calcination process.

In a similar study, Rujitanapanich et al. (2014) [41] reported XRD patterns for CaO obtained from oyster shells after being calcined at 1200°C for 2 hours. Their analysis revealed prominent CaO peaks at 37.4° and 53.8°, which closely correspond to the findings of the present study. This consistency across different research efforts highlights the reliability of the calcination method employed in this investigation for producing high-quality CaO precursors from various shell sources.



**Figure 5** XRD patterns of CaO precursors.

Figure 6 illustrates the XRD patterns of HA synthesized from three distinct sources: quail eggshells, oyster shells, and periwinkle snail shells. Prominent HA peaks can be seen at  $2\theta$  values of approximately 25.9°, 31.8°, 32.2°, 32.9°, 34.1°, 39.8°, 46.7°, and 49.5°. The intensity peak of the XRD diffraction pattern of the synthesized HA from the three shell types is compared and closely resembles the standard XRD pattern of HA based on ICDD 9-432, which authenticates the high crystallinity and phase purity of the synthesized HA. The well-defined nature and high intensity of these peaks are indicative of the synthesized HA's excellent crystallinity. Moreover, the absence of significant extraneous peaks suggests a high degree of phase purity in the synthesized HA samples. These results demonstrate the successful synthesis of high-quality HA from the three different shell sources, with diffraction patterns that closely align with established standards for pure HA. The confirmation of the successful and high quality of the synthesized HA also suggests excellent biocompatibility and bioactivity, which are crucial for successful integration with human bone tissue. The HA obtained from the three shell sources closely mimics the mineral composition of natural bone, verifying that they contain the properties of osteoconductive and possible cell attachment, which are essential for bone regeneration applications. Moreover, the high crystallinity and purity of the synthesized HA ensure that it maintains structural integrity for supporting new bone growth, making it highly suitable and useful for usage in orthopedic and dental applications, in which osseointegration is important. This enhances the

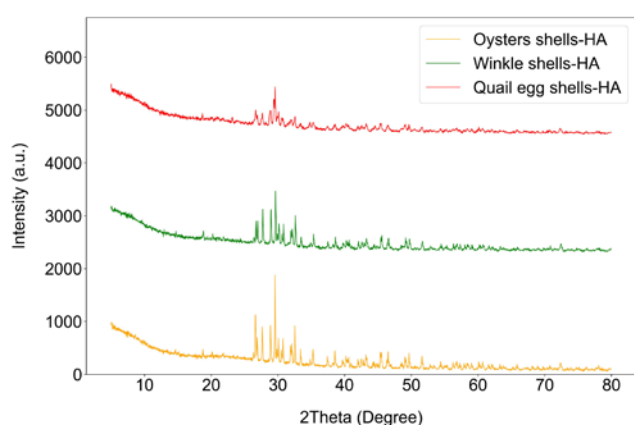


material's clinical performance in bone grafts and implants, highlighting its suitability for medical applications where bone regeneration is required [42].

Regarding the difference in the degree of crystallinity, the difference could be attributed to many different factors in the process that we used in the synthesis of HA. The difference in raw material is one possible explanation that could influence the crystallinity due to the variations in the mineral composition's organic content as well as impurities found in the raw material. Another possibility could be attributed to the conditions under which the HA was synthesized as well as post-synthesis treatment with factors such as temperature, pH, and concentration of reactants possibly affecting the crystallinity.

In a similar study, Shahabi et al. (2014) [43] reported that the standard XRD pattern based on ICDD 9-432 closely matches the XRD pattern of their HA samples, which also closely match the XRD pattern of the synthesized HA samples for further confirmation of the successful synthesis.

Venkatesan and Kim (2010) [44] investigated HA synthesis from fish bones. Their XRD results also revealed typical HA diffraction patterns similar to those observed in the present study, further corroborating the successful synthesis of HA from marine biowaste materials.



**Figure 6** XRD patterns of synthesized hydroxyapatite (HA).

## CONCLUSIONS

This study successfully produces synthesized HA from quail eggshells, oyster shells, and periwinkle snail shells using a wet precipitation technique, with periwinkle shell containing the highest percentage yield of producing HA compounds of 92.12%, followed by quail eggshell at 92.01%, respectively.

The oyster shell has a relatively lower percentage yield of 73.65% due to weight loss during the procedure of separation and purification of the HA compound as well as a crystallinity difference, particularly the greater prevalence of aragonite in the oyster shells. The XRD results for both CaO precursors and synthesized HA

aligned with previous studies, which verifies the reliability and credibility of the study's methodology. As the CaO precursors showed characteristic peaks at  $2\theta$  values of approximately  $37.4^\circ$  and  $53.8^\circ$ , they confirm the successful transformation of calcium carbonate to calcium oxide. Moreover, the synthesized HA compound revealed peaks at  $2\theta$  values of approximately  $25.9^\circ$ ,  $31.8^\circ$ ,  $32.2^\circ$ ,  $32.9^\circ$ ,  $34.1^\circ$ ,  $39.8^\circ$ ,  $46.7^\circ$ , and  $49.5^\circ$ , which indicate the high properties of crystallinity and purity of the HA compound.

The successful synthesis of high-quality HA from these shell sources demonstrates high crystallinity, phase purity, excellent biocompatibility, bioactivity, and osteoconductive property of the synthesized HA, which are essential for integration with human body tissues, foundation of bone growth, and bone regeneration applications. This suggests its suitability for orthopedic, dental, and medical applications due to its clinical effectiveness in bone grafts and implants.

Additionally, the environmentally friendly approach of repurposing waste shells aligns with the growing emphasis on sustainability in healthcare, potentially influencing the next generation of biomaterial development. The findings of this study open up the possibilities and pathways for further research into tailored HA composites, promoting innovations that improve patient outcomes while reducing environmental impact, thus bridging the gap between sustainable practices and advanced medical technologies.

The findings contribute to the potential development of recycling food waste in Thailand while addressing the waste management issues and aligning with sustainable practices in the food industry.

Future research could focus on optimizing large-scale production, exploring additional applications, and investigating the economic feasibility for industrial implementation. In the medical field, further studies could address the development of advanced, sustainable biomaterials or products such as bone scaffolds and coatings for medical implants to maximize the cost-effectiveness and environmental benefits of HA synthesized from shell waste.

Several key areas can be explored in future analysis to enhance the characterization of hydroxyapatite (HA) synthesized from quail eggs, oyster shells, and periwinkle shells. We could evaluate the mechanical properties, including compressive strength and fracture toughness, to ensure suitability for load-bearing applications. Biocompatibility could be assessed through in vitro cell viability assays and in vivo studies. Surface characterization could be conducted using SEM and AFM to analyze morphology and porosity. Chemical composition and purity could be verified with FTIR and ICP-OES, focusing on the Ca/P ratio and impurities. Thermal stability could be examined with TGA and DSC, while long-term stability and degradation could be tested in simulated body fluids. Additionally, process

optimization and cost analysis could be performed to facilitate large-scale production. Comparative studies with commercial HA and exploration of alternative synthesis methods could also be undertaken to benchmark performance and refine material properties.

### ACKNOWLEDGEMENT

The authors would like to acknowledge Mr. Thanadol Tuntiwongwat and Mr. Thananop Tummawai for their unwavering support and guidance.

### REFERENCES

- Gustavsson J, Cederberg C, Sonesson U, Van Otterdijk R, Meybeck A. Global food losses and food waste. FAO. 2011;1-29.
- Darkun K, Febrina L, Lutfansa A. Utilization a mixture of eggshells and husk ash to reduce environmental impact. *Environmental Research, Engineering and Management*. 2022;78(3):110-8.
- Laohavisuti N, Boonchom B, Boonmee W, Chaiseeda K, Seesanong S. Simple recycling of biowaste eggshells to various calcium phosphates for specific industries. *Sci Rep*. 2021;11(1):15143.
- Chilakala R, Thannaree C, Shin EJ, Thenepalli T, Ahn JW. Sustainable solutions for oyster shell waste recycling in Thailand and the Philippines. *Recycling*. 2019;4(3):35.
- Waheed M, Yousaf M, Shehzad A, Inam-Ur-Raheem M, Khan MKI, Khan MR, et al. Channelling eggshell waste to valuable and utilizable products: A comprehensive review. *Trends Food Sci Tech*. 2020;106:78-90.
- Mohd Pu'ad NAS, Alipal J, Abdullah HZ, Idris MI, Lee TC. Synthesis of eggshell derived hydroxyapatite via chemical precipitation and calcination method. *Mater Today-Proc*. 2021;42:172-7.
- Kristl M, Jurak S, Brus M, Sem V, Kristl J. Evaluation of calcium carbonate in eggshells using thermal analysis. *J Therm Anal Calorim*. 2019;138:2751-8.
- Hamester MR, Balzer PS, Becker D. Characterization of calcium carbonate obtained from oyster and mussel shells and incorporation in polypropylene. *Materials Research*. 2012;15:204-8.
- Silva TH, Mesquita-Guimarães J, Henriques B, Silva FS, Fredel MC. The potential use of oyster shell waste in new value-added by-product. *Resources*. 2019;8(1):13.
- Tunsaringkarn T, Tungjaroenchai W, Siri Wong W. Nutrient benefits of quail (*Coturnix coturnix japonica*) eggs. *International Journal of Scientific and Research Publications*. 2013;3(5):1-8.
- Ahmed N, Kamil F, Hasso A, Abduljawaad A, Saleh T, Mahmood S. Calcium carbonate nanoparticles of quail's egg shells: Synthesis and characterizations. *Mech Beh M*. 2022;31(1):1-7.
- Supriyanto NS, Sukarni S, Puspitasari P, Permanasari AA. Synthesis and characterization of CaO/CaCO<sub>3</sub> from quail eggshell waste by solid state reaction process. *AIP Conf Proc*. 2019;2120:40032.
- Department of Fisheries Ministry of Agriculture and Cooperatives. Statistics of Marine Shellfish Culture Survey 2019. Fisheries Development Policy and Planning Division, Fishery Statistics Group; 2020.
- Parveen S, Chakraborty A, Chanda DKr, Pramanik S, Barik A, Aditya G. Microstructure analysis and chemical and mechanical characterization of the shells of three freshwater snails. *ACS Omega*. 2020;5(40):25757-71.
- Potortì AG, Messina L, Licata P, Gugliandolo E, Santini A, Di Bella G. Snail shell waste threat to sustainability and circular economy: Novel application in food industries. *Sustainability-Basel*. 2024;16(2):706.
- Habibah TU, Amlani DV, Brizuela M. Hydroxyapatite dental material. In: StatPearls [Internet]. StatPearls Publishing; 2024 [cited 2024 Aug 1]. Available from: <https://pubmed.ncbi.nlm.nih.gov/30020686/>.
- Feng X. Chemical and biochemical basis of cell-bone matrix interaction in health and disease. *Current chemical biology*. 2009;3(2):189-96.
- Rivera-Muñoz EM. Hydroxyapatite-based materials: synthesis and characterization. *Biomedical Engineering-Frontiers and Challenges*. 2011:75-98.
- Szczęś A, Hołysz L, Chibowski E. Synthesis of hydroxyapatite for biomedical applications. *Adv Colloid Interfac*. 2017;249:321-30.
- Chen L, Al-Bayate S, Khurshid Z, Shavandi A, Brunton P, Ratnayake J. Hydroxyapatite in oral care products-a review. *Materials*. 2021;14(17):4865.
- Pu'Ad NM, Koshy P, Abdullah HZ, Idris MI, Lee TC. Syntheses of hydroxyapatite from natural sources. *Heliyon*. 2019;5(5):e01588.
- Saeri MR, Afshar A, Ghorbani M, Ehsani N, Sorrell CC. The wet precipitation process of hydroxyapatite. *J Mater Sci Lett*. 2003;57(24-25):4064-9.
- Azis Y, Alfarisi CD, Komalasari K, Khairat K, Sahan Y. Synthesis and characterization of hydroxyapatite from duck eggshell by wet precipitation process. *Journal of Applied Materials and Technology*. 2021;3(1):8-11.

24. Kareem Z, Eyiler E. Synthesis of hydroxyapatite from eggshells via wet chemical precipitation: a review. *RSC Adv.* 2024;14(30):21439-52.
25. Ibrahim M, Labaki M, Giraudon JM, Lamonier JF. Hydroxyapatite, a multifunctional material for air, water and soil pollution control: A review. *J Hazard Mater.* 2020;383:121139.
26. Nurfiana F, Kadarwati A, Putra S. Synthesis and characterization of hydroxyapatite from duck eggshell modified silver by gamma radiolysis method. *J Phys Conf Ser.* 2020;1436(1):012099.
27. Malau ND. Manufacture and characterization of hydroxyapatite from quail eggshell using precipitation methods. *International Journal of Progressive Sciences and Technologies.* 2021;29(1):484-90.
28. Viriya-empikul N, Krasae P, Puttasawat B, Yoosuk B, Chollacoop N, Faungnawakij K. Waste shells of mollusk and egg as biodiesel production catalysts. *Bioresource Technol.* 2010;101(10):3765-7.
29. Yoon GL, Kim BT, Kim BO, Han SH. Chemical-mechanical characteristics of crushed oystershell. *Waste Manage.* 2003;23(9):825-34.
30. Cho J, Kim S, Park KT, Rhee CH, Park HW, Jung JC. Eco-friendly CaO-based catalysts derived from waste oyster shells for the oxidative coupling of methane. *J Mater Cycles Waste.* 2023;25(6):3355-66.
31. Wu SC, Hsu HC, Hsu SK, Tseng CP, Ho WF. Preparation and characterization of hydroxyapatite synthesized from oyster shell powders. *Adv Powder Technol.* 2017;28(4):1154-8.
32. Boronat C, Correcher V, Virgos MD, Garcia-Guinea J. Ionising radiation effect on the luminescence emission of inorganic and biogenic calcium carbonates. *Nucl Instrum Meth B.* 2017;401:1-7.
33. Iwase K, Harunari Y, Teramoto M, Mori K. Crystal structure, microstructure, and mechanical properties of heat-treated oyster shells. *J Mech Behav Biomed.* 2023;147:106107-7.
34. Hoque ME, Shehryar M, Islam KN. Processing and characterization of cockle shell calcium carbonate ( $\text{CaCO}_3$ ) bioceramic for potential application in bone tissue engineering. *J Mater Sci Eng.* 2013;2(4):132.
35. Oyawoye MR, Momoh OR, Sani YM, Akande HF. Characterization of Periwinkle Shell from Nembe, Rivers State, Nigeria. *Nigerian Research Journal of Engineering and Environmental Sciences.* 2019;4(2):850-6.
36. Tan YH, Abdullah MO, Nolasco-Hipolito C. The potential of waste cooking oil-based biodiesel using heterogeneous catalyst derived from various calcined eggshells coupled with an emulsification technique: A review on the emission reduction and engine performance. *Renewable and Sustainable Energy Reviews.* 2015;47:589-603.
37. Akram M, Ahmed R, Shakir I, Ibrahim WA, Hussain R. Extracting hydroxyapatite and its precursors from natural resources. *J Mater Sci.* 2014;49:1461-75.
38. Luz GM, Mano JF. Biomimetic design of materials and biomaterials inspired by the structure of nacre. *Philos T Roy Soc A.* 2009;367(1893):1587-605.
39. Wu SC, Hsu HC, Hsu SK, Chang YC, Ho WF. Synthesis of hydroxyapatite from eggshell powders through ball milling and heat treatment. *Journal of Asian Ceramic Societies.* 2016;4(1):85-90.
40. Meshkatsadat MH. Facile and Eco-Friendly Method for Synthesis of Calcium Oxide Nanoparticles utilizing Pistacia atlantica leaf extracts and its characterization. *International Journal of New Chemistry.* 2023;10(1):27-34.
41. Rujitanapanich S, Kumpapan P, Wanjanoi P. Synthesis of hydroxyapatite from oyster shell via precipitation. *Enrgy Proced.* 2014;56:112-7.
42. Bayaty FA, Al-Obaidi MMJ, Lokman A, Yazid S, Ibrahim OE. Osteoconductive properties of synthetic eggshell hydroxyapatite: an experimental study in rats. *Arab Gulf J Sci Res.* 2023. Available from: <https://doi.org/10.1108/AGJSR-04-2023-0155>.
43. Shahabi S, Najafi F, Majdabadi A, Hooshmand T, Haghbin NM, Karimi B, et al. Effect of gamma irradiation on structural and biological properties of a PLGA-PEG-hydroxyapatite composite. *Sci World J.* 2014;2014(1):420616.
44. Venkatesan J, Kim SK. Effect of temperature on isolation and characterization of hydroxyapatite from tuna (*Thunnus obesus*) bone. *J Mater.* 2010;3(10):4761-72.





## Characterization and bioactive protein hydrolysates from two-spotted cricket (*Gryllus bimaculatus* De Geer) and short-tail cricket (*Brachytrupes portentosus* Lichtenstein)

Achara Chaiongkarn\*, Pattarawadee Kendkwasingh, Premsuda Saman and Supatjaree Ruengsomwong

Biodiversity Research Centre, Thailand Institute of Scientific and Technological Research, Pathum Thani 12120, THAILAND

\*Corresponding author: achara@tistr.or.th

### ABSTRACT

The two-spotted cricket (*Gryllus bimaculatus*) and short-tail cricket (*Brachytrupes portentosus*) are economically significant edible insects in Thailand, boasting up to 60% protein content. This study investigates the effects of different types of proteases on the production of protein hydrolysates and biological activities from two cricket species, divided into 4 groups based on extraction and digestion methods as proteins extracted by heat at 100°C, proteins digested with the protease SD-AY 10, pepsin, and a combination of protease SD-AY 10 and pepsin. None of the 4 protein groups inhibited pathogenic *E. coli*, *Salmonella enteritidis*, and *Salmonella typhimurium*. The total antioxidant capacity (TAC) assessment showed that proteins from *G. bimaculatus* digested with SD-AY 10 had a significantly higher antioxidant level (5.5 nmol/μl), while proteins from *B. portentosus* digested with pepsin had a similarly high antioxidant level (5.59 nmol/μl), both significantly higher than other groups ( $p < 0.05$ ). Proteins from both crickets digested by enzymes were safe for RAW 246.7 macrophage cells at concentrations from 1.56 to 25% (v/v) and effectively inhibited nitric oxide production. Protein hydrolysates from *G. bimaculatus* and *B. portentosus* inhibited nitric oxide production at a concentration of 25% (v/v) equivalent to β-glucan. Phagocytic activity was also observed in protein hydrolysates from both cricket species, stimulating RAW 246.7 cells at concentrations of 1.56–25% (v/v). However, protein hydrolysate from *B. portentosus*, digested with pepsin at a concentration of 1.56–12.5% (v/v) showed higher phagocytic activity values (152.52–163.86%) compared to β-glucan (149.18%). The results showed that protein hydrolysates from two cricket species, digested by enzymes, exhibited antioxidant activity, inhibited nitric oxide production, are safe for cells, and hold potential as future supplements for human food and animal feed additives.

**Keywords:** Edible insects, Protein hydrolysates, Bioactive compound

### INTRODUCTION

Population growth and global warming have significantly impacted food security. As protein sources may become insufficient to meet rising demand, prompting scientists to explore edible insects as an alternative protein source for humans and animals over the past decade. Edible insects have been investigated in various fields including breeding, food research, safety, storage, and packaging [1]. Thailand's high biodiversity provides up to 300 species of edible insects. The widespread consumption of insects began with the outbreak of the Patanga locust in 1978, which caused severe damage to agricultural crops, leading to a change from natural harvesting to insect farming practices [2]. Consequently, Thailand has witnessed a substantial expansion in its insect-related export market, encompassing a wide array of products such as fresh and frozen insects and processed forms such as fried, roasted, insect powder, protein shakes, and bars, with an estimated annual value of 28.57 million USD [3].

Edible insects are an emerging source of protein, and scientists are interested in using insect proteins to create functional foods and nutritional supplements such as protein extracts, protein hydrolysates, and peptides. These substances can exhibit biological activity including antioxidants, anti-diabetic agents, anti-hypertensive agents, anti-cancer agents, as well as pathogen inhibitors, immune stimulants, and growth promoters [4]. The production of protein hydrolysates and peptides is primarily through protease hydrolysis processes such as alcalase, pepsin, papain, bromelain, trypsin, chymotrypsin, neutral protease, and proteinase-k [5–8]. Enzymes utilized in the process of protein digestion to produce protein hydrolysate may yield different biologically active substances depending on the protein source, despite being the same type of enzyme. Zielinska et al. [9] studied the antioxidant and anti-inflammatory effects of using enzymes in the gastrointestinal tract to digest proteins from three species of edible insects: *Gryllodes sigillatus*, *Tenebrio molitor*, and



*Schistocerca gregaria*. Different types of enzymes, when digesting the same protein, can produce varying antioxidant activities. This variation results from differences in protein size and the number of positive and negative charges in the structure, which affect the biological activity [10], which is important for applications in the food, cosmetics, health products, and animal dietary supplement industries.

The two-spotted cricket (*Gryllus bimaculatus*) and short-tail cricket (*Brachytrupes portentosus*) are economically important insects cultivated for their high nutritional value. Protein, fat, and carbohydrate percentages of *G. bimaculatus* were 57.02%-70.2%, 13.90%-33.14%, and 13.90%, respectively with *B. portentosus* 48.69%-59%, 20.60%-26.15%, and 5.15%, respectively [8, 11, 12]. Hall et al. [13] studied insect protein hydrolysates from whole crickets (*Gryllodes sigillatus*) using alcalase for enzymatic hydrolysis to enhance functional properties. The hydrolysates, composed of smaller peptides and amino acids, showed improved solubility, emulsifying, and foaming abilities. These hydrolysates are widely applied in food products for their nutritional and functional benefits, contributing to better texture, stability, and overall product quality. This research used protease enzymes to produce protein hydrolysates and investigated the biological activities of these two species. The knowledge gained will promote the production of high-value insect products for use as health enhancers, cosmetics, and animal health supplements.

## MATERIALS AND METHODS

### Extraction of soluble proteins from crickets

The extraction process of the two species of crickets, *G. bimaculatus* and *B. portentosus* involved weighing 50 g of fresh cricket, adding 400 ml of distilled water, blending thoroughly and then packing the mixture in a 500 ml glass bottle before sterilization in an autoclave at 100°C for 30 min. After sterilization, the precipitate was separated by centrifugation at a speed of 5000 rpm for 15 min, and the supernatant was stored at -20°C.

### Protein hydrolysate production using enzymes

Three samples of cricket protein hydrolysates were used.

1. Protein hydrolysates were obtained from the action of the enzyme SD-NY10 (Amano, Japan) at a concentration of 300 units/100 ml of soluble protein extract. The water-soluble protein extract were adjusted to pH 7 and incubated in a temperature-controlled bath at 50°C for 8 h. After incubation, the enzyme reaction was stopped by boiling in water for 10 min and the samples were stored at -20°C.

2. 100 ml of the extracted soluble protein were adjusted to pH 3 using 0.5 N hydrochloric acid. The enzyme pepsin at a concentration of 300 units/100

ml of soluble protein extract. (Sigma-Aldrich, Germany) was then added and the mixture was incubated in a water bath shaker at 37°C for 2 h. The enzyme reaction was stopped by boiling the mixture in water for 10 min.

3. Protein hydrolysate samples digested with the enzyme SD-NY10 were then digested with the pepsin enzyme, as described above, and stored at -20°C.

### Protein analysis

Protein content was measured using the Bradford assay with ready-made Bradford reagent (Bio-Rad, USA) diluted with distilled water at a ratio of 1:4. A 0.5 ml sample was taken to determine the protein amount, and 5 ml of the diluted Bradford reagent was added. The mixture was thoroughly mixed, and the absorbance was measured at a wavelength of 595 nm. The experiment was repeated three times and compared with a standard curve of bovine serum albumin at concentrations of 0.0, 0.2, 0.4, 0.6, 0.8, 1.0, and 1.2 mg/ml (Sigma-Aldrich, Germany).

### Analysis of protein molecular weights by SDS-PAGE

Protein samples from the crickets and standard protein were transferred on precast acrylamide gels with continuous concentrations of 4-12% (Invitrogen, USA) using electricity of 170 volts for 45 min. Protein bands were fixed on the gel plates with the Fixing solution for 1 h, stained with Coomassie brilliant blue for 2 h, and then the stain was washed off with the Destain solution overnight. The molecular weight of the sample protein was compared with the standard band displayed on the gel. The procedure for staining the gel was adapted from Green and Sambrook [14].

### Pathogenic bacterial inhibition by the agar well diffusion method

The experiment used three bacterial strains: *Escherichia coli* TISTR 117, *Salmonella typhimurium* TISTR 292, and *Salmonella enteritidis* TISTR 2519. The bacteria were cultured in nutrient broth and incubated at 37°C for 18-24 h. The bacterial concentrations were then adjusted to  $1 \times 10^8$  CFU/ml using 0.85% sodium chloride and compared with the McFarland Standard 0.5. The bacteria were spread on nutrient agar using the 3-way streaking method. Wells were created with a No. 3 cork borer, and 100 µl of the substances from both species of crickets were added into each well. Each plate was replicated three times and incubated at 37°C for 18-24 h. The inhibitory effect was examined by measuring the diameter in millimeters of the clear zones formed.

### Antioxidant activity

The total antioxidant capacity was assessed using a total antioxidant capacity assay kit (TAC) from Sigma-Aldrich, Germany, and compared to the standard Trolox measurements at a wavelength of 570 nm using a microplate reader (Multiskan Go,

Thermo Scientific, Finland). A critical evaluation criterion was ensuring that the absorbance value of the cricket protein sample did not surpass the standard curve. If this occurred, then sample dilution was necessary.

#### *Cytotoxicity testing*

A RAW 264.7 cell culture (Mouse macrophage cell line ATCC® number TIB-71™), ATCC, Virginia, USA was used.

1. RAW 264.7 cell cultures were prepared in Dulbecco's Modified Eagle Medium (DMEM) supplemented with 10% fetal bovine serum and 1% antibiotic-antimycotic in a 75 cm<sup>2</sup> surface area cell culture flask and incubated at 37°C with 5% CO<sub>2</sub> until they reached a density of 80%. The cells were then dissociated into a single cell suspension and counted to a concentration of 1x10<sup>5</sup> cells/ml. Subsequently, the cells were cultured in a 96-well culture plate and incubated at 37°C with 5% CO<sub>2</sub>.

2. The six test samples were prepared as protein hydrolysates from the two species of cricket. These test samples were filtered through a 0.22-micron filter and then diluted in cell culture media to concentrations of 50, 25, 12.5, 6.25, 3.13, and 1.56% (v/v). The positive control solution was supplemented with 10% DMSO in the culture medium, while the negative control solution was used DMEM. Each experimental group was replicated three times, and cells were incubated for 24 h. After incubation, cell viability was assessed through succinate dehydrogenase enzyme activity in living cells according to the protocol in ISO 109935-5. 100 ml of MTT solution (1 mg/ml) were then added and incubated at 37°C for 2 h. After incubation, the MTT solution was removed, and 100 µL of DMSO were added to the cells. The formation of a purple substance was observed and measured, with light absorbance value at a wavelength of 570 nm (ABS<sub>570</sub>).

3. The cell survival percentage was calculated and compared between the test sample and control groups as follows:

$$\text{Cell viability \%} = \frac{\text{ABS}_{570} \text{ of test sample}}{\text{ABS}_{570} \text{ of the control group}} \times 100$$

Substances with a cell viability value below 70% were considered cytotoxic.

#### *Stimulating nitric oxide production in the macrophage cell line*

1. The cell line RAW 246.7 was cultured using the same method as in the cytotoxicity test but with a cell concentration of 2x10<sup>5</sup> cells/ml. The same procedure for testing and protein hydrolysate extraction from cricket samples was used in the cytotoxicity study. The positive control for this test was a lipopolysaccharide solution (L4931) from *Escherichia coli* of Sigma-Aldrich, Germany at a concentration

of 1 µg/ml in the culture medium, while the negative control was a diclofenac solution at a concentration of 40 µg/ml in the cell culture medium. Each group was replicated three times.

#### *2. Nitric oxide quantification*

The RAW 264.7 cell line was cultured in a cell culture medium with the test sample, positive, and negative controls for 24 h. Then, the obtained cell culture medium was analyzed to measure the quantity of nitric oxide using a Griess reagent kit (Thermo Fisher Scientific, USA). The quantity of nitrite produced by the cells was assessed by the spectrophotometric analysis of light absorption at a wavelength of 570 nm and compared with a nitrite standard. Nitric oxide quantification was calculated as follows:

$$\text{Nitric oxide (}\mu\text{mol)} = \frac{\text{ABS}_{570} \text{ of test sample}}{\text{the slope value on the standard graph}}$$

The method was adapted from Zhang et al. [15].

#### *Phagocytic activity analysis of macrophage cells*

The RAW 264.7 cell culture method and test substances were the same as in the cytotoxicity test, with β-glucan at a concentration of 100 µg/ml in the culture medium used as a positive control. The negative control group consisted of cells cultured in Dulbecco's modified Eagle's medium (DMEM). All experimental groups were replicated three times. After incubation for 24 h, the cell culture medium was removed, and 100 µl of neutral red solution (at a concentration of 0.075% in PBS) was added to each well and incubated for 3 h at 37°C. After this incubation, the neutral red solution was removed, the cells were washed once with PBS pH 7.4, and Destain was added for 1 h according to the method of Zhang et al. [15]. The absorbance was then measured at a wavelength of 540 nm to calculate the phagocytic activity as:

$$\text{Phagocytic activity} = (\text{ABS}_{540} \text{ of test sample} - \text{ABS}_{540} \text{ of the negative control unit}) \times 100$$

## RESULTS AND DISCUSSION

#### *Characterization of protein hydrolysates derived from two species of cricket*

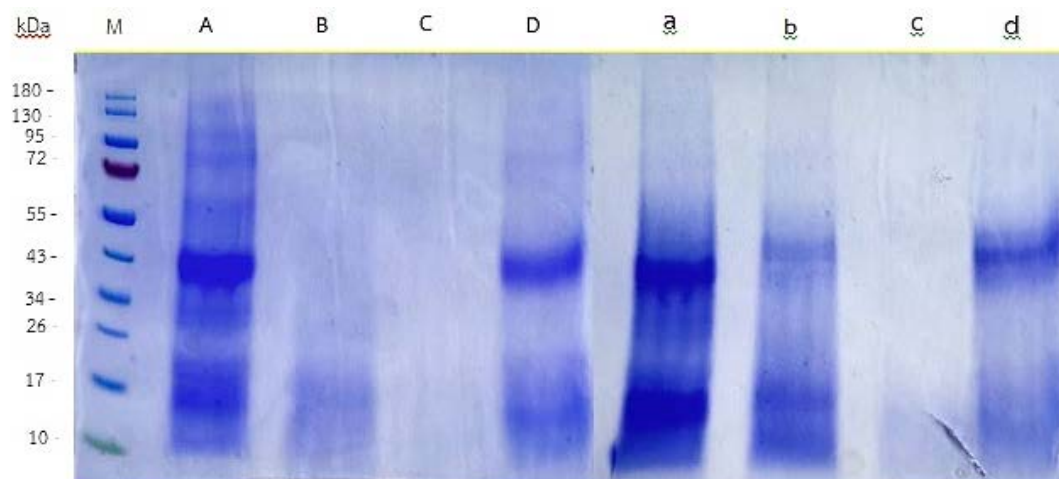
Water-soluble proteins from *G. bimaculatus* and *B. portentosus* were extracted using heat at 100°C for 30 min in an autoclave. The resulting water-soluble protein yields were 0.84 and 0.92 mg/ml, respectively. Subsequent enzymatic digestion of the water-soluble proteins produced three types of peptide hydrolysates: protein hydrolysates from digestion with the enzyme SD-AY 10, SD-AY 10 with pepsin, and pepsin. When different enzymes were used to digest the water-soluble proteins, the amounts of proteins digested varied. Peptides digested with SD-AY 10+pepsin from both cricket species had the highest

protein digestion values of 96-98%, followed by peptides digested with pepsin at 83-84%. The lowest

digestion was observed in peptides digested using the SD-AY 10 enzyme (Table 1).

**Table 1** Soluble protein hydrolysates (%) from two cricket species digested with pepsin and SD-AY 10.

Cricket species	Soluble protein hydrolysates (%)		
	SD-AY 10	Pepsin	SD-AY 10+Pepsin
<i>G. bimaculatus</i>	37	84	96
<i>B. portentosus</i>	72	83	98



**Figure 1** SDS-PAGE patterns of *B. portentosus* and *G. bimaculatus* proteins. A-D=proteins from *B. portentosus* and a-d protein from *G. bimaculatus*: A, a = protein extracted with heat 100°C, B b = protein hydrolysate by SD-AY 10; C c = protein hydrolysate by SD-AY 10+pepsin and D d = protein hydrolysate by pepsin.

The protein hydrolysate obtained from *B. portentosus* digested with SD-AY 10 had a higher level of digested protein compared to *G. bimaculatus* (Table 1). Different amino acid compositions in the protein structure impacted the specific binding site of the enzyme SD-AY 10 for the amino acid serine [16], leading to limited enzymatic activity. This observation aligned with Leni et al. [17]. They utilized the enzyme bromelain for protein digestion from larvae of *Alphitobius diaperinus* and *Hermetia illucens* and recorded distinct protein digestibility values that differed by 13.3% and 23.1%, respectively.

Analysis of protein hydrolysate solutions derived from both cricket species via SDS-PAGE at an acrylamide gel concentration of 4-12% revealed water-soluble proteins extracted at 100°C from *B. portentosus* with molecular weights of 10, 17, 30, 43, 60, 72, and 95 kDa. The proteins digested with SD-AY 10 exhibited bands in the molecular weight range of 17 kDa, while the proteins digested with SD-AY 10+pepsin resulted in no protein bands on the gel. Proteins digested with pepsin displayed bands at molecular weights of 43 and 15 kDa. Proteins extracted with heat from *G. bimaculatus* showed bands at 10, 17, and 43 kDa, while proteins digested with the enzyme SN-AY 10 demonstrated a lighter band at 43 kDa and more intense bands between 17 and 10 kDa. Proteins digested with SD-AY 10+pepsin and pepsin exhibited analogous outcomes to those from *B. portentosus* (Figure 1). Proteins

digested with SD-AY 10+pepsin showed 96-98% protein digestion (Table 1) with no protein bands on the gel, suggesting protein digestion to a size of less than 10 kDa. These findings align with previous research utilizing endo-proteases such as papain, bromelain, pepsin, and protease enzymes from microorganisms, which digested proteins extracted from water-based edible insect sources, yielding protein sizes ranging from 10 to 35 kDa [8, 18-20].

#### Biological activity

##### 1. Effective inhibition of pathogenic microorganisms

The protein samples derived from *G. bimaculatus* and *B. portentosus* were used to test the inhibition of pathogens *E. coli*, *S. enteritidis*, and *S. typhimurium* included heat-extracted soluble protein, and protein hydrolysates obtained through digestion with SD-AY 10, SD-AY 10 combined with pepsin, and pepsin using the agar well diffusion method. Results indicated that the protein samples from both species of crickets were unable to inhibit all three species of pathogens, consistent with results reported by Flores et al. [20]. They extracted proteins from the edible insects *Tenebrio molitor* and *Ulomoides dermestoides* digested with protease from *Aspergillus oryzae*, yielding peptides with molecular weights ranging from 45 kDa to less than 10 kDa, which were unable to inhibit *Salmonella* spp. Similarly, Sousa et al. [21] found that

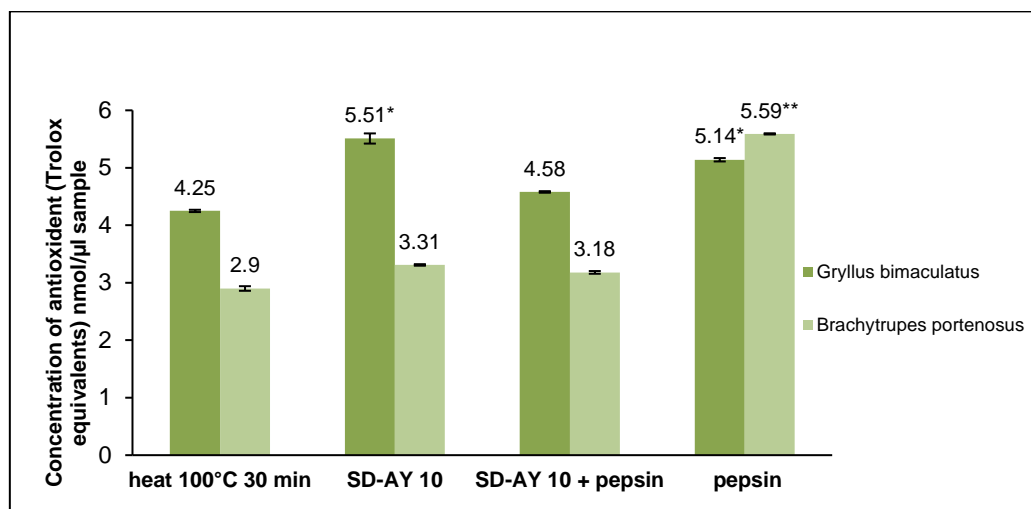


protein hydrolysates of the edible insect *Alphitobius cliperinus*, obtained from alcalase digestion, were unable to inhibit the growth of *E. coli* and *S. enteritidis*. These results highlighted that protein hydrolysates from the 150 insect species studied were ineffective in inhibiting pathogenic microorganisms.

### 2. Total antioxidant capacity

The total antioxidant capacity (TAC) assesses the resistance to free radicals generated within the body during the process of oxygen metabolism, which produces reactive oxygen species (ROS) including hydrogen peroxide ( $H_2O_2$ ), hydroxyl radical ( $HO^\bullet$ ), peroxy radical ( $ROO^\bullet$ ), and superoxide radical ( $O_2^\bullet$ ) [22]. This test evaluated the water-soluble protein extracts and protein hydrolysates from two species of crickets for their antioxidant efficiency. Compared to the standard Trolox, *G. bimaculatus* protein hydrolysates digested with SD-AY 10 exhibited the highest antioxidant efficiency at 5.5 nmol/ $\mu$ l,

significantly higher than the other protein solutions ( $p < 0.05$ ). Conversely, proteins extracted with heat at  $100^\circ C$  demonstrated the lowest efficiency. The heat-extracted protein exhibited lower antioxidant activity compared to the enzymatically hydrolyzed protein, particularly in the case of *G. bimaculatus*. According to the SDS-PAGE results, several large proteins were present, ranging from 43 to 130 kDa. The size of these proteins influences their antioxidant capacity, with smaller proteins demonstrating greater antioxidant activity. This observation aligns with findings that smaller proteins exhibit stronger antioxidant properties [23]. For *B. portentosus*, protein hydrolysates digested pepsin displayed efficient antioxidant activity, significantly higher than other protein solutions ( $p < 0.01$ ) with an efficiency value of 5.59 nmol/ $\mu$ l (Figure 2). Consistent with numerous studies exploring protein digestion in edible insects using alkaline protease enzymes and digestive enzymes [20, 21, 24, 25].



**Figure 2** Effect of protein hydrolysates from *B. portentosus* and *G. bimaculatus* on total antioxidant capacity  
\*Significant difference ( $p \leq 0.05$ ), \*\*significant difference ( $p \leq 0.01$ ).

The molecular weight of the peptides influenced the antioxidant properties. The experimental group digested with a single type of SD-NY10 of *G. bimaculatus*, with molecular weights ranging from 10 to 17 kDa, displayed better antioxidant efficiency than those utilizing SD-AY 10 with pepsin, which had a molecular size lower than 10 kDa, consistent with Jang et al. [26] and Flores et al. [20] within this molecular weight range. The antioxidant efficiency of peptides depends on various factors such as amino acid composition, hydrophilic-hydrophobic properties, polarity of the structure, enzyme types, and methods used to break down protein structures into peptides [4, 27].

### 3. Cytotoxicity

Peptide samples from the two cricket species were divided into three experimental groups: proteins digested with SD-AY 10, SD-AY 10+pepsin, and pepsin. Each experimental group utilized concentrations of protein solutions such as 1.56, 3.13, 6.25, 12.5, 25, and 50% (v/v) of RAW 264.7 cell culture medium. Results

revealed that peptides within the concentration range of 1.56-25% (v/v) in all experimental groups exhibited cell safety, with over 70% cell viability, especially peptides from each cricket species. When comparing peptides derived from hydrolysis using three different enzyme treatments, those from *G. bimaculatus* hydrolyzed with SD-AY10 exhibited the highest cell viability ( $p < 0.01$ ). In contrast, proteins from *B. portentosus* digested with pepsin demonstrated superior safety, with cell survival rates ranging from 104% to 109% ( $p < 0.01$ ). However, cell toxicity was observed across all experimental groups at a 50% (v/v) sample concentration, indicating that higher concentrations of cricket protein hydrolysates resulted in increased cytotoxicity. These findings are consistent with those of Riolo et al. [28], who reported that elevated concentrations of protein hydrolysates from black soldier fly (*Hermetia illucens*) were harmful to fibroblast cells (L-929). (Table 2).



**Table 2** Effect of protein hydrolysates from *B. portentosus* and *G. bimaculatus* on the viability of the RAW 264.7 cell line.

Cell viability of RAW 264.7 (%)					
Type of protein hydrolysates treatment	Sample concentration % (v/v)	SD-AY 10	SD-AY 10 + pepsin	pepsin	DMSO 10% (v/v)
<i>G. bimaculatus</i>	1.56	90.52±0.97 <sup>a</sup>	79.69±0.26 <sup>c</sup>	86.45±2.72 <sup>b</sup>	17.11±0.09
	3.13	87.48±0.87 <sup>a</sup>	75.60±0.46 <sup>c</sup>	83.63±2.30 <sup>b</sup>	
	6.25	86.86±1.29 <sup>a</sup>	76.37±0.86 <sup>c</sup>	82.29±3.08 <sup>b</sup>	
	12.5	84.79±0.66 <sup>a</sup>	73.09±0.68 <sup>b</sup>	76.47±2.88 <sup>b</sup>	
	25	82.69±0.66 <sup>a</sup>	73.68±0.82 <sup>b</sup>	73.50±2.08 <sup>b</sup>	
	50	61.00±1.33 <sup>a</sup>	50.36±0.82 <sup>c</sup>	53.40±0.51 <sup>b</sup>	
<i>B. portentosus</i>	1.56	88.09±1.26 <sup>b</sup>	84.36±1.96 <sup>c</sup>	109.36±1.53 <sup>a</sup>	17.11±0.09
	3.13	87.08±0.72 <sup>b</sup>	86.80±1.03 <sup>b</sup>	106.68±0.69 <sup>a</sup>	
	6.25	89.11±0.45 <sup>b</sup>	86.19±1.14 <sup>c</sup>	108.37±1.45 <sup>a</sup>	
	12.5	88.21±1.69 <sup>b</sup>	85.89±0.46 <sup>c</sup>	109.67±0.60 <sup>a</sup>	
	25	85.27±1.50 <sup>b</sup>	79.48±1.06 <sup>c</sup>	104.67±1.42 <sup>a</sup>	
	50	33.80±1.23 <sup>c</sup>	47.06±1.45 <sup>b</sup>	63.34±1.40 <sup>a</sup>	

Note: <sup>a,b,c</sup>Means within a row with different letters are statistically significant (p<0.01)

**Table 3** Effect of protein hydrolysates from *B. portentosus* and *G. bimaculatus* on nitric oxide production of the RAW 264.7 cell line.

Nitric oxide production of the RAW 264.7 cell line						
Type of protein hydrolysates treatment	Sample concentration % (v/v)	SD-AY 10	SD-AY 10 + pepsin	pepsin	LPS (1 µg/ml)	Diclofenac (40 µg/ml)
<i>G. bimaculatus</i>	1.56	35.48±0.27 <sup>b</sup>	33.72±0.56 <sup>b</sup>	86.45±2.72 <sup>a</sup>	34.02±0.54	15.51±1.50
	3.13	37.23±0.57 <sup>b</sup>	36.02±0.77 <sup>b</sup>	83.63±2.30 <sup>a</sup>		
	6.25	33.81±0.70 <sup>b</sup>	32.97±0.51 <sup>b</sup>	82.29±3.08 <sup>a</sup>		
	12.5	22.90±0.22 <sup>b</sup>	21.84±0.33 <sup>b</sup>	76.47±2.88 <sup>a</sup>		
	25	9.30±0.71 <sup>a</sup>	6.89±0.13 <sup>b</sup>	9.43±0.98 <sup>a</sup>		
	50	-	-	-		
<i>B. portentosus</i>	1.56	40.25±1.11 <sup>a</sup>	33.74±0.45 <sup>b</sup>	34.60±1.10 <sup>b</sup>	34.02±0.54	15.51±1.50
	3.13	39.56±0.46 <sup>a</sup>	33.30±0.56 <sup>c</sup>	34.75±0.86 <sup>b</sup>		
	6.25	34.34±0.91 <sup>a</sup>	30.64±0.27 <sup>b</sup>	30.47±0.60 <sup>b</sup>		
	12.5	22.26±1.00 <sup>a</sup>	19.73±0.29 <sup>b</sup>	21.01±0.57 <sup>a</sup>		
	25	7.66±0.36 <sup>a</sup>	6.73±0.94 <sup>ab</sup>	5.94±0.22 <sup>b</sup>		
	50	-	-	-		

Note: <sup>a,b,c</sup>Means within a row with different letters are statistically significant (p<0.01)

#### 4. Effect of protein hydrolysates on the production of nitric oxide (NO)

In all the experimental groups, protein hydrolysates derived from the two cricket species, at a concentration of 25% (v/v), exhibited a higher inhibitory effect on nitric oxide production than diclofenac (anti-inflammatory substance) at 15.51 µmol. The amount of nitric oxide ranged from 5.94 to 9.43 derived from *G. bimaculatus* hydrolyzed using SD-AY10+pepsin exhibited significantly reduced nitric oxide (NO) levels (p<0.01). Similarly, peptides obtained from *B. portentosus* hydrolyzed with pepsin also showed the lowest NO levels (p<0.01). Notably, at a concentration of 50% (v/v), NO was undetectable (Table 3).

In most experimental groups, protein hydrolysate concentrations ranged from 1.56% to 12.5% (v/v) and demonstrated the ability to trigger nitric oxide production comparable to the positive control using LPS (34.02 µmol) as a stimulant, except for protein from *G. bimaculatus* digested with pepsin, which stimulated high levels of nitric oxide production ranging from 76.47 to 86.45 µmol. Nitric oxide is considered harmful to cells and classified as a pro-inflammatory substance. An excessive amount of nitric oxide stimulates immune cells to produce more substances that induce cell inflammation [29, 30]. The stimulation and inhibition of nitric oxide production by protein hydrolysates from both cricket species depended on various factors including the type of

protein-digesting enzyme, insect species, protein molecular weight, and testing substance concentration. The reported of Yoon et al. [31] investigated the use of the enzyme Flavourzyme/alcalase and a combination of two enzymes in digesting proteins from the three insect species: *Tenebrio molitor*, *G. bimaculatus*, and *Bombyx mori*. The peptides tested had molecular weights ranging from less than 10 to 15 kDa. The protein concentration used in nitric oxide production was tested in RAW 624.7 cells at 0.1, 0.3, and 0.5 mg/ml. Protein hydrolysate from *B. mori* with both enzymatic digestions inhibited nitric oxide production better than the other two species, with a concentration of 0.5 mg/ml demonstrating the highest inhibitory effect.

#### 5. Effect of peptide hydrolysates on phagocytic activity

Phagocytic activity measures the response of white blood cells to the invasion of foreign agents such as bacteria, viruses, or substances (polysaccharides, proteins, hydrolysates, and herbal extracts) [29]. White blood cells destroy invaders by releasing pro-inflammatory substances including reactive oxygen species, reactive nitrogen species, interleukin-1 $\beta$ , and tumor necrosis factor- $\alpha$  [32]. Thus, measuring

phagocytic activity assesses the ability of white blood cells to destroy foreign substances when stimulated. Testing the protein hydrolysates from both cricket species revealed that at a concentration of 50% (v/v) in all experimental groups, the protein hydrolysates exhibited no phagocytic activity, which correlated with the production of nitric oxide and the cell survival rate. Notably, analysis of protein hydrolysates from *G. bimaculatus* revealed that proteins digested with pepsin at concentrations ranging from 1.56% to 12.5% (v/v) exhibited higher phagocytic activity than the positive control (149.18%), with activity values between 152.52% and 163.86%. Additionally, when comparing peptides hydrolyzed by the three enzymes, those treated with pepsin showed the highest phagocytic activity ( $p<0.01$ ). Conversely, protein hydrolysates from *B. portentosus* at concentrations of 12.5% and 25% (v/v) showed phagocytic activity between 154.16% and 158%, exceeding the positive control (Table 4). Peptides hydrolyzed predominantly by pepsin had the highest phagocytic activity ( $p<0.01$ ). These differences in macrophage activity and nitric oxide (NO) levels could be due to the distinct peptides generated by each enzymatic digestion.

**Table 4** Effect of protein hydrolysates from *B. portentosus* and *G. bimaculatus* on phagocytic activity of the RAW 264.7 cell line.

Phagocytic activity of the RAW 264.7 cell line						
Type of protein hydrolysates treatment	Sample concentration % (v/v)	SD-AY 10	SD-AY 10 + pepsin	pepsin	$\beta$ -glucan (100 $\mu$ g/ml)	control
<i>G. bimaculatus</i>	1.56	108.16 $\pm$ 2.29 <sup>c</sup>	141.11 $\pm$ 2.52 <sup>b</sup>	156.69 $\pm$ 2.88 <sup>a</sup>	149.18 $\pm$ 2.41	100
	3.13	138.58 $\pm$ 5.44 <sup>b</sup>	139.19 $\pm$ 1.36 <sup>b</sup>	159.01 $\pm$ 0.75 <sup>a</sup>		
	6.25	128.75 $\pm$ 4.57 <sup>c</sup>	141.59 $\pm$ 0.66 <sup>b</sup>	163.86 $\pm$ 2.90 <sup>a</sup>		
	12.5	137.21 $\pm$ 3.19 <sup>b</sup>	138.34 $\pm$ 0.38 <sup>b</sup>	152.52 $\pm$ 4.91 <sup>a</sup>		
	25	145.97 $\pm$ 1.39 <sup>a</sup>	131.43 $\pm$ 0.81 <sup>b</sup>	142.76 $\pm$ 5.53 <sup>a</sup>		
	50	-	-	-		
	1.56	128.9 $\pm$ 71.48 <sup>a</sup>	115.05 $\pm$ 1.65 <sup>b</sup>	131.19 $\pm$ 2.26 <sup>a</sup>	149.18 $\pm$ 2.41	100
<i>B. portentosus</i>	3.13	137.09 $\pm$ 0.24 <sup>a</sup>	116.01 $\pm$ 0.56 <sup>c</sup>	130.58 $\pm$ 2.77 <sup>b</sup>		
	6.25	138.92 $\pm$ 0.42 <sup>a</sup>	124.82 $\pm$ 2.69 <sup>b</sup>	139.02 $\pm$ 2.56 <sup>a</sup>		
	12.5	150.21 $\pm$ 3.41 <sup>a</sup>	130.70 $\pm$ 1.12 <sup>b</sup>	154.16 $\pm$ 3.32 <sup>a</sup>		
	25	136.98 $\pm$ 3.78 <sup>b</sup>	123.93 $\pm$ 0.92 <sup>c</sup>	158.60 $\pm$ 3.27 <sup>a</sup>		
	50	-	-	-		

Note: <sup>a,b,c</sup>Means within a row with different letters are statistically significant ( $p<0.01$ )

Results demonstrated that protein hydrolysates or peptides generated through protease digestion enhanced the phagocytic activity of macrophage cells. Various factors influenced cell activation including the molecular weight and concentration of the activating proteins, as well as their correlation with the cell survival rate [33-35].

## CONCLUSIONS

The protein hydrolysates utilized in this study, derived from *G. bimaculatus* and *B. portentosus*, were digested with the enzymes SD-AY 10, pepsin, and

a combination of SD-AY 10 and pepsin. Evaluation of biological activity revealed that *G. bimaculatus* protein digested with SD-AY 10 exhibited the highest antioxidant activity, while protein hydrolysates from *B. portentosus* hydrolyzed with pepsin had the highest antioxidant activity. Cytotoxicity assessment conducted on RAW 246.7 macrophages indicated that protein hydrolysates in all experimental groups were cell-safe at concentrations ranging from 1.56% to 25% (v/v). Protein hydrolysates from both cricket species inhibited nitric oxide production at a concentration of 25% (v/v), exerting anti-inflammatory effects. However,

concentrations of 1.56% to 6.25% (v/v) stimulated the immune system and induced phagocytic activity. Proteins from *G. bimaculatus* digested with pepsin exhibited the highest phagocytic activity at concentrations ranging from 1.56% to 12.5% (v/v), while *B. portentosus* proteins digested with pepsin displayed the highest phagocytic activity at concentrations of 12.5% to 25% (v/v). Results suggested that protein hydrolysates from *G. bimaculatus* and *B. portentosus* showed significant biological activity and acted as antioxidants, anti-inflammatory agent, and immune stimulants. Further investigations should explore the development of other novel bioactive compounds derived from Thailand's biological resources. These compounds hold promises for applications as pharmaceutical, cosmetic, and health supplements for both humans and animals, thereby enhancing the value and economic potential of insects in the country.

### REFERENCES

- Elhassan M, Wendin K, Olsson V, Langton M. Quality aspects of insects as food-nutritional, sensory, and related concepts. *Foods*. 2019;8(3):95.
- Dobermann D, Swift JA, Field LM. Opportunities and hurdles of edible insects for food and feed. *Nutr Bull*. 2017;42(4):293-308.
- Digital economy promotion agency, ministry of digital economy and society. Raising crickets through the utilization of valuable protein technology poised for future applications, 2022 [Internet]. [cited 2023 Mar 29]. Available From: <http://www.depa.or.th/article-view/cricket-futuchnology>.
- Hall F, Johnson PE, Liceaga A. Effect of enzymatic hydrolysis on bioactive properties and allergenicity of cricket (*Grylloides sigillatus*) protein. *Food Chem*. 2018;262:39-7.
- Hernández-Ledesma B, García-Nebot MJ, Fernández-Tomé S, Amigo L, Recio I. Dairy protein hydrolysates: Peptides for health benefits. *Int Dairy J*. 2014;38(2):82-100.
- Hou Y, Wu Z, Dai Z, Wang G, Wu G. Protein hydrolysates in animal nutrition: Industrial production, bioactive peptides, and functional significance. *J Anim Sci Biotechnol*. 2017;8:24.
- You SJ, Wu J. Angiotensin-I converting enzyme inhibitory and antioxidant activities of egg protein hydrolysates produced with gastrointestinal and nongastrointestinal enzymes. *J Food Sci*. 2011;76(6):801-7.
- Paulin IG, Parwanto MG. Nutritional characteristics of teak grasshopper (*Valanga nigricornis* Burmeister), cricket (*Brachytrupes portentosus* L.), and mealworm (*Tenebrio molitor*) as alternative food sources in Indonesia. *Indonesian journal of biotechnology and biodiversity*. 2020;4(1):52-61.
- Zielinska E, Baraniak B, Karas M. Antioxidant and anti-inflammatory activities of hydrolysates and peptide fractions obtained by enzymatic hydrolysis of selected heat-treated edible insects. *Nutrients*. 2017;9(9):970.
- Trinh BT, Supawong S. Enzymatic hydrolysis of cricket (*Grylloides sigillatus*) protein: influence of alcalase and neutrase enzyme on functional properties of recovered protein. *Biol Sci*. 2021;10(3):342-53.
- Taufek NM, Aspani F, Muin H, Raji AA, Razak SA, Alias Z. The effect of dietary cricket meal (*Gryllus bimaculatus*) on growth performance, antioxidant enzyme activities, and haematological response of African catfish (*Clarias gariepinus*). *Fish Physiol Biochem*. 2016;42(4):1143-55.
- Magara HJO, Niassy S, Ayieko MA, Mukundamago M, Egonyu JP, Tanga CM, et al. Edible crickets (orthoptera) around the world: distribution, nutritional value, and other benefits-a review. *Front Nutr*. 2021;7:1-23.
- Hall FG, Jones OG, O'Haire ME, Liceaga AM. Functional properties of tropical banded cricket (*Grylloides sigillatus*) protein hydrolysates. *Food Chem*. 2017;224:414-22.
- Green MR, Sambrook J. Molecular cloning: a laboratory manual. Vol. 1. 4th ed. New York: Cold Spring Harbor Laboratory Press; 2012.
- Zhang Y, Tang KY, Chen B, Zhou S, Li N, Liu C, et al. A polyethylenimine-based diazeniumdiolate nitric oxide donor accelerates wound healing. *Biomater Sci-UK*. 2019;7:1607-16.
- Hatta F, Matsumoto K, Honda Y. Bacilloolysin, papain, and subtilisin improve the quality of gluten-free rice bread. *J Cereal Sci*. 2015;61:41-7.
- Leni G, Soetemans L, Jacobs J, Depraetere S, Gianotten N, Bastiaens L, et al. Protein hydrolysates from *Alphitobius diaperinus* and *Hermetia illucens* larvae treated with commercial proteases. *Journal of insects as food and feed*. 2020;6(4):393-404.
- Luna GC, Gonzalez FSM, Mauer LJ, Liceaga AM. Cricket (*Acheta domesticus*) protein hydrolysates, impact on the physicochemical, structural and sensory properties of tortillas and tortilla chips. *Journal of insects as food and feed*. 2021;7(1):109-20.

19. Firmansyah M, Abduh MY. Production of protein hydrolysate containing antioxidant activity from *Hermetia illucens*. Heliyon. 2019;5(6): e02005.
20. Flores DR, Casados LE, Velasco SF, Ramlez AC, Velazquez G. Comparative study of composition, antioxidant and antimicrobial activity of two adult edible insects from Tenebrionidae family. BMC Chem. 2020;14(55):1-9.
21. Sousa P, Borger S, Pintado M. Enzymatic hydrolysis of insect *Alphitobius diaperinus* towards the development of bioactive peptide hydrolysates. Food Funct. 2020;11(4):3539-48.
22. Valko M, Rhodes CJ, Moncol J, Izakovic M, Mazur M. Free radicals, metals and antioxidants in oxidative stress-induced cancer. Chem-Biol Interact. 2006;10(1):1-40.
23. Kittiphattanabawon P, Benjakul S, Visessanguan W, Shahidi F. Effect of extraction temperature on functional properties and antioxidative activities of gelatin from shark skin. Food Bioprocess Tech. 2012;5:2646-54.
24. Batish I, Brits D, Valencia P, Miyai C, Rafeeq S, Xu Y, et al. Effects of enzymatic hydrolysis on the functional properties, antioxidant activity and protein structure of black soldier fly (*Hermetia illucens*) Protein. Insects. 2020;11(12):876.
25. Wonyoung J, Chulmin K, Na KA, Younggi C, Rae KJ, Myeongsoo J, et al. Comparisons of yield, amino acid composition and antioxidant activity of the ten extracts of *Gryllus bimaculatus* (Two-spotted cricket) prepared by different methods. Food Suppl Biomater Health. 2021;1(4):1-9.
26. Jang HY, Park CE, Kim KJ, Kim JH, Lee S. Comparison of antioxidant capacity of protein hydrolysates from 4 different edible insects. Korean J Food Sci Tech. 2019;51(5):480-5.
27. Ajilola CF, Fashakin JB, Fagbemi TN, Aloko RE. Effect of peptide size on antioxidant properties of african yam bean seed (*Sphenostylis stenocarpa*) protein hydrolysate fractions. Int J Mol Sci. 2011;12(10):6685-702.
28. Riolo K, Rotondo A, La Torre GL, Marino Y, Franco GA, Crupi R, et al. Cytoprotective and Antioxidant Effects of Hydrolysates from Black Soldier Fly (*Hermetia illucens*). Antioxidants (Basel). 2023;12(2):519.
29. Lee JH, Lee JE, Paik HD. Immunomodulatory activity of egg yolk protein hydrolysates prepared by novel two-step hydrolysis: A study of mechanism and stability after in vitro digestion model. Poult Sci. 2022;101(5):101802.
30. Ramesh A, Kumar S, Brouillard A, Nandi D, Kulkarni A. A nitric oxide (NO) nanoreporter for noninvasive real-time imaging of macrophage immunotherapy. Adv Mater. 2020;32(24): 2000648.
31. Yoon S, Wong NAK, Chae M, Auh JH. Comparative characterization of protein hydrolysates from three edible insects: mealworm larvae, adult crickets, and silkworm pupae. Food. 2019;8 (563):1-16.
32. Xin Y, Ji H, Cho E, Roh KB, You J, Park D, et al. Immune-enhancing effect of water-soluble beta-glucan derived from enzymatic hydrolysis of yeast glucan. Biochem Biophys Reports. 2022;30:101256.
33. Cai B, Chen H, Wan P, Luo L, Ye Z, Huang J, et al. Isolation and identification of immunomodulatory peptides from the protein hydrolysate of tuna trimmings (*Thunnus albacares*). LWT. 2022;164: 113614.
34. Huang D, Yang L, Wang C, Ma S, Cui L, Huang S, et al. Immunostimulatory activity of protein hydrolysate from *Oviductus ranae* on macrophage *In Vitro*. Evid Based Complement Alternative Med. 2014;1-11. Available from: <https://doi.org/10.1155/2014/180234>.
35. Lebrun I, Cavallaro V, Juliano L, Juliano MA, de Sousa e Silva MCC. Effects of 'casoparan', a peptide isolated from casein hydrolysates with mastoparan-like properties. Mediators Inflamm. 2004;13(4):263-8.





**Institute of Research and Development  
Rajamangala University of Technology Thanyaburi**

39 M.1 Klong 6, Thanyaburi, Pathumthani 12110, Thailand  
Tel. (02) 549-4492 Fax. (02) 577-5038, (02) 549-4680

Website : <https://ird.rmutt.ac.th>



THAIJO